MODELLING AND OPTIMIZATION OF GREEN PELLETS CLASSIFICATION ON ROLLER SCREENS USING THE DISCRETE ELEMENT METHOD

Benito Barbabela e Silva

Dissertação de Mestrado apresentada ao Programa de Pós-graduação em Engenharia Metalúrgica e de Materiais, COPPE, da Universidade Federal do Rio de Janeiro, como parte dos requisitos necessários à obtenção do título de Mestre em Engenharia Metalúrgica e de Materiais.

Orientadores: Luís Marcelo Marques Tavares
Rodrigo Magalhães de Carvalho

Rio de Janeiro
Julho de 2017

MODELLING AND OPTIMIZATION OF GREEN PELLETS CLASSIFICATION ON ROLLER SCREENS USING THE DISCRETE ELEMENT METHOD

Benito Barbabela e Silva

DISSERTAÇÃO SUBMETIDA AO CORPO DOCENTE DO INSTITUTO ALBERTO LUIZ COIMBRA DE PÓS-GRADUAÇÃO E PESQUISA DE ENGENHARIA (COPPE) DA UNIVERSIDADE FEDERAL DO RIO DE JANEIRO COMO PARTE DOS REQUISITOS NECESSÁRIOS PARA A OBTENÇÃO DO GRAU DE MESTRE EM CIÊNCIAS EM ENGENHARIA METALÚRGICA E DE MATERIAIS.

Examinada por:

_____

Prof. Luís Marcelo Marques Tavares, Ph. D.

_____

Prof. Rodrigo Magalhães de Carvalho, D. Sc.

_____

Prof. Fabio Pereira dos Santos, D. Sc.

_____

Eng. Valdirene Gonzaga de Resende, D.Sc.

RIO DE JANEIRO, RJ – BRASIL

JULHO DE 2017

Silva, Benito Barbabela e

Modelling and Optimization of Green Pellets Classification on Roller Screens Using the Discrete Element Method/ Benito Barbabela e Silva. – Rio de Janeiro: UFRJ/COPPE, 2017.

XXVIII, 153 p.: il.; 29,7 cm.

Orientadores: Luís Marcelo Marques Tavares

Rodrigo Magalhães de Carvalho.

Dissertação (mestrado) – UFRJ/ COPPE/ Programa de Engenharia Metalúrgica e de Materiais, 2017.

Referências Bibliográficas: p. 136-143.

1. Green pellets. 2. Screening. 3. The Discrete Element Method. I. Tavares, Luís Marcelo Marques *et al*. II. Universidade Federal do Rio de Janeiro, COPPE, Programa de Engenharia Metalúrgica e de Materiais. III.Título.

When you walk through a storm
Hold your head up high
And don't be afraid of the dark
At the end of a storm
There's a golden sky
And the sweet silver song of a lark
Walk on through the wind
Walk on through the rain
Though your dreams be tossed and blown
Walk on, walk on
With hope in your heart
And you'll never walk alone
You'll never walk alone
Walk on, walk on
With hope in your heart
And you'll never walk alone
You'll never walk alone

He was my friend
He trusted me
In memory of my beloved dad

Acknowledgement

I am very grateful to:

my family for my rising. To my mother and father for teaching me the values of education and hard work respectively.

VALE S / A and DIPE - Pelletizing Department - especially to Rodrigo Araújo, Fernando Quintão and Mauricío Max, for the opportunity of personal growth and for believing in R&D as a powerful tool for technological development in the search of operational excellence.

Virgino Xavier, Frederico Mayerhofer, Luis Dantas and José Paiva for the trust and belief in the work developed.

The advisors Prof. Luís Marcelo Tavares and Prof. Rodrigo Carvalho for all dedication, teachings and knowledge sharing during all stages of this journey.

To Master Pedro Cavalcanti and Doctor Emerson Reikdal for the unconditional support and for all the time spent on the work. All results would not be achieved without your friendly help.

To Evandro Lopes, Gleisson Ricardo and Evandro Madalena for their substantially supporting during the tests and for the execution of the routine in my absences.

To all LTM members.

Resumo da Dissertação apresentada à COPPE/UFRJ como parte dos requisitos necessários para a obtenção do grau de Mestre em Ciências (M.Sc.)

MODELAGEM E OTIMIZAÇÃO DA CLASSIFICAÇÃO DE PELOTAS VERDES EM PENEIRAS DE ROLOS USANDO MÉTODO DE ELEMENTOS DISCRETOS

Benito Barbabela e Silva

Julho/2017

Orientadores: Luís Marcelo Marques Tavares
Rodrigo Magalhães de Carvalho

Programa: Engenharia Metalúrgica e de Materiais

O presente trabalho estuda, através de simulações por Métodos de Elementos Discretos, a classificação de pelotas verdes em peneiras de rolos. Para tal, as propriedades individuais e a granel das pelotas verdes são determinadas em ensaios físicos para calibração e validação por comparação com dados industriais de modelos de contato que reproduzam com verossimilhança o movimento destes sólidos. De acordo com os resultados, o modelo JKR foi o que melhor se adequa para as interações de pelotas úmidas de baixa resistência entre elas e a superfície dos rolos. Simulações exploratórias avaliaram a sensibilidade do modelo à diferentes condições operacionais. A aplicação de metodologia e análise de experimentos permitiram o entendimento e amplitude da influência das principais variáveis de controle de processo. Com base nos resultados, propostas de otimização foram elaboradas e simuladas indicando perspectivas positivas. A peneira duplo *deck* em operação e o um novo projeto de peneira segregadora foram testados. Os resultados para a nova proposta demonstraram-se promissores: melhor eficiência e maior fração de vazios para o leito de pelotas no carro de grelha.

Abstract of Dissertation presented to COPPE/UFRJ as a partial fulfillment of the requirements for the degree of Master of Science (M.Sc.)

MODELLING AND OPTIMIZATION OF GREEN PELLETS CLASSIFICATION ON ROLLER SCREENS USING THE DISCRETE ELEMENT METHOD

Benito Barbabela e Silva

July/2017

Advisors: Luís Marcelo Marques Tavares
Rodrigo Magalhães de Carvalho

Department: Metallurgical and Materials Engineering

The present work studies the classification of green pellets in roller screens using the Discrete Element Method. For this, the individual and bulk properties of the green pellets are determined in physical tests for calibration and validation by comparison with industrial data of contact models that reproduce with verisimilitude the movement of these solids. According to the results, the JKR model was the one that best fitted the interactions of low resistance moist pellets among themselves and rolls surface. Exploratory simulations evaluated the sensitivity of the model to different operating conditions. The application of the methodology of design and analysis of experiments made possible the understanding of the main process control variables amplitude of influence. Based on the results, optimization proposals were elaborated and simulated indicating positive perspectives. The double deck screen in operation and a new segregator double deck design were tested. The results for the new proposal have shown to be promising: better efficiency and higher voidage fraction of the bed of pellets in the grid car.

LIST OF FIGURES

LIST OF TABLES

LIST OF SYMBOLS

Φ	seeds weighted mean
ϕ	sphericity shape factor

Latin

a	surface of contact
a_c	attractive cohesion force
a_n	acceleration on normal component
a_v	acceleration vector
b	adjustable/empirical parameter
c	adjustable/empirical parameter
A_1	independent constant of granule size
C	shape factor
Ca	Capillary number
C_f	fines shape factor
C_r	ratio of fines and seeds shape factor
C_s	seeds shape factor
D	damping matrix
D_{eff}	effective granule diameter
D^*	characteristic limiting size
d_p	grain/particle size
$d_{sp/sp}$	vertical distance between the first contact point to the mid-point in bridges neck

e	coefficient of restitution
E	granule elastic modulus
E^*	equivalent Young's modulus
E_a	energy of activation
E_1, E_2	Young's modulus of particles 1 and 2
$F_{boundary}$	bridge force estimated by capillary pressure at first contact point solid/liquid
F_n	normal force
F_n^d	normal damping
F_n^t	tangential damping
F_{gorge}	bridge force estimated by capillary pressure at mid-point (neck)
$F_{pullout}$	maximum cohesion force
F_t	tangential force
$Fcap$	capillary force
G	shear modulus
G^*	equivalent shear modulus
$g(y)$	desired granule size distribution
h	binder layer length
h_a	characteristic length scale of surface asperities
$k(x)$,$k_L(m)$	growth ratio
k_a	measure of granule deformability
k_s	diffusional temperature dependent parameter
K_L, K_U	loading/unloading stiffness

K_c	dimensionless granule compaction rate
k_0,k_1	arbitrary constants
l_0	initial grain mean size at sintering process
L	distance between pressure measures
m	particle mass
m_1,m_2	particles mass
m_{eff}	effective granules mass
M	mass matrix
M_L^{max}	maximum mass consumed by layering
n	distribution of energy impact energies
$n(t)$	number of agglomerates at time t
N_0	number or agglomerates at the beginning
P_{80}	80 % passing size of product stream
$p(x)$	fraction of fine particles of size x_f which act as nuclei
q	independent constant of granule size
r_1,r_2	radii of curvature
r_{c1}	granule mean radius at the end of random coalescence
Q	global stiffness matrix
R	Boltzmann constant
R_{min}	smaller particle radius in simulation
R_1,R_2	spheres radii
Re	Reynolds number
R_{eff}	effective granules radius

r_{neck}	curvature radius at the mid-point of a liquid bridge
R_p	sphere radius
S	half distance between two solid particles
S_n	normal stiffness
$s(m)$	granule surface area
S_{LP}	liquid pore saturation
S_t	tangential stiffness
St_c	capillary Stokes number
St_c^*	critical capillary Stokes number
St_{def}	Stokes deformation number
St_v	viscous Stokes number
St_v^*	critical viscous Stokes number
t	time
T_f	sintering final temperature
u_l	liquid phase velocity
u_o	initial velocity of a colliding granule
v_1	mean volume of granules at granulation beginning
$v(t)$	mean volume of granules at time t
$v_n^{\overline{rel}}$	normal relative velocity
v_r	Rayleigh wave speed
v_t	tangential velocity
$v_t^{\overline{rel}}$	tangential relative velocity

v_v	velocity vector
V_0	fluid velocity
V_{bridge}	bridge volume
W	moisture content
W_0	minimum feed moisture where layering cannot take place
W_A	adhesion work
W_{CL}	liquid cohesion work
W_{CS}	solid cohesion work
We	Weber number
x	half-gap distance between colliding granules
x_s	seed size
x_f	particle/fine size
$y(t)$	granule size
Y_d	granules plastic yield stress
z	temperature dependent parameter

Greek

α	correction for air bubbles presence in layering thick
α_c	centroids relative approach
α_p	particle local deformation
β	normal stiffness
γ_S	solid surface energy or solid surface tension
γ_{SL}	solid-liquid interface energy

γ_{LV}	liquid-vapor equilibrium surface tension
δ	particles overlap
δ_0	residual overlap
δ_n	normal component of particles overlap
δ_t	tangential component of particles overlap
δ''	plastic deformation
ΔP	pressure drop
ΔP_{cap}	capillary suction pressure
Δt	time step
Δt_{crit}	critical time step
Δx_d	reduction on interparticle gap distance
$\Delta\sigma$	pellets cold compression strength gain
ε	void fraction of a packed bed
θ_{LS}	contact angle of a liquid on a solid surface
λ^*	coalescence kernel
λ_0	random coalescence kernel
λ	non-random coalescence kernel
λ_{LS}	liquid spreading coefficient
λ_{SL}	solid spreading coefficient
μ	fluid viscosity
μ_n	friction normal coefficient
ρ	fluid density
ρ_f	apparent density of layered fines

ρ_l	water density
ρ_p	solid density
ρ_r	ratio of apparent densities of the layered mass and seed particles
ρ_s	apparent density of seeds
σ_{st}	granule tensile strength of the bond area
σ_t	granule tension strength
τ	dimensionless compaction time
τ_{bed}	semi-empirical bed tortuosity
υ	Poisson ratio for the material
υ_1, υ_2	Poisson ratio of particles 1 and 2
φ	filling angle
ζ	adjustable parameter for packing method

NOMENCLATURES

CAPEx	Capital Expenditure
DDRS	Double deck roller screen
DEM	Discrete Element Method
DOE	Design of experiments
FRE	Fines removal efficiency
GSE	Global screening efficiency
JKR	Johnson-Kendall-Roberts
LOI	Loss on ignition
LTM	Laboratório de Tecnologia Mineral COPPE/UFRJ
ÖMAG	Österreichische-Alpine Montangesellschaft
OPEx	Operational Expenditure
PSE	Product Screening Efficiency
VOEST	Vereinigte Österreichische Eisen und Stahlwerke

1 INTRODUCTION

The pelletizing process has begun in 1950's in the United States of America. The scenario which motivated it was a demolished Europe at the end of the Second World War. At that time the North American government launched a strong financial help called Marshal Plan. Its purpose was to increase American exports in order to supply financially the economic recovery of Europeans nations – mainly their allies United Kingdom and France.

From this moment on, industrial activity was boosted by the rising steel demand to rebuild all the transport, civil, industrial and market infrastructure. At that time, the development of new technologies made steel production in larger scales possible. The most important fact was the consolidation of LD converter by the Austrian companies VOEST in Linz and ÖAMG in Donawitz (MEYER, 1980). The average steel production growth was 4.2 %/y, and iron ore supply became a challenge due to natural impoverishment as high-grade reserves depleted. Beneficiation and concentration of lower grade iron ore became necessary. Flotation as a concentration method significantly increased its participation in industrial plants. Nevertheless, its success depended on better mineral liberation, where finer grinding is unavoidable. Production of finer fractions rapidly increased, compounding large amounts disposed in piles which became an important environmental issue to iron ore mining companies. Such fine high grade material occupied large extents of lands, increased OPEx costs due to its disposal operations and represented a reject of concentration process since it could not be fed into reduction reactors. Primary iron (sponge or pig iron) is obtained through the action of a reduction gas passing through particles where permeability is the key success factor to process kinetics and efficiency, therefore fines widespread close the voids among particles and do not allow flow percolation (CASTRO, 2006; VELLOSO, 2006).

In order to solve the disposal problem and increase high-grade ore supply/offer, pelletizing processes begun to beneficiate the afore mentioned fine powder into small spheres ranging from 8 to 18 mm in size, called pellets. From then on, such reject become the pellet feed and was turned into a premium raw material feed for reduction reactors. Burnt pellets increased blast furnaces productivity due to their narrower size distribution compared to lump ore and sinter, and reduced process thermal consumption due to adjusted chemical composition by limestone and dolomite additions.

Pelletizing process routes usually present the following stages:

i. Pellet feed reception: it depends fundamentally on plant location and how the raw materials are supplied. Pelletizing plants located next to concentration units usually have homogenizing tanks since they are fed as slurries containing typically 70 % solids in weight, which is the case of Vale´s Vargem Grande and Fábrica plants in Minas Gerais, Brazil. On the other hand, Vale Oman and Vale I to VIII plants, located next to port facilities, receive pellet feed by train and ship respectively and form piles trough windrow or chevron method.

ii. Grinding: iron ore fineness and/or specific surface area are adjusted to the requirements of balling and sintering stages. It is usually carried out wet in tubular ball mills, although in some locations, due to water unavailable, it is carried out dry, which is the case of the Vale Oman plant. In the latter case, dust control is essential since its generation is an inherent outcome of this process. Both unit operations can be used either in open or closed circuits, being the second one more indicated to achieve a finer product.

iii. Filtering: if grinding is wet, filtering is the downstream stage. Its only objective is obtaining cake moisture suitable for balling and it is usually done in rotating vacuum filters (discs, tumble or ceramic) or pressure filters. If the moisture content is low, water addition has to be done in mixers or in balling drums and discs in order to promote green pellets formation. In contrast to that, if filtration presents low efficiency, producing a moister cake, the stages downstream will be unavoidably penalized (higher raw materials consumptions such as bentonite in balling; oil or gas in sintering).

iv. Roller Pressing: this is the most recent advance in terms of technology used in pelletizing process route. Initially developed for cement production, it has been applied for hard rock comminution since the mid-1990s (THOMPSEN *et al.*, 1996). With the aim of increasing specific surface area, it can be placed upstream or downstream grinding mills. If positioned upstream, roller presses generate micro cracks which facilitate grinding in mills. When placed downstream from grinding and filtering, pellet feed with lower specific surface area is filtered and lower moisture contents in cake can be easily achieved. In such route, filter cake produced must be rigidly controlled. Moister material is

harmful to high pressure grinding rolls because it not only reduces comminution efficiency but accelerates rolls body and studs wear (ALVES, 2012).

v. Mixing: in this stage, additives such as limestone and dolomite are added for chemical control: binary, CaO/SiO_2 or quaternary basicity – $CaO+MgO/SiO_2+Al_2O_3$ determines the kind of produced pellet: if acid, basic or self-fluxed. Binder is also added at this stage. Bentonite clays are widely used, activated or not by caustic soda (KAPUR *et al.*, 1972; KAWATRA *et al.*, 2001; FORSMO *et al.*, 2006). Their high capacity of water absorption and adhesion forces promotes the agglomeration of fine powder making green pellets amenable to handling until they reach the induration stage. On the downside, they cause pellets impoverishment in iron due to their high silica content. Organic binders are also commonly used, combined or not to bentonite, mainly for direct reduction pellets when lower silica content is essential (EISELE *et al.*, 2003). Calcium oxide is a weaker binder rarely applied. Anthracite coal, petroleum coke or coke breeze are solid fuels added to improve pellets burning (COSTA, 2008; FONSECA *et al.*, 2009). Theses raw materials are then mixed in horizontal (Loedge, Pekay) or vertical (Simpson, Eirich) mixers.

vi. Balling: sector where green pellets are made in rotary drums or discs and, more seldom, cones. Capillary, adhesive and mechanical forces are responsible for production of agglomerates that will feed travelling grates and rotary kilns. It is "the heart" of a pelletizing plant. It is the object of study in this text and it is going to be discussed in greater detail.

vii. Sintering/firing: the mechanical strength of green pellets is not high enough to allow them to be transported by trucks, trains or ship vessels. In addition to that, they cannot support the weight of coke, sinter and even the weight of their own top layers inside reduction reactors. In order to increase their strength, green pellets are submitted to heat treatment consisting of drying, preheating, heating up to 1350 °C and cooling in traveling grates, rotary kiln or shaft furnace facilities. This process is called induration.

viii. Screening: in the last stage, indurated pellets are classified on vibrating screens to remove material finer than 5 mm, generated due to process inefficiency. Part

of production, around 20~25%, is recirculated to compose the hearth layer in the induration furnace.

Nowadays, iron ore companies have just faced the end of China effect which took place in first decade of the 21th century and created a greater demand than the available supply. Prices of commodities were then boosted to record values never experienced before. Each ton of iron ore fines containing 62 % Fe was sold by an astounding 180 US$/t during the first semester of 2011. Since then, as steel demand has become weaker and new plants have started operation, stimulated by this environment of increased offer, the commodity quotation have fallen to the minimum baseline values, around 40-45 US$/t (Figure 1.1) during the first quarter of 2016, i.e., a 75 % depreciation in price. Mining players' scenario turned upside down and companies had to quickly modify the strategy model. New projects were interrupted, marginal operations were forced out of the market as they could not compete with larger scale and more efficient operations, and the drive exclusively for higher throughputs was replaced by lower breakeven costs, higher productivity and more attractive quality products as key indicators to a successful business (GILROY, 2015).

Figure 1.1. Iron ore (62 % Fe) fines prices (Source: indexmundi.com/commodities).

When it comes to pelletizing, it is remarkable how important fuel costs are. In Brazilian pelletizing plants, natural gas supply for traveling grate burners represents about 37 % of the total costs of production. In addition, the power consumption of process fans is around 1.7 % of the total costs of production (Figure 1.2). In order to

achieve the afore mentioned global strategy goals, attention to the balling sector becomes of key importance.

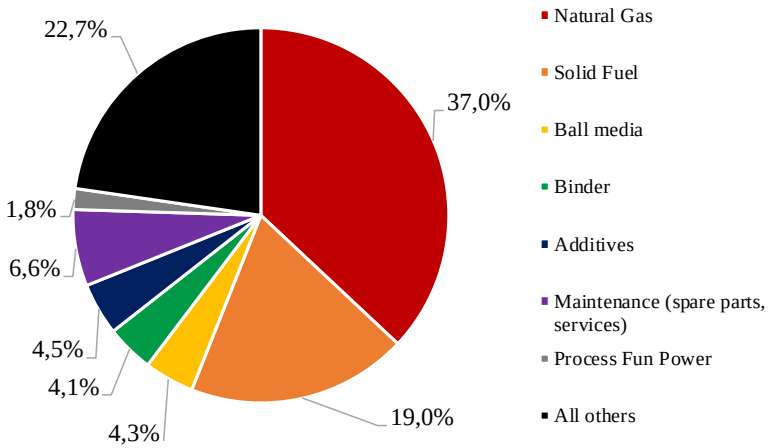

Figure 1.2. Brazilian pelletizing costs shares.

The success of high quality burnt pellets production and lower specific fuel and electrical energy consumptions in travelling grate furnaces depends fundamentally on heat exchanges efficiency among bed particles and fluid percolation flow. Better permeable conditions of packed bed are reached when particles size distribution are narrower. MCGEARY *apud* STANDINSH (1988) and STANDISH *apud* YU and STANDISH (1988) measured how voidage fraction vary in a binary (Figure 1.3) and ternary system of spheres (Figure 1.4). As ratio of smaller and larger particles increases and their proportion equalize, the bed become more packed. Such less porous conditions are very harmful in metallurgical process such as sintering of pellets or reduction in blast furnaces because they reduce gas phases percolation flow among particles.

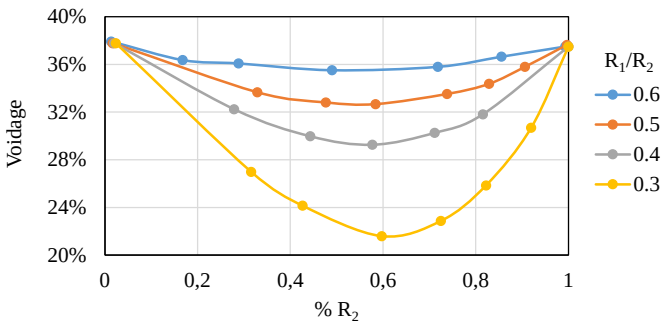

Figure 1.3. Measured voidage fraction for a binary system of spheres (Adapted from YU and STANDISH, 1988).

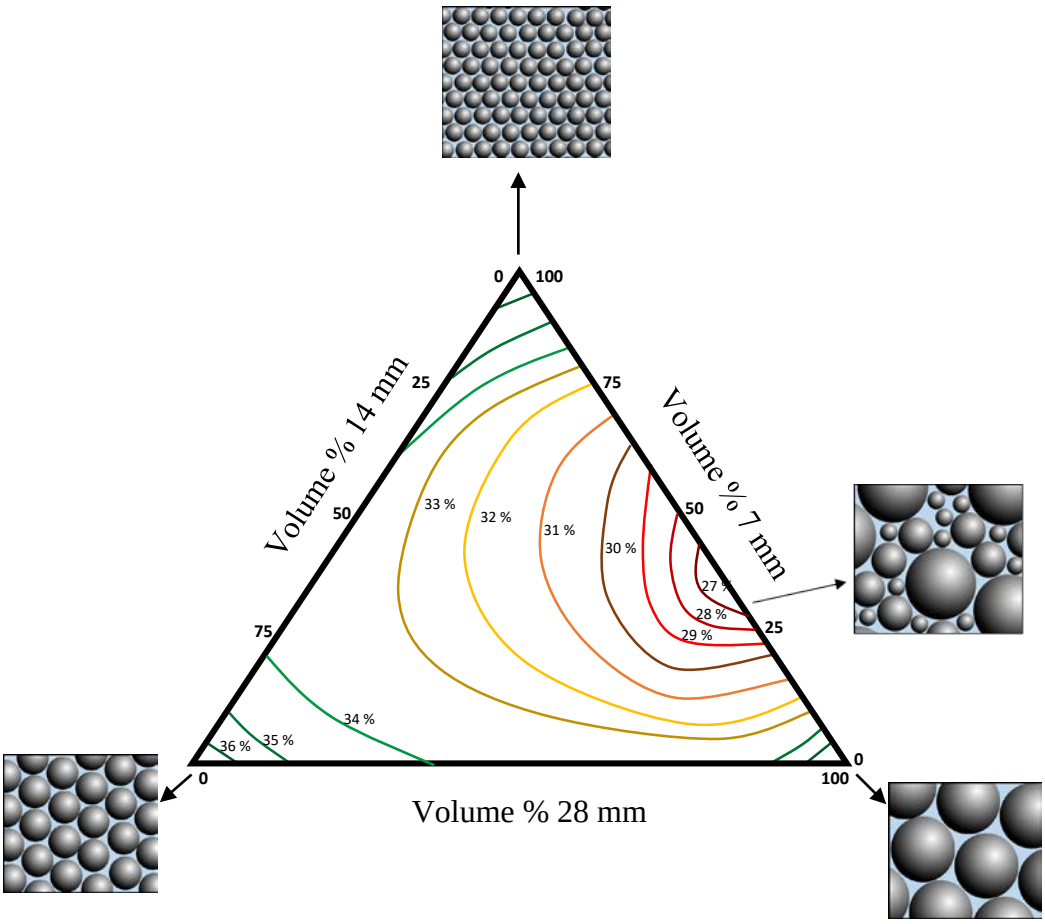

Figure 1.4. Measured voidage fraction for a ternary system of spheres (Adapted from YU and STANDISH, 1988).

ERGUN (1952) mathematically described how gases fluxes depend on voidage fraction in packed bed through the unification of Blake-Kozeny pressure drop in laminar regime due to viscous attrition and Burke-Plummer contribution where pressure drop is associated to convective inertial mechanisms in turbulent regime, given by

$$\frac{\Delta P}{L} = \frac{150\mu V_0 (1-\varepsilon)^2}{\varepsilon^3 d_p^2 \phi^2} + \frac{1{,}75(1-\varepsilon)\rho V_0^{\,2}}{\varepsilon^3 \phi d_p} \qquad (1.1)$$

Where,

μ is the gas percolating phase viscosity;

ε is porosity;

ϕ is particles roundness;

d_p is mean particles diameter;

V_0 is the gas fluid velocity.

It establishes a relationship between the bed porosity, fluid interstitial velocity and the pressure drop. Figure 1.5 shows that modest reductions in bed porosity cause significant increases in pressure drop, which is, itself directly related to the required power in the process fans and travelling grate fuels consumption.

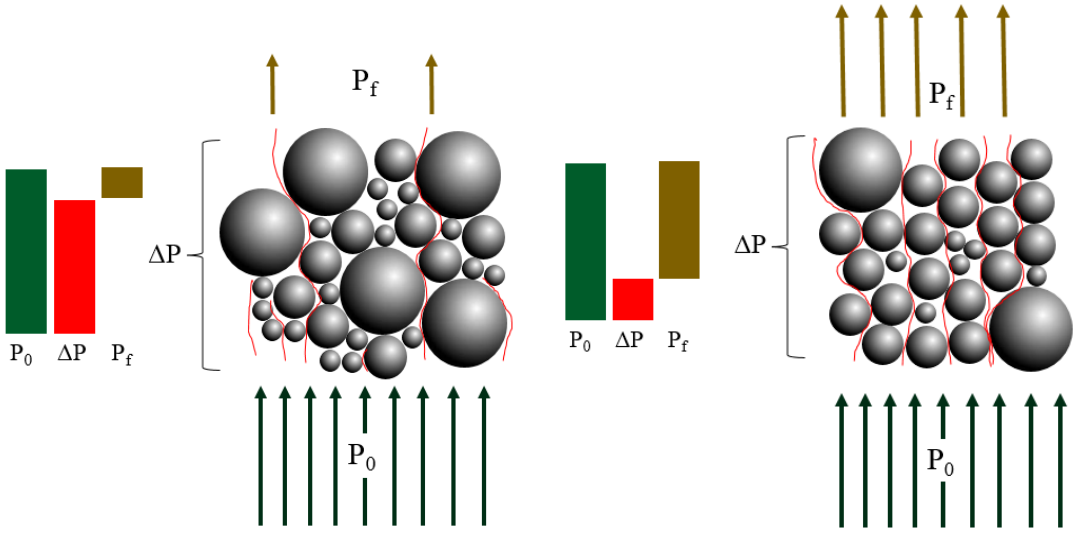

Figure 1.5. Pressure drop through a packed bed.

The permeability of a green bed of pellets (Figure 1.6) is directly influenced by the operations of balling in discs/drums and their classification on roller screens. As such, balling yield importance and influence on pellets induration process is, so, worldwide recognized due to beds permeability formation. Nevertheless, studies that attempt to correlate sintering process and balling yield are quite rare.

Figure 1.6. Snapshot of pellets bed in straight travelling grate.

Recently, CAVALCANTE *et al*. (2015a) analyzed the effect of bed permeability on fuel and electric energy consumption costs and also estimated its impact on productivity of an industrial plant based on a model of void fraction extracted by CAVALCANTE *et al*. (2015b). In such model, they correlated operational control response parameters collected by optical images analyzers and demonstrated that maximizing pellets bed permeability through optimal control of balling discs rotation speed, variable costs could be reduced in approximately 5.5 %.

BORIM and FREITAS (2009) detailed the gains on size dispersion optimization by automation of balling disc control. If pellets kinetics is affected by some changeable variable such as moisture, mean particle size or specific surface area, the camera analyzer can capture the change in pellet size and modify disc speed in order to maintain a constant pellet mean diameter. The effectiveness of such advanced control is notable if the camera is properly used (Figure 1.7). Usually, the camera is placed at the discharge of the discs (1) but it can also be located at the production belt at roller screen downstream (2). In the second case, any operational change or failure can introduce harmful errors to system control. For example, if there is an excessive opening gap between rolls placed at the bottom of the roller screen, larger pellets which are supposed to be part of oversize can be misguided to the on-size stream and have their image analyzed. The camera then indicates to the control process that the mean diameter size captured increased. As a result, disc rotational speed is reduced in order to reduce the size of pellets produced, i.e., a gap distance fail on roller screen misconduct a control action to discs which can increase the amount of fines and result in a wider dispersion of pellet sizes. As such, installation of devices for size analysis after the roller screen is only recommended if there is not enough room at the discharge of either discs or drums.

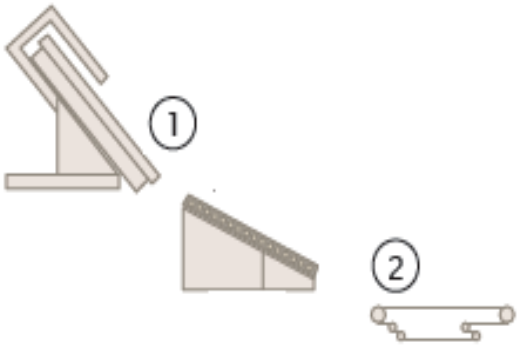

(a)

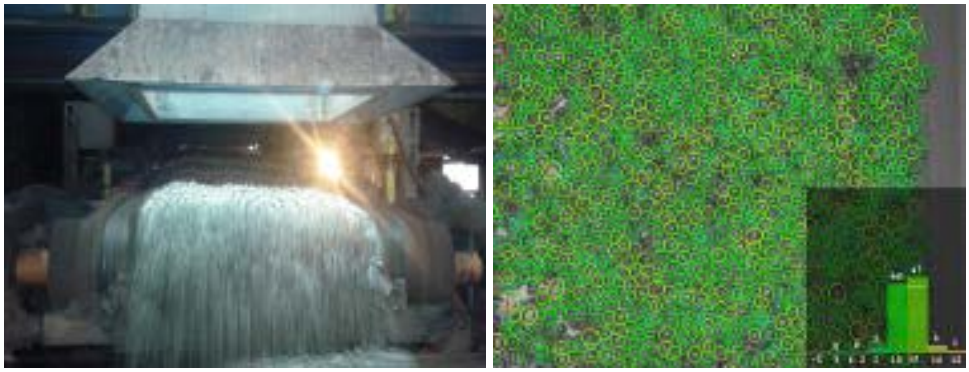

(b) (c)

Figure 1.7. (a) Installation positions for size analysis device: 1- disc discharge; 2- production conveyor at roller screen downstream; (b) camera device in operation; (c) image capture and processing

However, it is evident that the continuous search for beds of pellets more permeable through the optimization of the balling process has been done in a partial way. Throughout all these decades, works have focused exclusively on the study of variables that influence the formation of green pellets, whether on discs or drums. The handling and screening of this product that have great relevance for bed formation have been either only little studied or neglected by researchers.

From a population mass balance point of view, the balling process can be viewed in a way that is analogous to closed-circuit grinding: particles birth and death rates are also defined but in the opposite sense for each of these processes. Their success and efficiency is due to the sum of an excellent operation of agglomeration or fragmentation

equipment (mills, roller presses, crushers) and classifying devices (screens, hydrocyclones). However, while in grinding process circuits both equipment are equally and extensively studied (NAGESWARARAO, 1978; LYNCH, 1979; NAGESWARARAO, 1995), the roller screens, a separator that is exclusively used in green pellets classification, continue in the shade of the light of the knowledge. Green pellets handling circuit (conveyors belts, transfers chutes and roller screens) are still today an unexplored area responsible for part of losses in balling and in great need for optimization.

Nevertheless, analyses of balling work performance may be much tougher than grinding/classification in some aspects. Balling circuits usually do not have any sampling apparatus and manual samples done are hardly representative because green pellets easily degrade when handled due its low strength and moisty properties.

Numerical simulation of granular materials is an important tool both for advancing the fundamental understanding of many natural phenomena in material science and geophysics, and for the design, control and optimization of systems for processing, manufacturing, storage and transportation of granular materials, e.g., grains, corn, pharmaceuticals pills, pellets, soil and minerals. In the mineral processing industry, experiments and in situ measurements are many times prohibitive for practical and economic reasons, and in these cases, modeling and simulation play an essential role in reaching a deeper understanding of the process, making radical improvements and the search of completely innovative solutions possible (WANG *et al.*, 2015). SASTRY (2008) suggested that advances on balling process will forcefully pass through numerical simulations.

2 SCOPE OF WORK AND OBJETIVES

Since its start-up in 2009, Vale's Vargem Grande pelletizing unit, located in Nova Lima (Minas Gerais, Brazil) faces an important challenge. Pellet feed is coarser than the design criteria and its loss of ignition has also increased due mining mineralogical variety (Table 2.I). Such physical and physicochemical properties of the product are harmful for sintering in travelling grate.

Table 2.I. Summary of designed and actual ground concentrate parameter for Vargem Grande pelletizing (Vargem Grande Final Technical Report)

Parameter	Designed	Actual
LOI (loss of ignition) (%)	1.10	2-2.5
<0.045 (%)	90	78

BAKER *et al.* (1973) and LEONEL (2011) detailed the effect of LOI content on sintering heat process of pellets.

MAYERHOFER (2012) highlighted how the relationship between specific surface area and P_{80} is altered when iron ores of distinct physicochemical and mineralogy characteristics are ground under the same conditions. As LOI of iron ores increases, the gain in specific surface area increases linearly but reduction in particle size does not increases significantly, following an exponential decay.

SOUZA *et al.* (2014) presented how the expected operational conditions had to be changed in each phase of the production when higher LOI iron fines was processed. According to the authors, pellets produced with higher LOI concentrates are more plastic and moist. When they are fed into the traveling grate, the occurrence of the spalling phenomena, partial degradation of pellets with generation of fines, is more likely to happen in down draught drying zone. STATNIKOV *et al. apud* BATTERHAM (1986) presented how pellets strength is based upon Arrhenius relation, e.g., a time-temperature dependence process (Equation 2.1). Moist pellets and lower void fraction reduce heat exchange rates, cause temperature drop and, as a result, produce lower strength burnt pellets which generate more fines (< 5mm). It can be

noted in Equation 2.1 that the cold compression strength, $\Delta\sigma$, of pellets produced in Vargem Grande is inversely proportional to pellet feed grains mean size, l_0:

$$\Delta\sigma = \frac{\Delta l}{l_0} = k_S t^z \exp\left(\frac{-E_a}{RT_f}\right) \quad (2.1)$$

Where: $\Delta\sigma$ is the increase of pellets resistance strength

Δl is the mean linear grain growth

l_0 is the gran initial mean size

k_s is the diffusional temperature dependent parameter

t is the sintering treatment time

z is a temperature dependent parameter

Ea is the energy of activation of the sintering reaction

R is Boltzman constant

T_f is sintering final temperature

In order to produce world class pellets that are able to resist transoceanic transport, and since the actual pellet feed processed is not as fine as it was designed (Table 2.I), temperatures at the end of burn zone of traveling grate must be higher or the thermal cycle must last more, although this implies in productivity losses. In addition to the aforementioned mineralogical issue, the geographic factor plays an important role. The handling operations of Vargem Grande (Figure 2.1) pellets is more severe if compared to products made in Vitoria (ES) where the pelletizing plants are located inside the port complex. Some additional stages of reclaiming, conveyors transferring and wagon discharging take place since railroad transport is part of the route for overcome the 500 km distance between Vargem Grande and Tubarão port in Vitoria (ES). TAVARES *et al.* (2015a, 2015b) analyzed in great detail the mechanical degradation (size distribution alterations and fines generation) of indurated pellets during handling, starting from pelletizing plants until final domestic or overseas clients.

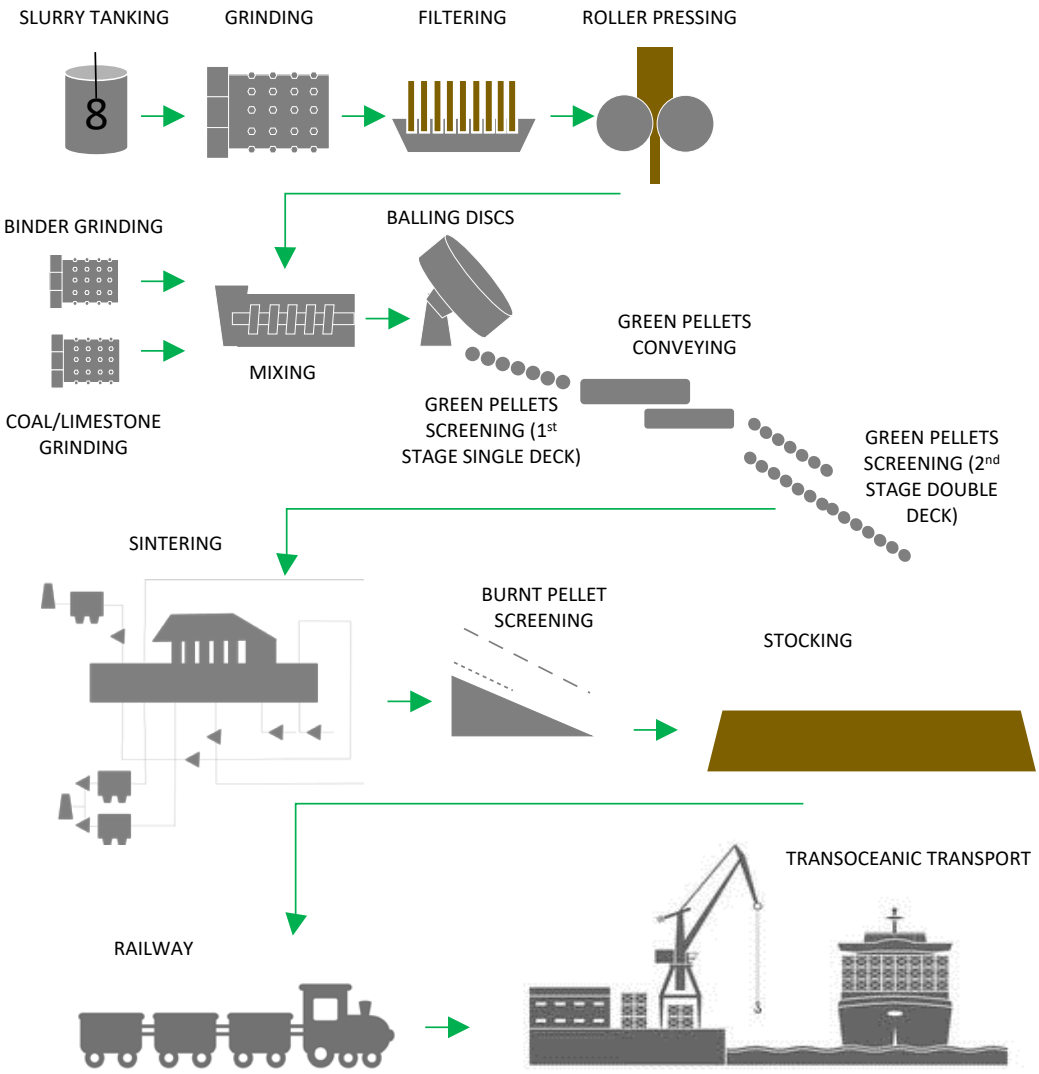

Figure 2.1. Simplified Vargem Grande production flowsheet.

Nevertheless, if well burnt, pellets produced from high LOI ground concentrates present better reducibility (ISO 7215) as shown in Table 2.II.

Table 2.II. LOI of raw material and pellets reducibility for selected plants from Vale

Plants	Raw material	LOI (%)	Reducibility (%)
Plants I-VIII (Vitoria/ES)	PFFF08, PFFE08	1.00	AF08 – 69.00
Vargem Grande (Nova Lima/MG)	PFFF40	2.80	AF40 – 75.00

Source: Vale's internal specifications EPS 000668 and sales internal report 2015

Increase of productivity is always a strategic driver pursued by any pelletizing unit. At Vargem Plant, such task unavoidably passes through the limitation (1490 t/h) of the conveyor which feeds the balling stage. Its feed consists of the sum of the fresh feed coming from the previous stage (mixers), and the return, given by the oversize green pellets (>16 mm) and the fines (<8 mm) declassified on roller screens. If, by any reason, the formation of green balls is not performed successfully, higher return rates will represent a greater proportion of the feed to the conveyor, thus limiting its availability to receive fresh feed. Still according to the Vargem Final Technical Report, the return rate should be, ideally, around 20 %, but actual rates are around 29 % (Figure 2.2). Each 0.5 % of return rate represents approximately 280 t/day. This issue becomes more challenging because plant the budgeted yearly plant production demand is continuously increasing (Figure 2.3).

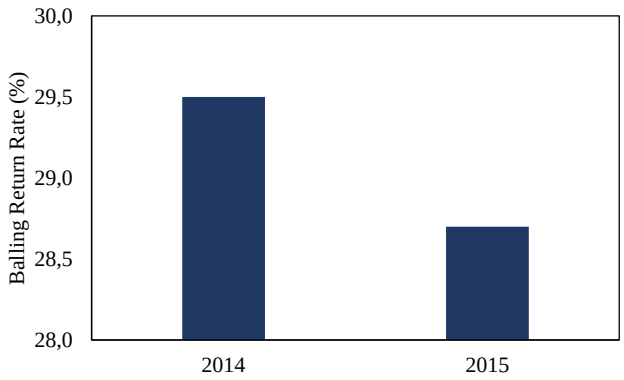

Figure 2.2. Return rates practiced in the balling circuit at Vargem Grande in recent years

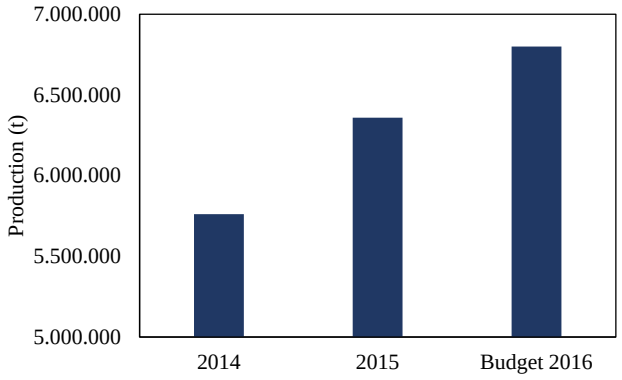

Figure 2.3. Vargem Grande yearly production.

In order to have a holistic view to maximize balling productivity (reduce return rates), have a better understanding on the formation of pellet beds and reduce fines in final product delivered at the clients, a proper assessment of the performance of separation of pellets in roller screens is necessary. Such screen is very particular, being almost exclusively employed throughout industry in separation of green pellets. The control parameters of these screens are the diameters of the rolls, the number of rolls, their speed, the screen angle and the feed rate.

The understanding of their effect is still very limited by both users and manufacturers, mainly due to:

i. Difficulties to analyze an inherently unstable process. Although optical measurement systems have presented good results in recent years by supplying information to advanced process controls, such analysis by scanning is done only to objects placed on the top of the bed. They also have limitations of resolution that hardly identify objects smaller than approximately 8 mm (OptProcess Manual, 2009) and are totally unable to distinguish pellets smaller than 5 mm.

ii. Circuits used for transporting pellets are very compact in order to reduce green pellets drops heights and distances in handling. As a result, belts used in each balling line do not have the necessary length to allow installing dynamic scales for continuously weighing the charge;

iii. Even when room is available, CAPEx costs required to install such dynamic scales are significant and seldom have short or intermediate payback times;

iv. Pelletizing units usually have more than five production lines, equipped with drums, discs or both, which share conveyor belts to transport the green pellets. As such, the impact of small changes on any control variable in a production line is difficult and complex to evaluate and determine the extent of its influence, unless a huge effort is made and the given variable is changed simultaneously in all lines at same time. This procedure is usually inefficient because many noisy variables can misguide conclusions.

v. Pellet feed physical properties have a significant effect on balling yield and quality of green pellets. Its gradual impoverishment and mineralogical changes

are more often challenges which many plants have been facing nowadays. As such, it is imperative that new arrangements of the process, which may not be of common usage in the past, be tested;

vi. Productivity increases inversely to bed permeability, since indurating furnaces operate at faster speeds or with more vertical layers requiring even more work from the fans. Higher bed permeability must then be continuously pursued in order to optimize process conditions;

vii. Green pellets sampling, handling and sieve screening in the laboratory are difficult, given their low strength, their amenability to easily lose weight and to have their shape altered if improperly handled;

viii. Simulation tools such as the discrete element method (DEM) have been increasingly used to analyze particle motion (CLEARY *et al.*, 1998; CLEARY, 2001), collision energies and amenability to produce wear in machines (CLEARY, 2000), mainly in mineral processing (WEERASEKARA *et al.*, 2013). Limited research and application has been dedicated to understand balling granulation (LIAN *et al.*, 1998; MISHRA *et al.*, 2002; WANG *et al.*, 2015).

Therefore, any physical modeling of balling is quite challenging. In order to reach optimal balling yield (e.g. controlled return rates) and permeability of indurating furnace, a proper mathematical model becomes necessary.

To achieve this objective, the plan of the present work is described as:

i. Characterize green pellets shape, strength, resilience and size distribution: obtain pellet feed mixed with additives and binder from Vargem Grande plant, determine its chemical, physical and physicochemical characteristics and reproduce pellets similar to the ones made in industrial scale;

ii. Choose the appropriate contact model and calibrate contact parameters (rolling friction, restitution and static friction coefficients) of green pellets under the domain of conditions relevant to simulate roller screens: conduct dynamic tests on devices and reproduce their motion on EDEM® platform with reliability, validate the parameters with real cases by comparisons to available industrial

data; run exploratory simulations in order to verify if results obtained may reproduce similar real situations;

iii. Simulate classification on roller screens at the discharges of discs at Vale´s Vargem Grande pelletizing plant using the Discrete Element Method (DEM). Analyze the effects of rolls diameter and speed, pellets feed rate, undersize gap lengths and screens inclination on balling yield (both qualitatively and quantitatively);

iv. Optimize such analyzed parameters in order to apply to the industrial unit;

v. Propose new designs for roller screens;

vi. Simulate using DEM different double deck (also called feeder) roller screen configurations (partial double deck and segregator upper deck) at the entrance of the indurating travelling grate;

In order to initiate the characterization of the green pellets, the understand of the process and the principles involving the formation of iron ore fines agglomerates must be approached.

3 LITERATURE REVIEW

Balling is considered the heart of the pelletizing process since it determines the pace of production and plays an important role on bed formation and permeability. Due to its position at the boundary between mineral processing (grinding, filtering, regrinding and mixing) and high-temperature metallurgical processing, it acts as an interface, being strongly governed and affected by the response of the previous stages but also carrying great influence to downstream operations, namely: pellets burning in Lurgi travelling grate, rotary or shaft kiln.

3.1 Initial studies on drums

In the 1950s, DOR *et al*. *apud* WELLSTEAD *et al*. (1978) were concerned about the lack of understanding of balling operations, which was considered more an art than a science since the beginning of pelletizing. Effective control strategies had not yet been put in practice and most installations were overdesigned to compensate for such limitations. Drums, which were the only type of balling equipment in operation until 1956, present some inherent surging phenomena (Figure 3.1) at their production discharge which are harmful to indurating machine feed rate and pellets quality. Such non-linear oscillating response (similar to a sine wave trend) is result of drums and screens constitutive relations in a closed loop circuit. The result is that fluctuations on production and recycle load rates usually drift 20 % around their own average. According to MEYER (1980), drums are usually at angles from 6 to 10 ° and have lengths ranging from 6 to 10 m. Their rotational speed varies from 8 to 14 rpm, with diameters from 1.8 to 3.66 m. As a result, their production rates vary from 20 up to 170 t/h and their recycle loads range from 200 to 500 %, being strongly dependent not only on machine dimensions but also on pellets consolidation. Operational conditions such as moisture content, binder addition and pellet feed fineness have significant influence on pellets growth rate and, as consequence, on production and recycle load.

The main purpose of the approach proposed by WELLSTEAD *et al*. (1978) was to evaluate by digital simulation and control-theory analysis the response of four different balling circuit flows which could limit surging, making it less harmful to induration machine yield downstream. In conventional circuits, the control by water sprays demonstrated to be useful although harmful to pellets quality (and also for sintering fuel

consumption). The following outcomes were observed using different operation strategies in circuit redesign:

- tandem operation (crossed recycled loads between different drums) (Figure 3.2a) was responsible for reaching lower surging amplitudes in one drum but increased in the second;
- recycle load hold-up (use of bin to retain the excess/lack of recycled seeds) smoothly reduced the oscillatory output (Figure 3.2b), and,
- partial feedback technique was considered to be the most effective method in simulations (Figure 3.2c). Since surging amplitude is 20 % of its mean value, decreasing its amount means also reduction of oscillatory amplitudes.

Much later, SILVA *et al*. (2013) confirmed the benefits of partial feedback. More recently, SASTRY (2008) proposed balling drums circuits' controls. Further information such as influence of feed rate, roller screen gaps and different points of water sprays additions are discussed as well.

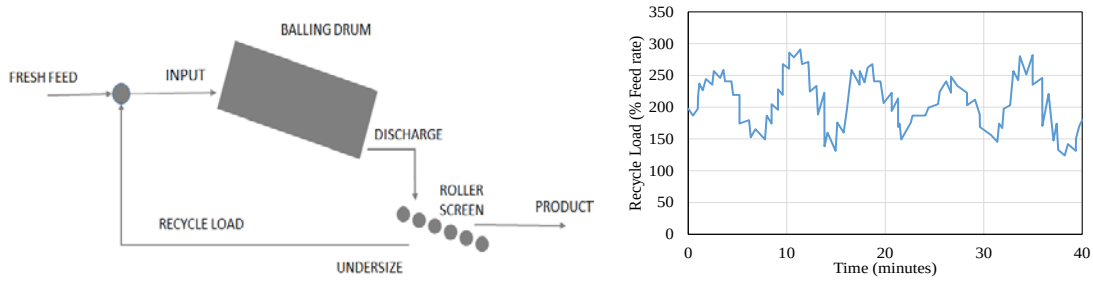

Figure 3.1. Drum balling circuit scheme and surging phenomena response (Adapted from WELLSTEAD *et al.*, 1978).

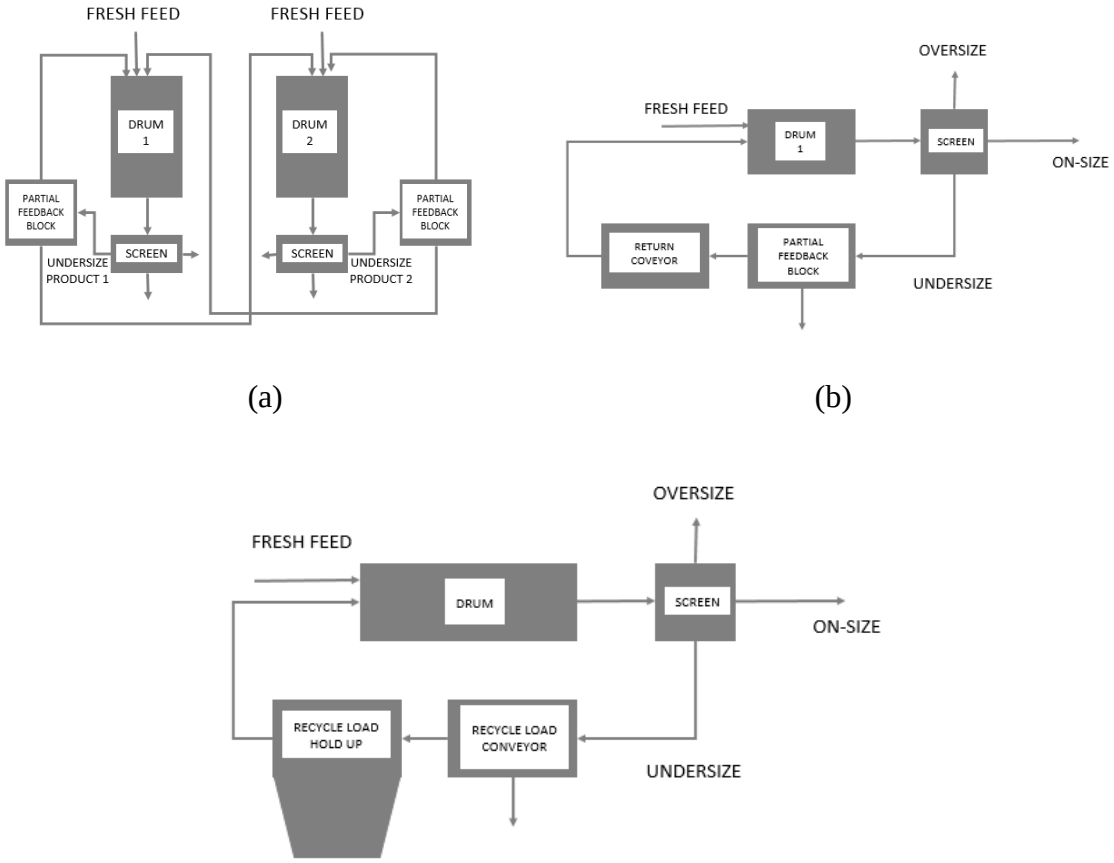

Figure 3.2. Schematic circuits tested (a) cross tandem controller; (b) partial feedback; and (c) recycled hold up device. (Adapted from WELLSTEAD *et al.*, 1978)

From that time to nowadays some authors have been investigating mechanisms of agglomerate growth, kinetics and controlled parameters which most directly impact and explain balling performance in order to maximize process yield, i.e., reduce return and recycle rates (HALEY *et al.*, 1962; BALL *et al.*, 1973; WELLSTEAD *et al.*, 1978).

3.2 Agglomerate formation

SASTRY and FUERSTENAU (1973) explain that the mechanisms responsible for agglomeration are result of the combination between natural and induced forces. Electrostatic forces are result of iron ore ground fines which exhibit charge on their surfaces due to the breakage of metallic bonds and exhibit low bonding strength forces that take place during granulation. Van der Waals forces are induced and instantaneous interactions between oxide charges among themselves. Magnetic forces are associated

to the paramagnetic nature of the material. Physical forces such as capillarity between liquid phase and solids, particle interlocking and adhesion forces promoted by viscous binders, play an important role due to their higher magnitude (Figure 3.3). According to RUMPF (1962) and RHODES (1998), such frictional and liquid/solid bridges are the only significant forces in wet system for particles with sizes larger than 10 μm. Induced forces are basically the mechanical movement promoted by rotation of balling devices.

In the aforementioned study, the authors clearly identified the mechanisms of agglomerate growth by applying tracer techniques. Two calcites, one from Texas and the second from New Jersey, presenting approximately the same kinetics behavior, could be identified on agglomerates when submitted to ultraviolet light. IVESON *et al*. (2001) discussed about each mechanism in greater detail.

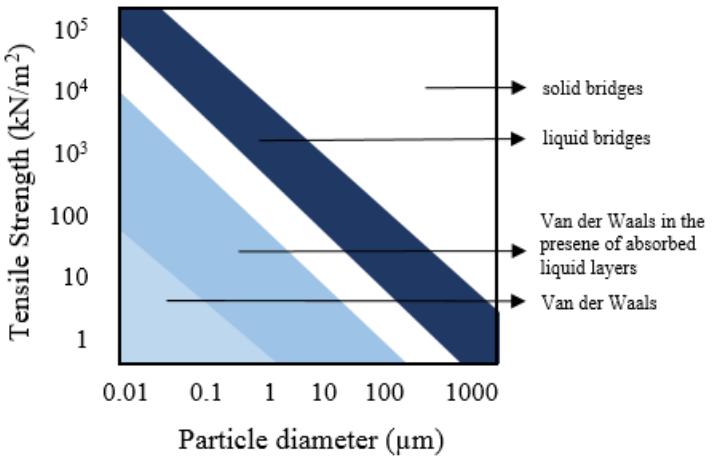

Figure 3.3. Theoretical tensile strength of agglomerates with different bonding mechanisms (Adapted from HELE, 2006).

3.2.1 Nucleation

According to IVESON *et al*. (2001), nucleation is the first step to produce granules. It happens when the powder is in contact with water. Nucleation takes place within the first meters of the drum entrance, as soon as fresh powder and recycled seeds start to roll. Seeds are the first stable agglomerates, ranging from 1 to 3 mm in size (KAWATRA, 2008). In discs, nucleation takes place just nearby the feed region. For such reason, moisture content is the most important parameter in nucleation, being water sprays strategic positioned over the mentioned areas in balling devices.

Binder added also plays an important role on nucleation yield since it strongly affects powder wettability by modifying its hydrophilic behavior. Young-Dupre approach (SCHADER, 1995) defined the thermodynamic relationship between solid and liquid phases. But first of all, it is fundamental to define adhesive and cohesive forces. The first occurs between different materials, e.g., liquid (water) and solid (ore grains); the latter takes place inside the liquid and is responsible to keep the integrity of a drop avoiding its spread over the solid surface (Figure 3.4).

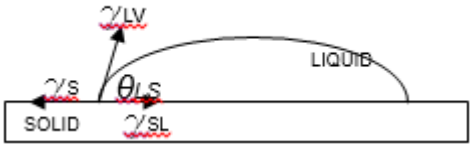

Figure 3.4. Solid wettability.

Where γ_{LV} is the liquid-vapour equilibrium surface tension, γ_S is the solid surface tension, γ_{SL} is the solid-liquid surface tension and θ_{LS} is resultant contact angle of the liquid on the solid surface.

At equilibrium, it reaches the point of minimum energy:

$$\gamma_S = \gamma_{SL} + \gamma_{LV} \cdot (\cos\theta_{LS}) \tag{3.1}$$

$$\gamma_{LV} \cdot \cos\theta_{LS} = \gamma_S - \gamma_{SL} \tag{3.2}$$

The adhesion work, W_A, made on surface as the drop interface moves forward is done:

$$W_A = \gamma_S + \gamma_{LV} - \gamma_{SL} \tag{3.3}$$

Combining Equations 3.2 and 3.3, gives:

$$W_A = \gamma_{LV} \cdot (\cos\theta_{LS} + 1) \tag{3.4}$$

Works of cohesion for liquid, W_{CL}, and solid, W_{CS}, can be estimated under extreme idealized conditions of perfect wettability, that is, θ_{LS}=0 °.

$$W_{CL} = 2\gamma_{LV} \tag{3.5}$$

$$W_{CS} = 2\gamma_{S} \tag{3.6}$$

Young-Dupre equation is valid for all real cases, i.e., θ_{LS}>0 °. If contact angles between solids and water range from 1 ° to 89 °, the liquid phase spread all over the solid which presents a hydrophilic surface, i.e., it is easier to the liquid roll over a different matter than over itself. When contact angles vary between 90 ° e 180 °, cohesion forces prevail over adhesion ones and solid surface exhibit a hydrophobic wettability characteristic. IVESON *et al*. (2001) refers, as a way to explain such cases, to the spreading coefficients, λ_{LS} and λ_{SL}, being them the difference between adhesion and cohesion forces. Such coefficients indicate if spreading is thermodynamic favorable:

$$\lambda_{LS} = W_A - W_{CL} \tag{3.7}$$

$$\lambda_{SL} = W_A - W_{CS} \tag{3.8}$$

If λ_{SL} is positive, the difference between adhesion to solid cohesion is positive, so the particles bond to liquid phase at the contact points between such two phases without a liquid film formation once cohesion work is stronger. As a result, weak and porous granules are made. If λ_{LS} is positive, a film of liquid phase spontaneously surrounds particles, forming dense and strong granules.

Nucleation is driven by capillarity phenomena. After wetting, interlocking particle forces appear between liquid binder and solids surfaces (Figure 3.5 and 3.6).

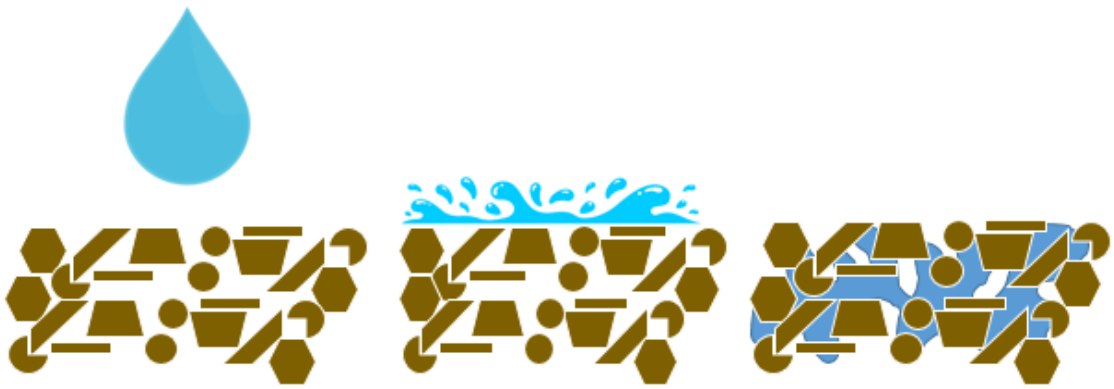

Figure 3.5. Nucleation (Adapted from IVESON *et al.*, 2001).

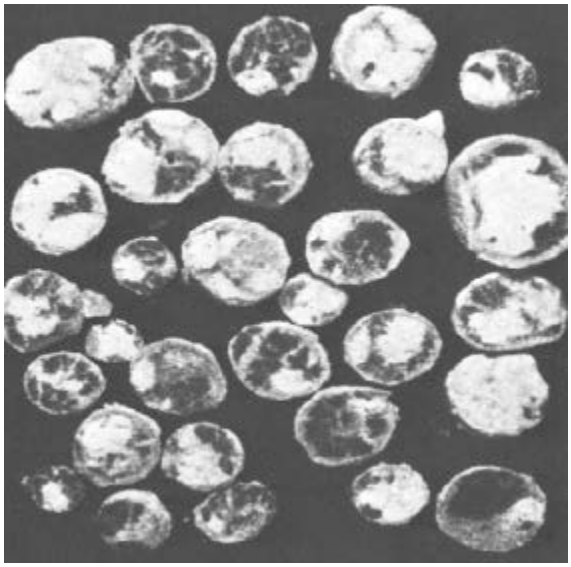

Figure 3.6. Granules formation of New Jersey (white) and Texas (black) calcites, at nucleation stage (SASTRY and FUERSTENAU, 1973 – Authorized reproduction).

As powder fines are moisten by adhesion of viscous binder spreading and tumbling forces move particles inside balling devices, granules migrate from pendular to droplet phase passing by funicular and capillary intermediary stages (Figure 3.7). Bridges between particles thermodynamically reduce free surface energy and establish bonds at points of contact. As agglomerates are agitated, particles rearrange themselves through the liquid film, pulling air out and becoming denser. At the end, viscous binder is finally squeezed out to granules surfaces.

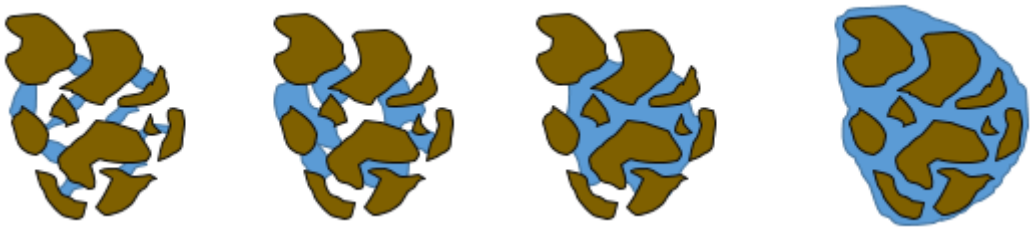

Figure 3.7. Structure evolution of porous agglomerates in balling (Adapted from KAMINSKA and DANKO, 2011).

The combination of interfacial solid-liquid tension due to the force of adhesion and suction pressure caused by the curvature of liquid interface result on the pendular liquid bridge static strength (IVESON *et al.*, 2001) as it can be seen in Figure 3.8. Capillary suction pressure, ΔP_{cap}, is defined by Laplace-Young equation as:

$$\Delta P_{cap} = 2\gamma_{LV}\left(\frac{1}{r_1} - \frac{1}{r_2}\right) \tag{3.9}$$

Where r_1 and r_2 are the main radii of curvature of the bridge profile formed between two particles.

For an inviscid liquid, the critical separation distance, S_C, for rupture is proportional to the cubic root of the liquid volume, V_{bridge}:

$$S_C = (1 + 0.5\theta_{LS})V_{bridge}^{1/3} \tag{3.10}$$

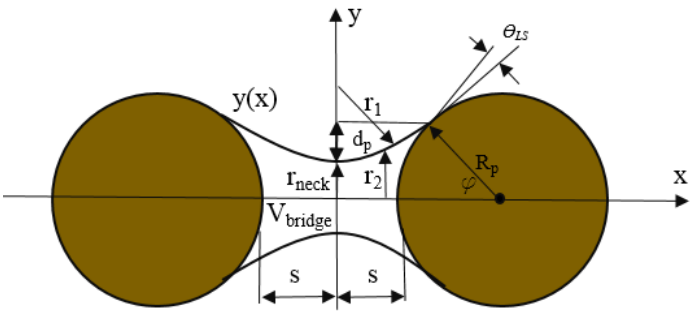

Figure 3.8. Schematic representation of a liquid bridge (Adapted from HELE, 2006).

There is no unanimous opinion about the position where capillary pressure terms should be evaluated. The bridge structure does not present a constant mean surface curvature (IVESON *et al.*, 2001) and approximations to toroids and hyperbolic arcs are used to describe the bonding volume. HOTTA *et al.* (1974) present results using such approximation by the boundary method (Equation 3.11), which takes into account the pressure at the first contact point between liquid and one of the spheres. LIAN *et al.* (1993) considered the mid-point at the neck of the bridge as reference to determine both surface tension and capillary pressure in the gorge method (Equation 3.11). IVESON *et al.* (2001) and HELE (2006) argues that the gorge method presented more accurate estimates for the resultant force.

$$F_{boundary} = \pi \cdot \Delta P_{cap} \cdot R_p^2 \cdot \sin^2(\varphi) + 2\pi \cdot R_p \cdot \sin(\varphi) \cdot \sin(\varphi + \theta_{LS}) \quad (3.11)$$

$$F_{gorge} = \pi \cdot \Delta P_{cap} \cdot r_{neck}^2 \cdot \sin^2(\varphi) + 2\pi \cdot r_{neck} \cdot \gamma_{LV} \quad (3.12)$$

Where r_{neck} is the curvature radius at mid-point of a liquid bridge and f is the filling angle of the viscous bridge and the particles.

WILLET *et al*. (2000) numerically solved Young-Laplace equation for equal spheres:

$$F_{boundary} = \frac{2\pi \cdot R_p \cdot \gamma_{LV} \cdot \cos(\theta_{LS})}{1 + 2.1 \cdot \left(\frac{S^2 R_p}{V_{bridge}}\right)^{\frac{1}{2}} + 10 \cdot \left(\frac{S^2 R_p}{V_{bridge}}\right)} \quad (3.13)$$

Where *S* is the half distance between two colliding particles.

RABINOVICH *et al*. (2005) presented the latest approximations of the pendular force between unequal spheres and considerations based on an effective particles radius, R_{eff}, for capillary bridges formed between spheres of different sizes:

$$F_{boundary} = -\frac{2\pi \cdot R_{eff} \cdot \gamma_{LV} \cdot \cos\theta_{LV}}{1 + \left(\frac{S}{d_{sp/sp}}\right)} - 2\pi \cdot R_{eff} \cdot \gamma_{LV} \cdot \sin\varphi \cdot \sin(\theta_{LV} + \varphi) \quad (3.14)$$

Where $d_{sp/sp}$ is the vertical distance between the first contact point to the mid-point in bridges neck:

$$d_{sp/sp} = S \cdot \left[-1 + \sqrt{1 + V_{bridge}/(2\pi \cdot R_{eff} \cdot S^2)}\right] \quad (3.15)$$

$$R_{eff} = \frac{R_1 R_2}{R_1 + R_2} \quad (3.16)$$

It can be seen that the capillary suction pressure is directly proportional to liquid binder surface tension and to its wettability behavior. Combined to inter-particle contacts, capillary suction pressure activates inter-particle friction forces which determines granule static bond strength (IVESON *et al.*, 2001). RUMPF (1962) describe such static tensile bond strength of granules in funicular and capillary states:

$$\sigma_t = S_{LP} \cdot C \cdot \frac{1-\varepsilon}{\varepsilon} \cdot \frac{\gamma_{LV} \cos\theta_{LV}}{d_p} \tag{3.17}$$

Where S_{LP} is the liquid pore saturation and C is particles shape factor.

FORSMO *et al.* (2006) studies pore saturation (figure 3.9) in iron ore green pellets as a function of moisture content, W, water and particles density, ρ_l and ρ_p respectively:

$$S_{LP} = \frac{100W}{100-W} \cdot \frac{1-\varepsilon}{\varepsilon} \cdot \frac{\rho_p}{\rho_l} \tag{3.18}$$

It was inferred in such study that granules integrity is proportional to solid surface hydrophilic affinity and binder surface tension. Nevertheless, it is inversely proportional to particle size and porosity. Porosity filling saturation, although it seems to affect proportionally granules strength, it presents an optimal value. After 90-95 % saturation internal pores are completely filled, so that concave surfaces are formed in pore openings. This observation is verified by ABOUZEID *et al.* (1979) on investigations carried out on Egyptian iron ore from El-Gedida deposit (Figure 3.10). According to them, beyond a certain level of water content, capillary forces decreases due to formations of capillaries of large diameter, i.e., cohesive forces begin to be predominant over adhesive ones.

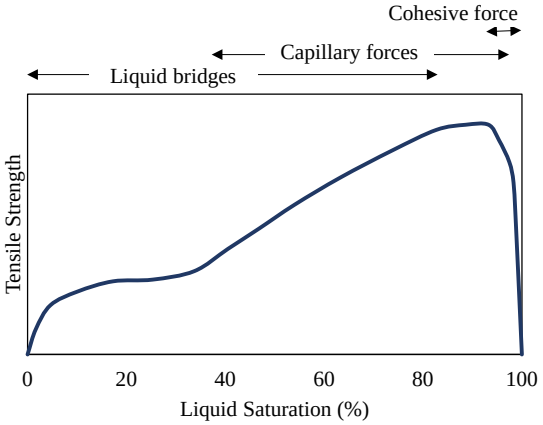

Figure 3.9. Tensile Strength as function of pore filling (Adapted from FORSMO *et al.*, 2006).

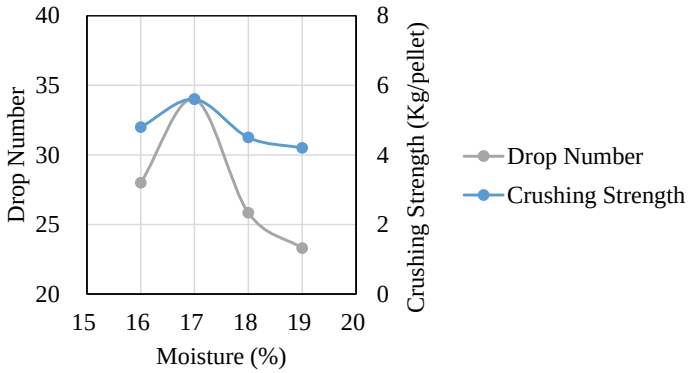

Figure 3.10. Green pellets strength, made from El-Gedida iron ore, as function of water content (ABOUZEID *et al.*, 1979).

KAPUR and FUERSTENAU (1964) were the first to describe the kinetics of green pellets balling. They verified how significant is the influence of moisture content during nucleation. Nuclei growth and size are directly proportional to moisture content (Figure 3.11).

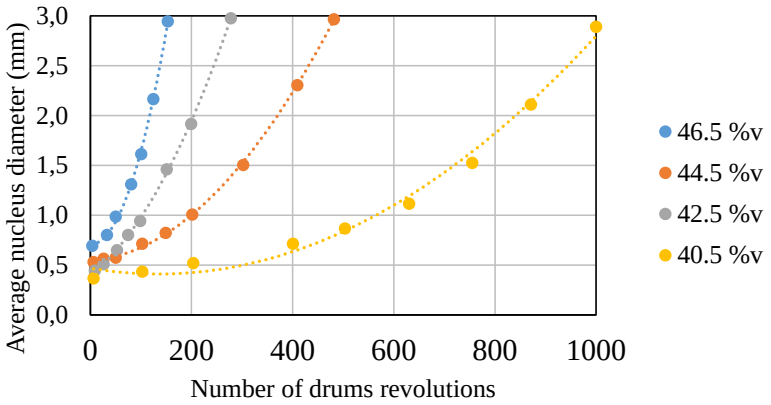

Figure 3.11. Evolution of average diameter of nuclei as function of balling drum for different moisture contents (% volume) (Adapted from KAPUR and FUERSTENAU, 1964).

3.2.2 Coalescence

Although it explains well the capillary influence on granules tensile strength, Equation (3.17), proposed by RUMPF (1962), presents some limitations by under-predicting agglomerates resistance made from fines widely sized particles. Besides that, it incorrectly estimates binder content effect (IVESON *et al.*, 2001). In such cases, inter-particle forces and viscous forces are equally important or could be even more important than capillary forces. For instance, excesses of binder content lubricate solid-liquid contacts and decreases agglomerates strength.

Moreover, SASTRY and FUERSTENAU (1973) clearly describe that without mechanical action of rolling, tumbling, agitating or/and kneading the wet material, agglomeration would not take place. The relative impact velocity promoted by granulation devices become of significant relevance when viscous binders are involved. According to ENNIS *et al.* (1990), under industrial conditions, the strength of a dynamic bridge may exceed that of the static by at least an order of magnitude due to the additional energy dissipation resulting from binder viscosity and the minute interparticle gap distance involved. ENNIS (1991) proposed a model (Figure 3.12) of two nearly touching spherical particles approaching each other. In the inner capillary region, when r=0, a viscous lubrication region exists, starting its influence from distances shorter than $S^{1/2}$. In the outer capillary zone, spheres are quite distant apart, the contribution of capillarity to bridge strength is dominant and viscous effects may be neglected at leading order in capillary number, which represents the ratio between viscous to surface tension forces:

$$Ca = \frac{We}{\mathrm{Re}} = \frac{\mu u_l}{\gamma_{LV}} \tag{3.19}$$

Where Ca is the capillary number, We is Weber number, μ is liquid viscosity and u_l is liquid phase velocity.

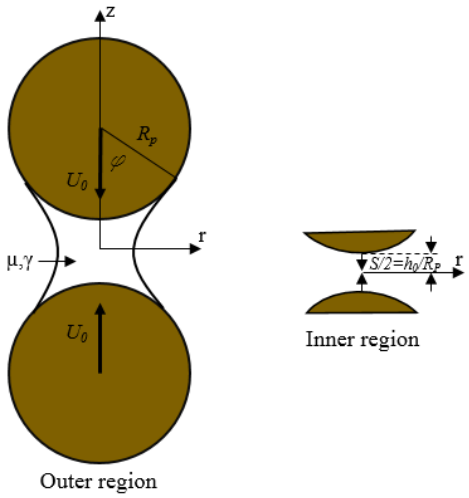

Figure 3.12. Regions of expansion for the pendular bridge (Adapted from ENNIS, 1991).

Through a balance of energy, ENNIS (1990) established the condition for successfully coalescence between two colliding solids. It happens when the kinetic energy given by their mass (proportional to r_1 and r_2 and their velocity, u_o) is insufficient to overcome the retarding force or strength of the liquid bridge. For such colliding particle, viscous Stoke number, St_v, and critical viscous Stoke number, St_v^*, are given by:

$$St_V = \frac{2mu_o}{3\pi\mu R_p^2} \tag{3.20}$$

$$St_V^* = \left(1+\frac{1}{e}\right)\ln\left(\frac{h}{h_a}\right) \tag{3.21}$$

For unequal colliding spheres, an analogous approach proposed by RABINOVICH *et al.* (2005) for capillary case is applied to Stokes numbers, with R_p being replaced by R_{eff} and also for the effective mass, so that:

$$m_{eff} = \frac{m_1 m_2}{m_1 + m_2} \tag{3.22}$$

When the viscous Stokes number exceeds the critical viscous Stokes number, the kinetic energy is greater than granules energy dissipation by the viscous binder layer. In such case the granule rebounds with velocity eu_o.

Three extensions of coalescence are determined based on the Stokes number aforementioned. If it is smaller than the critical one, all collisions are successful. As long as agglomerates grow, St_v approximates to St_v^*, and inertial regime takes place. When St_v becomes greater than St_v^*, all collisions do not form larger agglomerates and the system is under coating regime (IVESON *et al*., 2001). Not only the size but other inferences of viscous Stokes definitions are verified as well. For example, as more binder is added, the viscous layer increases. As consequence successful collisions are extended due to St_v^* proportional relation to such layer film, h (Figure 3.13). Nevertheless, if binder viscosity is risen (for example, in green pellets case, by adding more bentonite), at first it would appear to increase growth rate, but due to its swelling ability allowing water retention, lower volume of water is squeezed to granules surface. As such, an increase in binder viscosity indirect results in a St_v^* decrease due to reduced h (ENNIS, 1990). The relative velocity of granules is done by the operational speed of the balling equipment operational speed. Although St_v increases as velocity increases indicating less successful collisions by coalescence, the frequency of collisions also increases and other mechanisms of agglomerate growth are also benefited. Influences of operational conditions of balling devices are not simple to evaluate since growth rate is also dependent on residence time which changes when speed is modified.

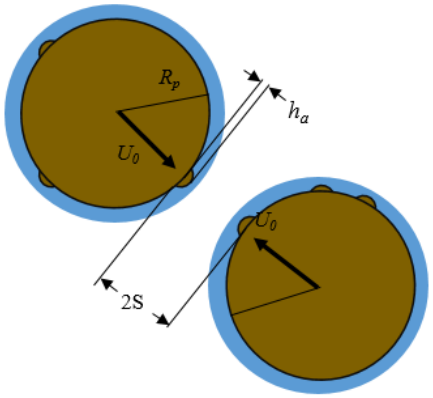

Figure 3.13. Schematic of two colliding granules (Adapted from ENNIS, 1990).

The model of Ennis has limitations because it omits viscous forces since his studies are based on non-deformable species. OUCHIYAMA and TANAKA *apud* IVESON *et al.* (2001) observed dry deformable granules during motion inside drums. They observed that granules changed their shape due to the action of compressive forces. A

contact area between such colliding agglomerates is generated and plastic deformation absorbs an important share of the kinetic energy involved in the collision. The authors observed that the compressive force was independent of granule size, i.e., it was product of the balling device conditions, but observed that separating forces were proportional to granule volume. Such analysis is very relevant and explains why collisions that successfully result in coalescence rapidly become less frequent as agglomerates sizes increase. In contrast to that, diameter of agglomerates would increase without limits. The prediction of the probability of coalescence of two granules is carried out in terms of characteristic limiting size *D**.

$$D^* = A_1\left(k_a{}^{3/2}\sigma_{st}\right)^q \tag{3.23}$$

Where A_1 and q are an independent constants of granule size, k_a and σ_{st} granule tensile strength of the bond area.

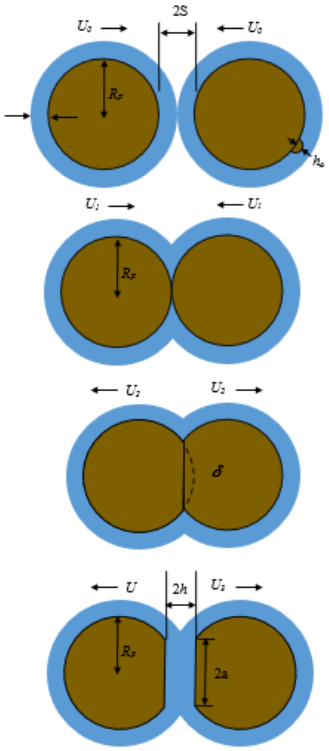

Figure 3.14. Schematic coalescence stage for wet deformable granules (Adapted from LIU *et al.*, 2000).

LIU *et al.* (2000) extended Ennis model and included granules elastic behavior done by their elastic modulus, *E*, and their plastic deformation when subjected beyond their plastic yield stress, Y_d (Figure 3.14). The authors describe two types of coalescence: type I, when kinetic energy of granules is entirely deadened on viscous layer, i.e, $St_v << St_v^*$; type II coalescence that happens as a consequence of plastic deformation, δ'', of agglomerates in situations done by:

$$\left(\frac{Y_d}{E}\right)^{1/2}\left(St_{def}\right)^{-9/8} < \frac{0{,}172}{St_v}\left(\frac{D_{eff}}{h}\right)^2\left[1-\frac{1}{St_v}\ln\left(\frac{h}{h_a}\right)\right]^{5/4}\cdot \left[\left(\frac{h^2}{h_a^2}-1\right)+\frac{2h}{\delta''}\left(\frac{h}{h_a}-1\right)+\frac{2h^2}{(\delta'')^2}\ln\left(\frac{h}{h_a}\right)\right]\cdot \left[1-7.36\left(\frac{Y_d}{E}\right)\cdot(St_{def})^{-1/4}\cdot\left(1-\frac{1}{St_v}\ln\left(\frac{h}{h_a}\right)\right)^{-1/2}\right]^2 \tag{3.24}$$

Where the Stokes deformation number is given by:

$$St_{def} = \frac{m_{eff}u_o^2}{2D_{eff}^3 Y_d} \tag{3.25}$$

D_{eff} is the effective diameter granule analogously calculated as m_{eff} and r_{eff} and h_a is a characteristic length scale of surface asperities.

The plastic deformation is given by:

$$\delta''=\left(\frac{8}{3\pi}\right)^{1/2}\left(St_{def}\right)^{1/2}D_{eff}\left[1-\frac{1}{St_v}\ln\left(\frac{h}{h_a}\right)\right]\cdot \left[1-7{,}36\left(\frac{Y_d}{E}\right)\left(St_{def}\right)^{-/4}\cdot\left(1-\frac{1}{St_v}\ln\left(\frac{h}{h_a}\right)\right)^{-1/2}\right] \tag{3.26}$$

According to LIU *et al.* (2000), granules which present limited deformations during collisions follow Ennis model. Nevertheless, when agglomerates exhibit deformation plastic, the probability of coalescence becomes greater (Figure 3.15) due to the higher capacity of granules to dissipate the kinetic energy involved in the collisions. Plastic deformation promotes not only an increase in surface area but also particles rearrange inside agglomerates as well. Collisions in such system squeeze water to the surface, increasing the thickness of the viscous layer and, therefore, successful coalescence

events. The authors' inferences show that St_{def} is proportional to granules velocity, u_o, although there are limitations to the model. If velocity is raised beyond a level, the granule will break. On the other hand, St_{def} is inversely proportional to agglomerate diameter, i.e., small granules are more susceptive to stick than larger ones. Finally, coalescence events become less likely to occur (Figure 3.16).

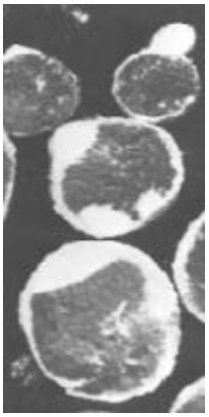

Figure 3.15. Granule formation by coalescence mechanism of New Jersey (white) and Texas (black) calcites (SASTRY and FUERSTENAU, 1973 – Authorized reproduction).

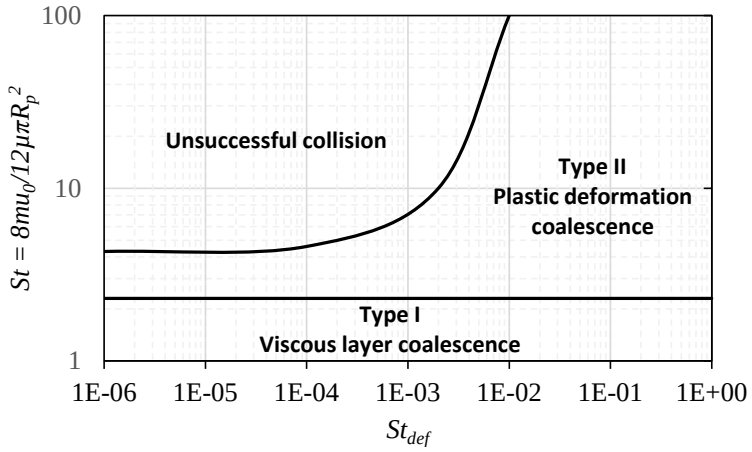

Figure 3.16 Rebound and coalescence regions for wet deformable granules (LIU *et al.*, 2000).

3.2.3 Layering

According to SASTRY and FUERSTENAU (1972), when new moist feed is added into a system containing pellets, they are collected by such seeds as shown in Figure 3.17. This mechanism is also called snowballing. Later, SASTRY *et al.* (2003) described the layering mechanism as a continuous growth of well-formed species by fine consumption of moist fines where there is no change on the total number of pellets but does account for increase in their mass.

LITSTER *et al.* (1986) first showed the proportional relationship between the adhering layer of seeds and the nuclei particle size, i.e., their exposed surface area. Their remarkable work postulates that nucleation of wet fine powder and layering cannot be analyzed apart because particles which are consumed by seeds can also act as nuclei. According to KAPUR *et al.* (1993), the granule size, $y(t)$, is related to particle size, x_f, by a granule ratio, $k(x)$:

$$y(t) = k(x) \cdot x_f \tag{3.27}$$

The layer thickness is given by:

$$t(x) = \frac{y(t) - x_s}{2} \tag{3.28}$$

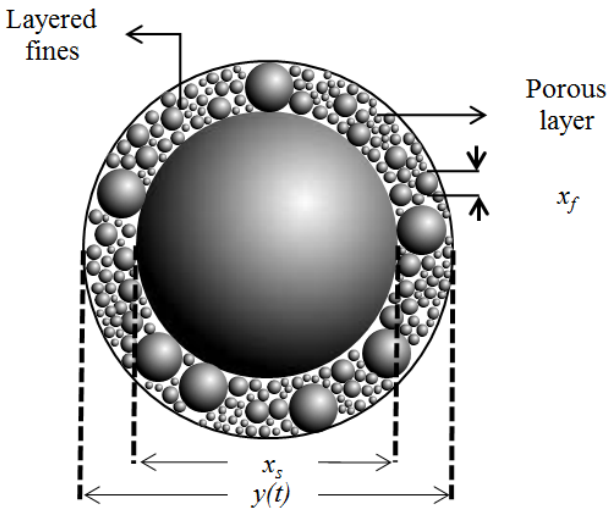

Figure 3.17. Fines layered by a seed (Adpated from KAPUR *et al.*, 2003).

The partition function, $p(x)$, defines the fraction of particles of size x_f which act as nuclei. M_L is the mass layered onto all seeds:

$$M_L = \rho_r \int_0^\infty f(x_f)\, p(x_f) \left[C_r k^3(x_f) - 1 \right] dx_f \tag{3.29}$$

Where, ρ_r, is the ratio of apparent densities of the layered mass and seed particles:

$$\rho_r = \rho_f / \rho_s \tag{3.30}$$

C_r is the ratio of geometric factors for granule and seed shapes and k is the granule growth index:

$$C_r = C_f / C_s \tag{3.31}$$

$$k^3 = \frac{1 - \Phi + \rho_r \Phi}{C_r \rho \Phi} \tag{3.32}$$

Where Φ is the mean weight of the seeds, given by:

$$\Phi = \int_0^\infty f(x_f)\, p(x_f)\, dx_f \tag{3.33}$$

The desired granule size distribution is function of transformation of particle size x_f to granule size, $y(t)$, so that:

$$g(y) = \frac{1}{k(x_f)} f\left(\frac{y(t)}{k(x_f)} \right) \tag{3.34}$$

Later, KAPUR *apud* KAPUR *et al.* (2003) showed that $p(x)$ could be calculated by exploiting the water balance in the granulating material:

$$p(x_f) = \left(\frac{\alpha \varepsilon \rho_l + W \varepsilon \rho_p}{\alpha \varepsilon \rho_l + W \varepsilon \rho_p + W \rho_s} \right)^{\frac{1}{3}} \tag{3.35}$$

Being α a correction for air bubbles trapped in the layering area. It can be inferred that as the moisture content, W, increase the cut off size acting as seed reduces. Same tendency is verified as higher solid specific density are.

SASTRY *et al.* (2003) evaluated the amount of feed layered by varying the amount of feed added and the moisture content in a laboratorial pelletizing drum. They concluded that the rate of layering is fast in the beginning and then it decreases continuously, coming to zero. The cut-off size of seeds used was 4 mm. Authors verified that the percentage of feed layered decreases, as more fresh feed fines were added to the granulation process because others faster mechanisms such as nucleation and coalesce increase their participation. Following the aforementioned Kapur model, layering mechanism dependence on moisture content was demonstrated in such study as follows:

$$M_L^{\max}(W) = k_0 \exp\left[-k_1(W - W_0)\right] \tag{3.36}$$

Where k_0 and k_1 are arbitrary constants, M_L^{max} is the maximum layered feed and W_0 is the minimum moisture content where layering mechanism occurs. GODIN and WILHELMY (2008) have analyze the quality of layered pellets. Its mechanism is clearly identified in Figure 3.18.

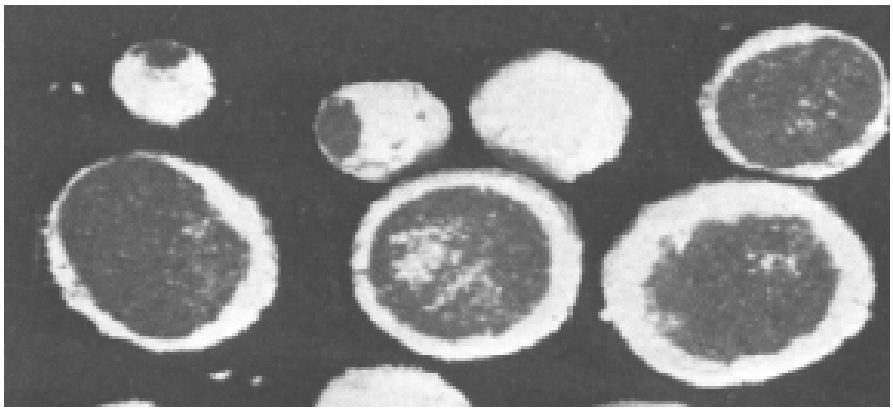

Figure 3.18. Layering growth of pellets (SASTRY and FUERSTENAU, 1972 – Authorized reproduction).

SASTRY and FUERSTENAU (1972) summarized the regimes of agglomerate growth by analyzing the rate of change of the average diameter of pellets made using taconite iron ore with 0.5% of bentonite and 10.8% of moisture (Figure 3.19).

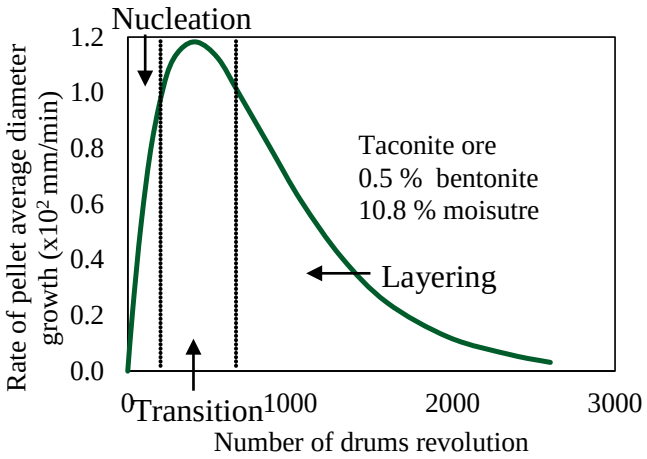

Figure 3.19. Differential growth rate curve for taconite concentrate (Adapted from SASTRY and FUERSTENAU, 1973).

According to them, and later verified by other authors (IVESON *et al.*, 2001; KAPUR and RUNKANA, 2003; SASTRY *et al*., 2003), the hardest task in granulation is to be able to analyze in separate each of the mechanisms since they happen simultaneously, having important influences on each other and also changing as compaction occurs. The nuclei region is characterized by nucleation and a maximum rate of coalescence. In the transition region, the coalescence extent governed by Equations 3.19 and 3.24 reaches its end, while the layering mechanism increases in importance. From then on, ball growth kinetics reduces asymptotically to zero as SASTRY (2003) modeled later. Such exponential kinetic decay was also observed by OUCHIYAMA and TANAKA *apud* IVESON *et al.* (2001) who assumed that granules were held together by capillary pressure of binder, ignoring viscous layer influence:

$$\frac{d\varepsilon}{d\tau} \cong -\left[1 - \frac{(1-\varepsilon)^3}{\varepsilon K_\varepsilon}\right]^n \tag{3.37}$$

Where K_ε is the dimensionless granule compaction rate which is proportional to the impact energy, particle size and inversely proportional to interparticle friction and binder adhesion. The parameter n describes the distribution of granule impact energies and τ is the dimensionless compaction time which is proportional to the frequency of impacts.

ENNIS (1991) model only considered viscous binder forces on coalescence growth although they have estimated the error of capillary negligence. According to the author the exponential decay is done by:

$$\frac{\Delta x_d}{h} = 1 - \exp(-St_V) \tag{3.38}$$

Δx_d is the reduction on interparticle gap distance.

3.3 Mass/population balance models applied to agglomeration and screening

SASTRY and FUERSTENAU (1973) listed formally the pellet growth mechanisms in order to assess the change of population species due to occurrence of them (Table 3.I).

Table 3.I. Change of population and mass during pellet growth (adapted from SASTRY and FUERSTENAU, 1973)

Mechanisms of pellet growth	Total Number	Total Mass	Agglomerate size change	
			Discrete	Continuous
Nucleation	Yes (+1)	Yes	Yes	No
Binary Coalescence	Yes (-1)	No	Yes	No
Layering	No	Yes	No	Yes

SASTRY (2008) summarized the population balance model for iron ore balling process considering the three mechanisms of agglomerate growth:

$$\frac{\partial n(m,t)}{\partial t} = -N^0(m,t) - \frac{\partial}{N(t)}\int_0^\infty \lambda^*(m,m',t)n(m,t)n(m',t)dm' + \\ + \frac{1}{2N(t)}\int_0^\infty \lambda^*(m',m-m',t)n(m't)n(m-m',t)dm' - \frac{\partial}{\partial m}\left[k_L(m)s(m)n(m,t)\right] \tag{3.39}$$

As mentioned before, N^0 is driven by powder wettability, i.e., its hydrophobic or hydrophilic relationship and the spontaneity characteristic or not of the spreading coefficient. The second and third terms on the right of the equation correspond to death/disappearance and birth/appearance functions of binary coalescence between colliding granules of masses *m* and *m'*. λ^* is the coalescence kernel, i.e, the rate function

for the agglomerate of such granules. In 1975, SASTRY discussed about two different rates of colliding regimes: random, λ_0, and non-random, λ, coalescence:

$$\lambda^*(m,m',t) = \lambda_0(t)\lambda(m,m') \tag{3.40}$$

ADETAYO *et al.* (1995) presented a more detailed description of kernels behavior during coalesce. According to the authors, in the first stage, called non-inertial, the probability of successful coalescence is independent of particles sizes and velocity. It depends exclusively on binder distribution, which is a direct function of operating conditions such as device rotational speed, feed size distribution and moisture content. In such study, the first-stage kernel is defined as a constant. During this period, the growth of granules takes place very quickly in accordance to SASTRY and FUERSTENAU (1972) and described by KAPUR and FUERSTENAU *apud* KAPUR and RUNKANA (2003). The numbers of granules, *n(t)*, decays exponentially while their volume grow, *v(t)*, in the same opposite trend:

$$n(t) = N_0 \exp\left(\frac{-\lambda_0 t}{2}\right) \tag{3.41}$$

$$v(t) = v_1 \exp\left(\frac{\lambda_0 t}{2}\right) \tag{3.42}$$

Where v_1 is the mean volume of granules at granulation beginning.

The mean granule size at the end of random coalescence, r_{c1}, is given by application of Kapur and Fuerstenau Equation (3.41) on Ennis model:

$$r_{c1} = \frac{9\mu}{8\rho_p v(t)} St_v^* \tag{3.43}$$

During the second stage, coalescence collisions are size dependent and larger diameter granules are favored due to their increased inertia upon impact (ADETAYO *et al.*, 1995). Compaction plays an important role since the rearrangement of particles is responsible to squeeze the excess of water to surface, extending the growth regime. Such sequence of events takes place following a first order kernel until agglomerates become rigid enough to deformation and St_v becomes greater than St_v^* when collisions are ineffective to glue granules together:

$$\lambda(m,m') = \lambda_0(t).\left[\frac{(m+m')^b}{(m\cdot m')^c}\right] \tag{3.44}$$

where, *b* and *c* are empirical constants of materials.

Finally, the last term on the right of Equation 3.38 is the net change due to layering mechanism, which is dependent of granules surface area, $s(m)$, or size, which acts as seeds and a kinetics constant $k_L(m)$.

3.4 Roller Screens

Roller screens (Figure 3.20) are worldwide applied on green pellets classification. In Brazil, such devices started being used in the 1990's and rapidly replaced vibrating screens which presented lower separation efficiency and caused some breakage of green pellets. Roller screens consist on a slightly angled structure in relation to horizontal (usually 10 to 19 °) assembled by parallels rolls meticulously gapped to separate fines, product and coarse agglomerates.

Fines removal is done through the gaps, usually greater than 9 mm (WELLSTEAD *et al.*, 1978) until 10 mm, on the first three quarters of the screening area. In the last quarter, the product is selected by gaps ranging from 14 to 18 mm. Coarse pellets are declassified at the ending roll discharge (Figure 3.20a). In drum pelletizers (Figure 3.20b), they are unavoidably part of each line of production since pellets are made in close circuit (analogous to close grinding mill circuit).

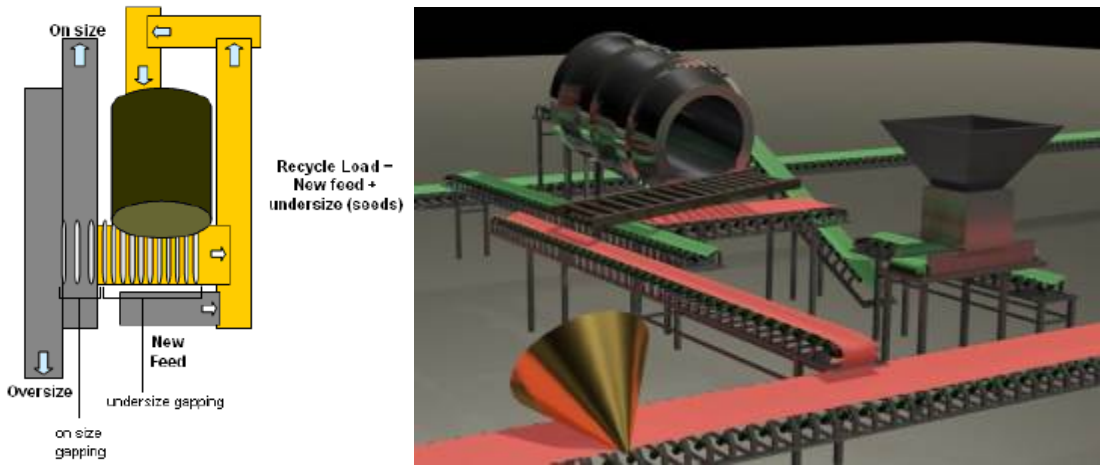

(a) (b)

Figure 3.20. 2D (a) and 3D (b) schematic view of drums pelletizers circuits.

For balling discs, roller screens are, in some cases, optional downstream. Their use depends on the type of double deck roller screen, also called feeder, installed

immediately before travelling grate or rotary kiln sintering furnaces. If such feeder removes oversize pellets and presents great capacity to remove undersize fines inherently generated during handling, the presence of roller screens at the discharge of discs may be optional. However, even in these cases, when the scale of production increases (larger than 5 Mt/y), roller screens at the discharge of discs are advisable because the quantity of fines to be screened (the amount of discs output summed to the generation due to green pellets broken during handling) is quite considerable. A huge area of feeder would be necessary to avoid excessive fines among green pellets in bed formation on pallets cars. It would force the application of wider (>4000 mm) conveyors (Figure 3.21) to collect the undersize return making its installation/change still more challenging. This maintenance activity is very tough being usually the critical path on a scheduled shutdown.

Figure 3.21. Conveyor belt for transport of fines sieved on double deck roller screen at Vargem Grande induration machine entrance.

At Vargem Grande, the structures of the roller screens are made in steel ASTM-A-36 and two 10 mm width guides built in UHMW-1900 polyethylene limit the screening area. The rolls have an ASTM-A-297 HE (SAE 312) stainless steel body and SAE-1045 shafts. Ceramic-coated rolls can also be applied in some cases. At the discharge of discs (Figure 3.22), the 75 mm diameter rolls are 1800 mm in length and the screens rated capacity is 125.7 t/h, which is not high enough to reach plant nominal production rate since return rate is around 29 % (Figure 2.2). Their nominal capacity is 163.4 t/h. A

three-phase 25 HP motor assembled to a 1:32 gear reducer promotes rolls' motion by a double gear driven wheel and two parallel double chains ASA-80 tensed by two pneumatic cylinders at 3 to 3.5 $kgcm^{-2}$ (Figure 3.23a). Rolls rotational speed is given by the transmission of the relative linear movement of the chains on crown wheels key stuck to rolls shaft (Figure 3.23b). Chains are constantly lubricated by gravity by five extensions from the lubrication system. Such roller screen devices weight around 8000 kg. Rolls speed can range from 70 rpm to 175 rpm.

Figure 3.22. Roller screen in operation downstream from the disc pelletizer.

(a) (b)

Figure 3.23. Roller screens driver system (a) Double gear driven wheel tensed by pneumatic cylinders and lubrication system (b) double and crown wheels (key stuck to rolls shaft) movement transmission.

At the travelling grate feed, a double deck roller screen (usually inclined 17° to 23° to horizontal) assembled with 94 mm diameter / 4000 mm length rolls removes the fines. The upper deck is gapped at 18 mm in order to reduce the pellets bed thickness on the lower deck, which is typically gapped at 8.2 mm, with the aim to facilitate and improve fines removal. Roll speeds can range from 10 to 108 rpm at Vargem Grande. The rotation of the rolls motion is driven by three-phase 1.1 kW individual helical geared motors, key stuck to cardan shafts. The complete structure weights around 25000 kg. Its feed rated capacity is 1144 t/h (1000 t/h of production) which is not high enough to reach Vargem Grande nominal grate index (26.5 $tm^{-2}d^{-1}$ or 29290 t/d).

As previously mentioned, green pellets classification on roller screens is of relevant importance although not further investigated. The challenges imposed by physical limitations such as inaccessibility and difficulties to collect representative samples and change of properties of solids while handling/testing guided the approach of the problem to the application of the mathematical model: the Discrete Element Method.

3.5 The Discrete Element Method

The Discrete Element Method is a numerical model first developed by Cundall and Strack (1979) that aims to describe the mechanical behavior of solids displacing independently from each other and which interact at their contact points. With the aid of a software code named BALL, the motion of assemblies of discs in a two-dimensional system and their interactions among themselves were first evaluated numerically.

Since then, DEM has increased its importance and has become widely accepted as an effective tool of addressing engineering problems in granular and discontinuous materials, especially in granular flows, powder mechanics, rock mechanics, comminution (WEERASEKARA et al., 2013; CLEARY,1998; CLEARY *et al.*, 2000, CLEARY *et al.*, 2009), chemical and pharmaceutical industries (ZHU *et al.*, 2008). The difficulty to analyze agitated systems where a great number of variables, noise and physical phenomena occur at the same time is the main reason for the success of this numerical method. In contrast to any physical modeling, it allows to reproduce, repeat and/or stop any granulation system simulation at any stage in order to get information that guide the understanding and clarify the mechanisms involved.

DEM is based on a time step cycle, Δt, calculation taken over small periods over which assembly velocities and accelerations are assumed constant and particles interactions influences can only be resultant on their immediate neighbor particle that is in contact in order to capture the inherent non-linearity of the system (CUNDALL and STRACK *apud* O'SULLIVAN, 2011). CLEARY (2000) explains that around 20 and 50 segments are necessary to accurately integrate each collision, i.e., time steps usually range from 10^{-3} to 10^{-6} s depending on the simulation scale and particle sizes and velocities. The accuracy, stability and robustness of the time integrations algorithm are relevant in simulations which attempt to replicate real situations. Approximations and limitations, given by the set time step are the round off and truncation (more relevant) errors, came from introduced calculations of particle displacement through the calculated accelerations.

SHENG *et al. apud* O'SULLIVAN (2011) defined the critical time step, Δt_{crit}, for DEM simulations with spheres and a Hertzan contact model:

$$\Delta t_{crit} = \frac{\pi R_{\min}}{0.1631\upsilon + 0.876605}\sqrt{\rho_p G} \tag{3.45}$$

Where R_{min} is the smallest particle radius, υ is its Poisson ratio and G is the shear stiffness. THORNTON *apud* O'SULLIVAN (2011) took in account the Rayleigh wave speed of propagation for elastic materials:

$$v_r = \left(0.1631\upsilon + 0.876605\right)\sqrt{G\rho_p} \tag{3.46}$$

The choice of the time step vale is not trivial to reach convergence and stability respecting the law of conservative energies in the system. It must be smaller when: non-linear contact models are used (due to stiffness matrix change during contact area modification); particle numbers and their contacts increase; particles are smaller, stiffer or less dense.

DEM approach is categorized in two different main models for particles: soft and hard. For hard particles, there is no interpenetration amongst solids and collisions are instantaneous events of less relevance. Momentum equations are solved and energy is dissipated by plastic deformations and heat. Such model does not provide accurate information in multiple concomitant collisions and present limited measures about

tangential and frictional forces involved (O'SULLIVAN, 2011). According to CLEARY (1998), in the soft particle method, the elastic deformation of individual particles is simulated by overlaps, δ, where the normal and tangential relative velocities determine the collisional forces respectively over a contact area, a, in simultaneous contacts.

DEM processing considers particles (or assemblies) as independent bodies able to freely translate and rotate. When a binary collision happens, a stiffness matrix is updated. Particles overlap each other until a given extent that is directly proportional to their intrinsic rigidness and energy of collision and begin to move backwards. In the opposite sense, when a contact is broken, the stiffness matrix has a spring index removed. The calculations perform alternatively the application of Newton's second law and force-displacement law at the contacts which gives assemblies motion and rotation done by resultant force. Therefore, the system follows the solution of matrix calculus for linear and angular dynamic equilibrium given by:

$$Ma_v + Dv_v + Q = \Delta F \tag{3.47}$$

Where M is the mass matrix, a_v is the acceleration vector, D is a damping matrix, v_v is the velocity vector, Q is the global stiffness matrix and ΔF is an applied external force vector.

The application of DEM must be therefore carefully carried out in order to successfully reproduce real systems on simulations (BARRIOS *et al.,* 2013). The appropriate choice of the contact model and a reliable and accurate parameterization of such model entries are the key factors to achieve/observe credible behaviors of particles motion and interactions among themselves and with the geometry of the system. The knowledge about solids intra and inter characteristics is equally relevant to characterize their responses to external stimulus not only as an individual particle but also when they are part of set of particles and the neighborhood. Any scale factor transformations must be deeply evaluated since forces of different nature can have their influences increased or decreased by such change.

3.5.1 EDEM® software

The software chosen to run the DEM simulations in this work for assessing of roller screens was EDEM®, developed by DEM Solutions from Edinburgh, Scotland, and

licensed to Laboratório de Tecnologia Mineral at COPPE/UFRJ. Its platform is divided in three different parts (EDEM 2.6 User Guide, 2010):

• EDEM Creator: where the environment and granular media are built. It involves the definition of contour parameters such as the geometry limits, the contact model selection and its respective inputs, interactions and motion parameters among the particles themselves and the geometries, gravitational or electromagnetic field actions, particles properties such as size distribution, shapes, density, Poisson coefficient, shear modulus, initial velocity.

• EDEM Simulator: definition of time step and simulation of total time. The grid simulator and its size are defined in order to refine the calculations, although it can upscale simulation time. The process can be stopped to be manipulated at any time to obtain qualitative or quantitative information/observation.

• EDEM Analyst: where data is collected and extracted for analysis at a post-processing stage. Information about particles and geometry can be captured and visualizations resources as videos or pictures are available to qualitatively and quantitatively identify the mechanical phenomena.

3.5.2 Contact Models

EDEM® provides several contact models to describe elements behavior when put in contact with each other and with the geometry:

- Hertz-Mindlin (no-slip)
- Hertz-Mindlin (no-slip) with RVD (Relative Velocity Dependent) Rolling Friction
- Hertz-Mindlin with Bonding
- Hertz-Mindlin with Heat Conduction
- Temperature Update
- Hertz-Mindlin with JKR (Johnson-Kendall-Roberts) Cohesion
- Linear Cohesion
- Hysteretic Spring

The choice between the models is based on phenomenological observations of particle motion and the object of study. Literature review indicated four potential contact models (or their combination) which may represent green pellets motion/stick

behavior on rollers screens and among each other: Hertz-Mindlin (no slip), Hertz-Mindlin JKR cohesion (indicated to capillary state), hysteretic spring (plastic deformations inclusion) and linear cohesion.

Previous studies by BOECHAT (2013) and BARRIOS *et al.* (2013) aimed to simulate indurated pellets motion during handling. In these cases, the authors used the no-slip Hertz Mindlin model which is based on Hertz theory of contact for the normal force component (Equation 3.48) and on studies of Mindlin-Deresiewicz for the tangential force (Equation 3.52).

$$\delta = u_0 \Delta t = \left(\frac{9F_n^2}{16R_{eff} E*^2} \right)^{1/3} \tag{3.48}$$

Where F_n is the normal force and E^* is the equivalent Young's modulus is given by (O'SULLIVAN, 2011):

$$\frac{1}{E*} = \frac{1-\upsilon_1^2}{E_1} + \frac{1-\upsilon_2^2}{E_2} \tag{3.49}$$

$$F_n = \frac{4}{3} E^* \sqrt{R_{eff}} \delta_n^{\frac{3}{2}} \tag{3.50}$$

Where δ_n is the normal overlap. During collision, solids surface of contact is done by:

$$a = \left(\frac{3F_n R_{eff}}{4E*} \right)^{1/3} \tag{3.51}$$

The tangential component follows the Mindlin theory:

$$F_t = \min(\mu_n F_n, \int S_n v_t dt + F_t^d v_t) \tag{3.52}$$

Where S_n is the normal stiffness, v_t is the tangential velocity, and F_t^d is the dashpot damping coefficient. For the following time steps, particles velocity, normal composition of acceleration (a_n), direction, rotation and resultant force are calculated based on successive application of Newton's second law of motion:

$$a_n = \frac{d^2x}{dt^2} = \frac{F_n}{m} \tag{3.53}$$

The damping force is:

$$F_n^d = -2\sqrt{\frac{5}{6}}\beta\sqrt{S_n m_{eff}}\,v_n^{\overline{rel}} \tag{3.54}$$

Where $v_n^{\overline{rel}}$ is the normal component of relative velocity, β and S_n the normal stiffness:

$$\beta = \frac{\ln e}{\sqrt{\ln^2 e + \pi^2}} \tag{3.55}$$

$$S_n = 2E^*\sqrt{R_{eff}\delta_n} \tag{3.56}$$

Tangential force, F_t, depends on the tangential overlap, δ_t, and the tangential stiffness, S_t:

$$F_t = -S_t\delta_t \tag{3.57}$$

Where δ_t is the tangential component of particles overlap.

$$S_t = 8G^*\sqrt{R_{eff}\delta_n} \tag{3.58}$$

G^* is the equivalent shear modulus. Tangential damping is analogous to normal one:

$$F_n^d = -2\sqrt{\frac{5}{6}}\beta\sqrt{S_t m_{eff}}\,v_t^{\overline{rel}} \tag{3.59}$$

CLEARY (1998) demonstrated schematically how Hertz-Mindlin contact model works at two bodies' collisions and how forces dissipation occurs in normal and tangential directions (Figure 3.24).

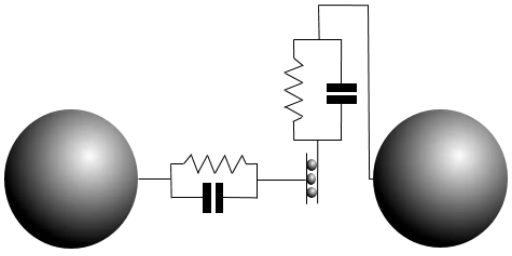

Figure 3.24. Hertz-Mindlin (no slip) contact model scheme (Adapted from CLEARY, 1998).

A difference between BOECHAT (2013) and BARRIOS *et al.* (2013) is that the former simulated the pellet as a perfect sphere aiming to reduce processing time since the number of particles was very large. Processing time is directly proportional to the number of particles (as population increases, the number of collisions raise considerably and making the routine of calculations for each of them long and heavy), their mean size (as smaller particles are, smaller is the time step, Δt, in order to register important changes in the system) and the geometry of the particles assembly (irregular shapes can present many different edges and higher specific surface which raise the probability of collisions to other particles in the system and, as consequence, the calculations). Processing time must be considered as a critical variable on simulation experiments. BARRIOS *et al.* (2013) carried out their studies in a lab rotational drum where the number of particles was quite limited, the authors showed the difference between a shape factor for a perfect sphere model and an assembly of spheres which represents irregular solids. The assemblies of spheres demonstrated to be the most representative model to simulate indurated pellets for the selected contact parameters. The contact parameters can be set to reproduce real situations with confidence for different solids shapes.

CLEARY *et al.* (2009a, 2009b) also applied the standard Hertz-Mindlin (no slip) to evaluate similar study objective carried out to double deck banana type vibrating screens (Figure 3.25). The authors analyzed the influence of operational variables on size segregation of a generic rock containing particle sizes ranging from 15 to 200 mm in each product stream and the pressure on the screen cloth in order to predict its wear. The stationary regime was reached after about 20s (10 times the minimum residence time of particles in the system) after the feed of material on the screens upper deck.

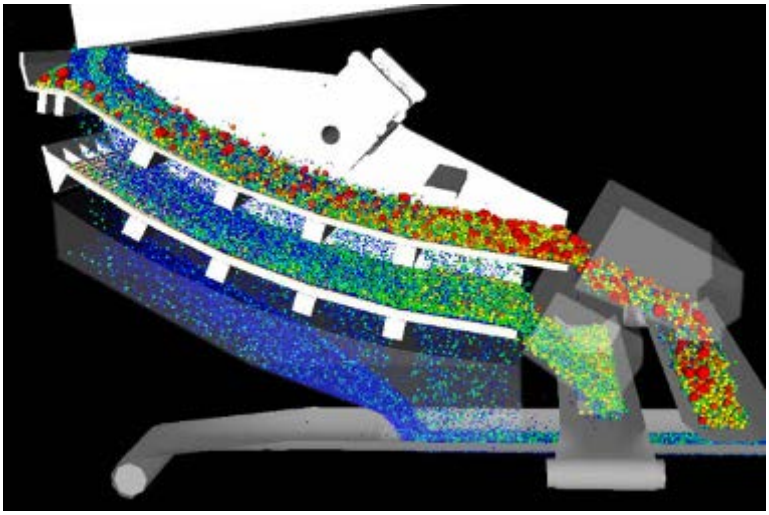

Figure 3.25. Simulation of solids segregation on double deck banana vibrating screen (CLEARY, 2009b)

As previously reviewed, green pellets are complex agglomerates that exhibit sticky behavior due to the external viscous layer at their final consolidation point (Figure 3.7). In EDEM®, the model JKR and linear cohesion are usually applied to describe systems of solids whose interfaces exhibit some adhesive behavior. Such contact models represent well the motion of fine dry powders or moist material where Van der Waals and/or capillary forces play significant influence.

JOHNSON *et al.* (1971) observed that attractive forces appeared between solids when put close to each other. Although such forces are of little significance at high loads they become increasingly important as the external load is reduced to zero. The authors identified that the total energy of the system was made up of three contributions: stored elastic and mechanical (both present on Hertz-Mindlin theory) and from the surface. This latter energy is dependent on particles overlap and on an interaction parameter, γ_{JKR} , which is analogous to surface tension. The normal force is then, given by:

$$F_{JKR} = -4\sqrt{\pi\gamma_{JKR}E^*}a^{\frac{3}{2}} + \frac{4E^*}{3R_{eff}}a^3 \tag{3.60}$$

$$\delta = \frac{a^2}{R_{eff}} - \sqrt{\frac{4\pi\gamma_{JKR}a}{E^*}} \tag{3.61}$$

The model provides attractive cohesion forces even if the particles are not in physical contact. The gap of attractive force action, a_c, is (EDEM® Users Guide, 2016):

$$\delta_c = \frac{a_c^{\,2}}{R_{eff}} - \sqrt{\frac{4\pi\gamma_{JKR}a}{E*}} \tag{3.62}$$

and,

$$a_c = \left[\frac{9\pi\gamma_{JKR}R_{eff}^2}{2E*}\left(\frac{3}{4} - \frac{1}{\sqrt{2}}\right)\right]^{\frac{1}{3}} \tag{3.63}$$

The maximum cohesion force, $F_{pullout}$, is given when particles are extremely close, but do not touch each other:

$$F_{pullout} = -\frac{3}{2}\pi\gamma_{JKR}R_{eff} \tag{3.64}$$

LIAN *et al.* (1998) investigated two colliding agglomerates made from 1000 particles during coalescence phenomena (Figure 3.26). The authors varied the impact relative velocity (from 0.5 to 5 m/s) and viscous binding properties as well (from 1 to 100 mPas). The authors verified that about 60 % of the energy of collisions of granules in pendular state coalescence is dissipated due to interparticle friction, while 35 % by the viscous damping effect of the liquid layer and the remaining 5 % due to bridge bond ruptures. The simulations are in perfect accordance to Liu's model for deformable spheres where the critical impact velocities increase and, as consequence, the Stokes deformation number, St_{def}, as the interstitial fluid viscosity rises.

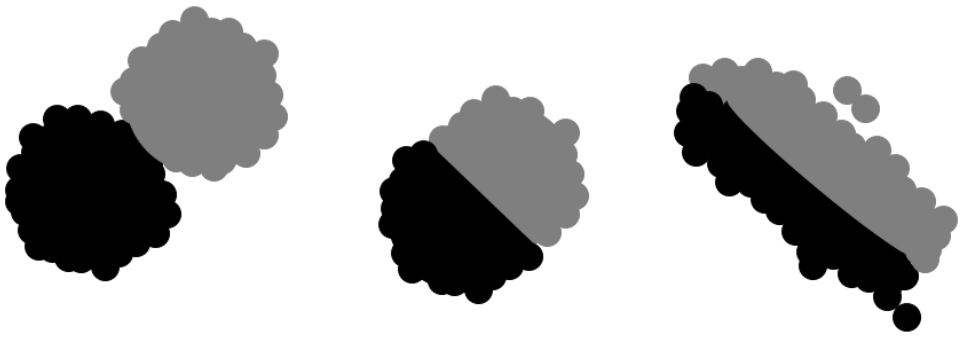

(a) (b) (c)

Figure 3.26. Agglomerates collision during coalesce phenomena for different relative velocities. (a) 0.5 ms^{-1} (a) 2.0 ms^{-1} (a) 5.0 ms^{-1} (Adapted from MISHRA, 2002)

Yet another parameterization is presented by WANG *et al.* (2015), who used a variant of DEM, called Nonsmooth Discrete Element Method (NDEM), to simulate discharge of green pellets from a rotary balling drum (Figure 3.27). Although interesting the findings of this study were questionable because of their choice of parameters. The magnitude of the coefficient of restitution between pellets used by the authors was quite high (0.18) in the referred semi-smooth DEM that according the authors can combine the numerical stability at larger step-size of an instantaneous non-overlapped event collision and the possibility of modeling the viscoelastic nature of contact forces. However, it is not advisable to treat green pellets sticky viscous and deformable characteristics which do not restitute as much as pointed with such strategy. Recently, for example, THORNTON *et al.* (2017) have concluded in their studies on elastic-plastic normal contact force model for solids with adhesion that linear models that ignore the permanent plastic deformation and assume the end of contact at a given relative approach are unphysical. Indeed, this value is likely to be overestimated around 7 to 10 times. The other parameters are very reasonable including the mass density since the object of study were iron pellets made from magnetite ore.

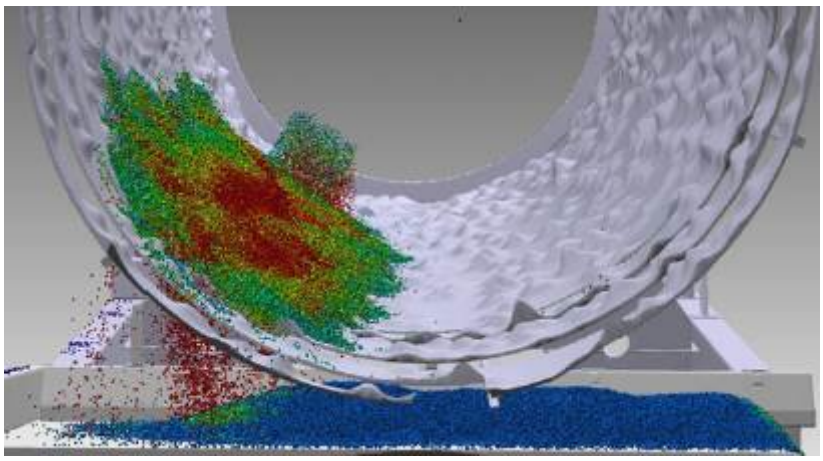

Figure 3.27. Simulation of green pellets on rotary drum pelletizer discharge (WANG *et al.*, 2015).

Studies by MISHRA *et al.* (2002) used Hertz-Mindlin with JKR Cohesion to simulate the agglomeration process in a rotating drum mixer at 60% of critical speed. The authors varied the interfacial energy from 0.5 to 1.5 Jm^{-2} and used the software

GRANULE in the simulations where surging phenomena could be observed by capturing mill torque variations as well as breakage and nucleation mechanisms at different positions on the tumbler device.

Green pellets deformation (Figure 3.28) is very relevant as LIU (2000) demonstrated when modified Ennis model. In EDEM® platform, plastic changes on solids volume can be integrated through the use of hysteretic spring contact model (Figure 3.29) based on the work by WALTON and BRAUN (1986) work.

Figure 3.28. Cylindrical-shaped green pellets, evidencing their plastic deformation between rolls.

When particles collide against each other or against a solid surface, the normal force follows a linear relation described by the loading stiffness, K_L. After reaching the maximum overlap, force is unloaded as the unloading stiffness, K_U, indicates. All the force magnitude is ceased but a residual overlap, δ_0, remains. If another force is applied to the particle, the trend followed is described by K_U relationship. Such greater overlap might reproduce deformation on roller the deformation of green pellets whose diameter is approximately equal to the gap.

$$F_n = \begin{cases} K_L\delta_n & \left[K_L\delta_n < K_2(\delta_n - \delta_0)\right] \\ K_U & \left[\delta_n > \delta_0\right] \\ 0 & \left[\delta_n \le \delta_0\right] \end{cases} \tag{3.65}$$

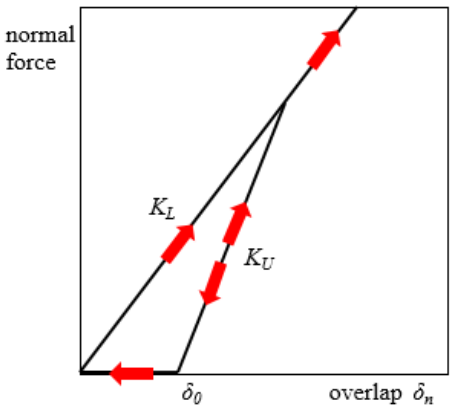

Figure 3.29. Load/unload forces representation for two colliding particles with hysteretic spring contact model (Adapted from EDEM® Users Guide, 2016)

Loading stiffness is related to the yield strength of the material. The deformation, as saw in theory of plastic agglomerates coalescence, is larger for the most plastic participating particle:

$$K_L = 5R_{eff}\ \min(Y_1, Y_2) \tag{3.66}$$

If the restitution coefficient governs the amount of energy absorbed in the collision, it is given by the ratio of load/unload relationship (EDEM ® Users Guide, 2016):

$$e = \sqrt{\frac{K_L}{K_U}} \tag{3.67}$$

With the comprehension of mechanisms and properties of the solids in the system, the roller screens equipment where the process of classification takes part and the potential contact models available on EDEM®, it is necessary to characterize green pellets and calibrate input parameters used to reproduce agglomerates motion and interactions among themselves and with others surfaces.

4 MATERIALS AND METHODS

4.1 Characterization of green pellets and calibration of input parameters

Characterization tests (static and dynamic) were carried out to determine the properties of agglomerates and to calibrate the input parameters asked in the EDEM® creator platform to simulate particles motion with good accordance to physical phenomena.

4.1.1 Static tests

4.1.1.1 Green pellets making and preparation

Balling feed material was sampled at Vargem Grande plant. Such pellet feed is already wet reground in ball mills, filtered in vacuum rotary filters, pressed by high-pressure roller press and mixed with limestone additive, anthracite coal and bentonite binder (Figure 2.1). Table 4.I summarizes such physical and chemical properties.

Table 4.I. Chemical and physical characteristics of balling mixture.

	Parameter	Value
Chemical composition	Fe_{total} (%)	62.2
	SiO_2 (%)	2.7
	CaO (%)	2.2
	Mn (%)	0.088
	MgO (%)	0.050
	P (%)	0.046
	TiO_2 (%)	0.101
	Binary basicity	0.82
Physical characteristics	Surface area (cm^2/g)	1860
	<0.045 mm (%)	80.4
	LOI (%)	4.75
	Bentonite dosage (%) – dry basis	0.56
	Anthracite coal (70.7 % C_{fix}) addition (kg/t)	17.05

Green pellets were then prepared in the lab in a one-meter diameter Eirich mixer (Figure 4.1), TR10 model and angled 68° from horizontal. Rotational speed was maintained constant at 16 rpm, i.e., 37 % of critical speed. Water spraying was carefully applied to promote agglomeration.

Pellet size distribution was determined by hand sieving.

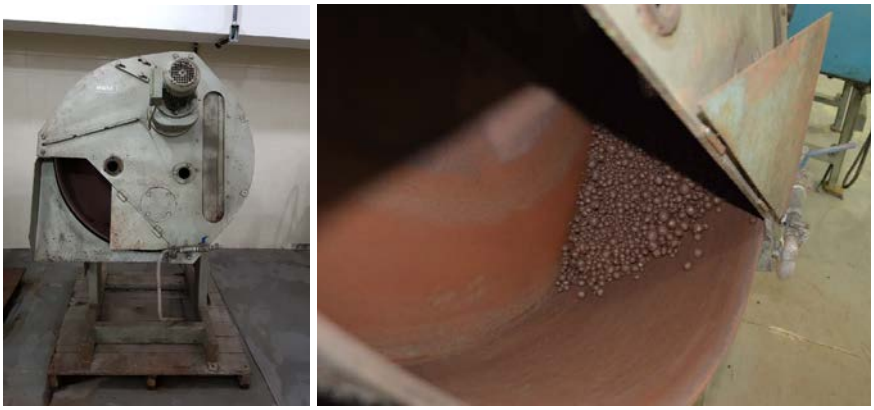

Figure 4.1. Eirich mixer used in green pellets preparation (left), and detail of green pellets produced (right).

Produced pellets were then quartered to determine their individuals and bulk properties.

4.1.1.2 Bulk density

Hydrostatic density of moist pellets was measured for 50 pellets individually. Such pellets were sieved between 9.5 to 12.5 mm. The test is based on Archimedes' principle where a body immersed in a fluid experience a buoyant force equal to the weight of the liquid displaced. A two-digit precision scale and a density measurer were used (Figure 4.2).

Figure 4.2. Hydrostatic density test setup.

4.1.1.3 Moisture content

A sample containing approximately 150 g was dried in oven at 105 °C for 1 h in order to determine green pellets moisture content. Moisture content, as observed in consolidation model and mechanisms of green pellets growth, plays an important role to define solids sticky behavior.

4.1.1.4 Drop number

The standard drop number test proposed by MEYER (1980) was carried out with 20 pellets sieved between 9.5 mm e 12.5 mm. They are individually dropped from a 46 cm height platform repeatedly until their breakage. The drop number is the average of drops each pellet resisted and it is an indirect measurement of evaluation of solids ability to absorb energy of collision.

4.1.1.5 Shape

Green pellets produced were sieved. A single pellet, in the fraction between 10 and 12.5 mm, was randomly selected to characterize their shape using the in DAVID Laserscanner (Figure 4.3). Three-dimensional (3D) images were collected by means of a laser source with camera capture. Images are instantly transferred to software to post processing and elaboration of the object volume.

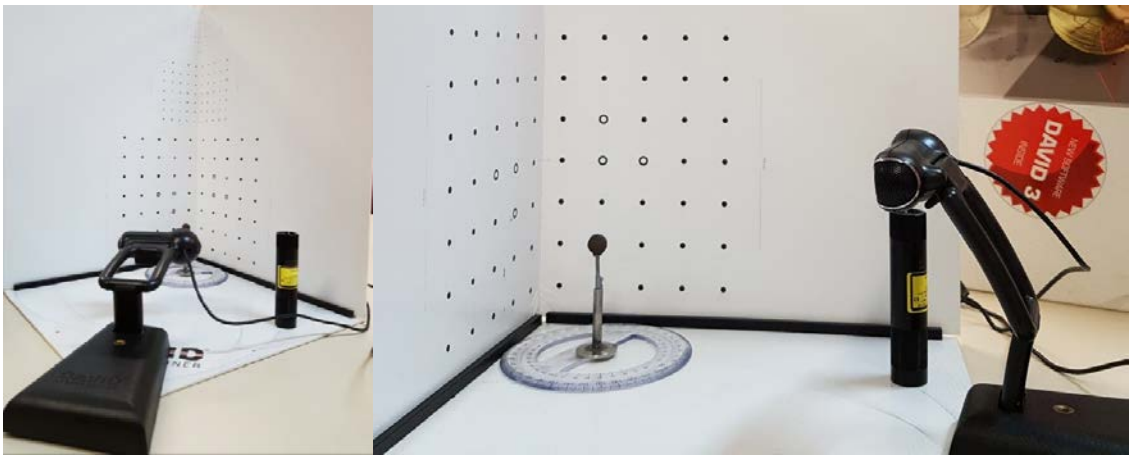

Figure 4.3. DAVID laser scanner.

The target object is positioned in front of the camera for data acquisition. Behind it, two quoted plans are placed as size references. A laser emission focuses on the surface of the object. Repeated laser scanning and continuous comparison to the plans gradually create the image on the software platform.

The object is rotated 20° to avoid three-dimensional distortions of its surface. This procedure is repeated until the complete turn. All sides are sequentially and complementary put together to acquire the final 3D image (Figure 4.4).

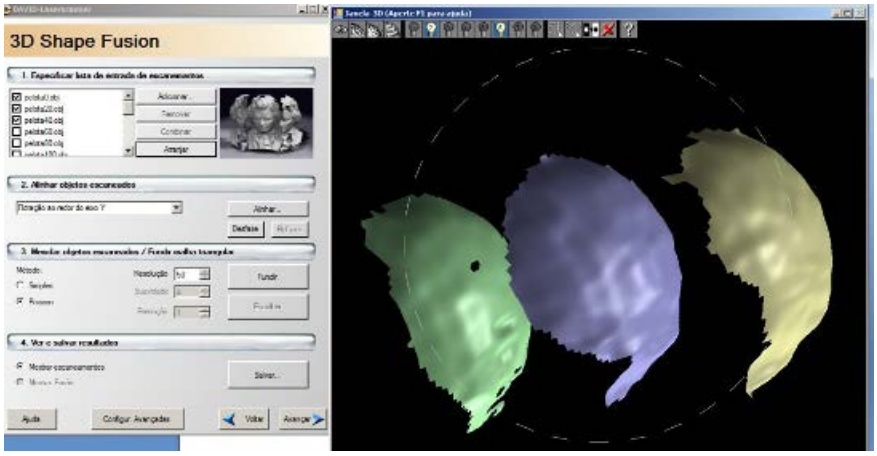

Figure 4.4. 20° sections of a green pellet projection.

4.1.1.6 Green and dried pellets resistance strength

Green and dry compression strengths of pellets were evaluated according to ISO 4700:2007. Sieved between 9.5 and 12.5 mm, a batch of 80 randomly picked pellets were tested for each compression procedure. Green moist pellets were collect just after pelletizing in the laboratory. Dried pellets were collected from the moisture content determination test, i.e., after the heat treatment at 105 °C for 1 h. The press piston advance velocity was set at 10 mm/min. A EMIC model DL1000 10 kN load cell registered the data (Figure 4.5).

Figure 4.5. Compression test on EMIC 10 kN press.

The relation between the force applied by the press embolus on the particles tested and their deformation determine the particle stiffness during elastic regime, given by Equation 3.68 (TAVARES and KING, 1998) and enunciated in the theoretical Hertzian contact relationship for spheres:

$$E = \frac{3F_n}{d_p^{\frac{1}{2}} \alpha_p^{\frac{3}{2}}} \tag{4.1}$$

Where α_p is the particle total deformation.

4.1.2 Bulk dynamic tests

Three physical dynamic tests were carried out in order to support the estimation of contact parameters input for the contact model: angle of repose, tumbling and handling

bench tests. The tests were conducted with green pellets produced in the laboratory, as previously discussed, with the size distribution produced.

4.1.2.1 Angle of repose

A 195 mm diameter hollow cylinder (Figure 4.6) was filled with 10 kg of green pellets produced in lab. The cylinder was then removed and pellets dropped on a rubber plate. The procedure was repeated three times to determine the angle of repose to horizontal.

Figure 4.6. Hollow cylinder filled with pellets.

4.1.2.2 Restitution

The restitution coefficient was estimated with the aid of a high-speed camera (240 fps). Single pellets were dropped from 1 m height on a 10 mm compacted mixture layer (same material which pellets are made of, i.e, pellet feed, bentonite, limestone and anthracite coal), a 5 mm steel plate and a 10 mm rubber piece (cut from conveyor belt) (Figure 4.7). Restitution is given by Equation 3.67 and it represents to the amount of energy which was not absorbed/consumed in the contact of colliding solids as deformation, sound and cracks propagation for example, and remains on solids after the collision. Kinetic energy is directly proportional to the square of velocities. Through a simple replacement on Equation 3.67, the restitution coefficient may be given by the ratio between the maximum velocity before the contact on the base and the immediate initial velocity of the pellet after the collision. In practice, the simplest calculation of

restitution is given by the ratio between the height reached by the pellet after the collision on the base and initial height it was abandoned, 1 m.

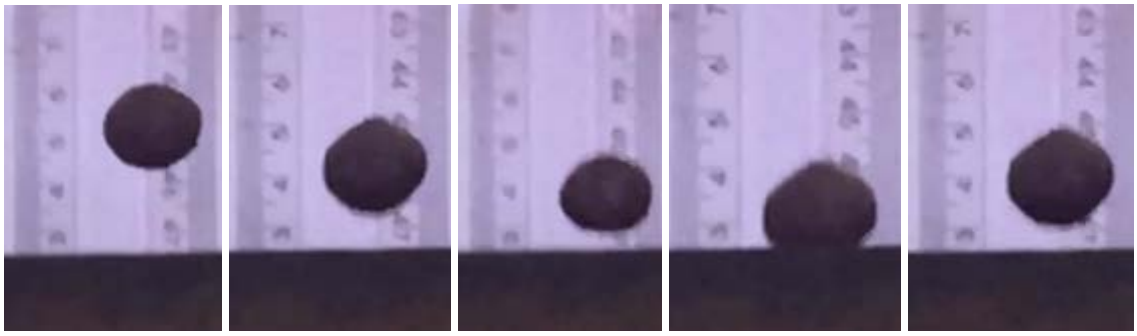

Figure 4.7. Sequential snapshots of a green pellet drop test on a rubber plate.

4.1.2.3 Handling bench test

At last, the handling bench test was carried out in an apparatus originally designed by researchers of the Rock Processing Group at Chalmers University of Technology, Sweden (QUIST, 2017). The LTM version was built in a larger scale that allows testing of samples containing particles of the size range of pellets. A 10 kg sample is fed at the upper part of the device. Its bottom is then opened and pellets flow by gravity over an inclined bulkhead following to the apparatus bottom (Figure 4.8). Such as in the mill test, a translucent acrylic top closes the device and allows the observation of the material behavior.

(a) (b) (c)

Figure 4.8. (a) Handling bench device; (b) physical test start point and (c) simulation representation.

The main focus at this stage was to evaluate how well different contact models could represent/simulate green pellets complex behavior of motion. The droplet (and final) state of consolidation of these solids is, at the same time, sticky due to the viscous binder layer present on covering surface, and elastic-plastic deformable due to their low strength resistance.

4.1.2.4 Tumbling

In the tumbling test (Figure 4.9), 1.96 kg of pellets were fed into a 30.5 cm diameter x 30.5 cm length steel mill. Such quantity corresponds to an apparent filling degree of 10 % in volume. A translucent acrylic top let the visualization of solids motion inside the mill when put in operation. Two different rotational speeds were tested: 40 and 54 rpm. Pellets trajectories and the moments of inertia are carefully observed. The main purpose of tumbling test is to allow estimation of the rolling and static friction coefficients that are most suitable to reproduce pellets motion during the simulations.

Figure 4.9. Tumbling mill test.

4.2 Validation

In order to demonstrate the reliability of estimated parameters for contact model selected from the calibration tests, exploratory simulations of green pellets classification on roller screens were carried out taking into account industrial data collected in the field (Table 4.II, Table 4.III and Figure 4.10). All dimensions of the devices were measured in the field and drawn/reproduced in real scale (1:1).

Table 4.II. Summary of base characteristics of the screen simulated

Input parameter	
Feed rate	130 t/h
Feed conveyor speed	0.36 m/s
Rolls speed	80 rpm
Rolls diameter	75 mm
Rolls length	1.800 mm
Feed conveyor angle	15°

Table 4.III. Green pellets historical size distribution results.

Diameter (mm)	Cumulative passing mass (%)
20.0	100.0
16.0	87.4
12.5	38.8
10.0	9.2
8.0	2.2
6.3	1.0
5.0	0.6

Figure 4.10. Feed conveyor and roller screens in EDEM® creator platform.

At this point, a definition of relevant terms that will be used in the study is relevant, since they will be used in the analysis of roller screens operation:

- Product: pellets contained in the size range of interest, nominally from 8.0 to 18.0 mm;
- Fines: pellets smaller than 8.0 mm in size;
- Coarse: pellets larger than 18.0 mm in size;
- Undersize: mass flow of material screened at roller screens´ first 3/4 length (green rolls in Figure 4.11);
- On-size: mass flow of material screened at roller screens´ last 1/4 length (yellow and blue in Figure 4.11);
- Oversize: mass flow of material not screened through gaps, passing over all rolls and discharged after the last roll;
- Fines removal efficiency: ratio of fines removed as undersize and fines fed, i.e., the complement of the screen by-pass;

- Product screening efficiency: Ratio of pellets ranging from 8 to 18 mm screened as on-size and the same range of pellets fed;

- Loss of production: amount of product pellets screened as undersize or oversize.

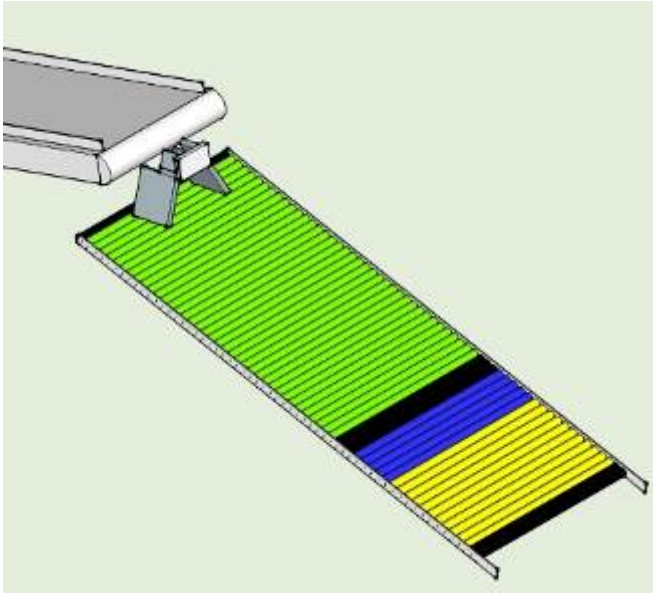

Figure 4.11. Schematic drawing of roller screen classifying areas in EDEM® creator platform.

A base case was analyzed to compare industrial information to simulated results. It is relevant to briefly mention again all limitations encountered in the field and presented in chapter 2 (topics i to vii). Restrictions as closed transfers for screened undersize and oversize make sampling impossible. The only reliable data is the discs return rate (undersize and oversize) recorded by the unique dynamic scale positioned at balling exit return belt.

In EDEM® Analyst platform, all pellets identification, volume and coordinates x, y and z were extracted. Post processing was carried out in Matlab® R2010a from The MathWorks™ and licensed to LTM to determine sizes and masses of pellets that compose all flows classified by the roller screen (Figures 4.12 and 4.13).

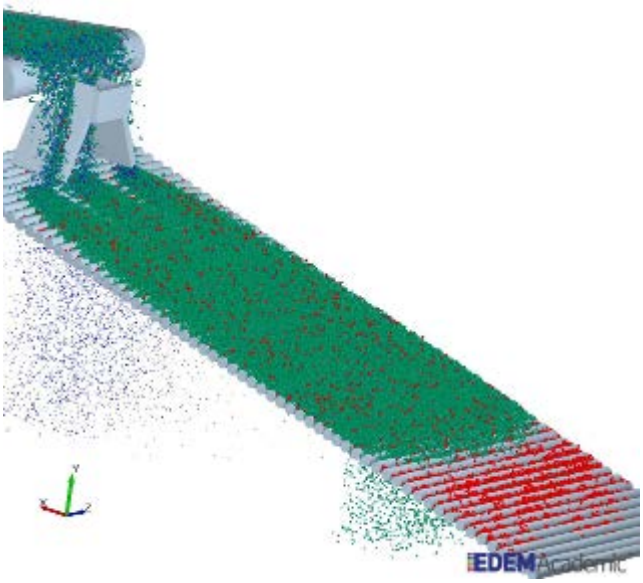

Figure 4.12. Base case simulation of green pellets classification in the roller screen.

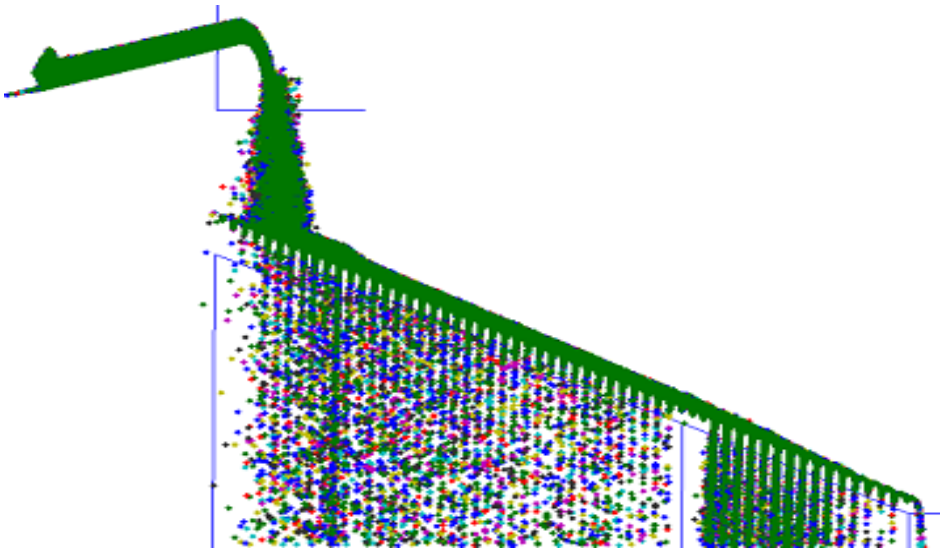

Figure 4.13. Matlab® R2010a analysis for the base case simulation of green pellets classification.

4.3 DOE – Single deck roller screen

In order to evaluate the single deck roller screens operation, a general full factorial DOE was created with 5 two-level factors without blocks, center points and replicates as it follows in Table 4.IV. The variables considered were gap, angle, roll speed and diameter and feed rate. The choice of factors levels was based on historical data

practiced at Vargem Grande plant, roller screen designed production capacity; discs nominal rate and 1800 mm length rolls available diameters on market.

Table 4.IV. Design of experiments for the single deck roller screen

Standard Order	Run Order	A gap (mm)	B angle (°)	C rolls speed (rpm)	D rolls diameter (mm)	E feed rate (t/h)
1	1	8.5	11	80	63.5	130
2	2	9.0	11	80	63.5	130
3	3	8.5	15	80	63.5	130
4	4	9.0	15	80	63.5	130
5	5	8.5	11	120	63.5	130
6	6	9.0	11	120	63.5	130
7	7	8.5	15	120	63.5	130
8	8	9.0	15	120	63.5	130
9	9	8.5	11	80	75.0	130
10	10	9.0	11	80	75.0	130
11	11	8.5	15	80	75.0	130
12	12	9.0	15	80	75.0	130
13	13	8.5	11	120	75.0	130
14	14	9.0	11	120	75.0	130
15	15	8.5	15	120	75.0	130
16	16	9.0	15	120	75.0	130
17	17	8.5	11	80	63.5	160
18	18	9.0	11	80	63.5	160
19	19	8.5	15	80	63.5	160
20	20	9.0	15	80	63.5	160
21	21	8.5	11	120	63.5	160
22	22	9.0	11	120	63.5	160
23	23	8.5	15	120	63.5	160
24	24	9.0	15	120	63.5	160
25	25	8.5	11	80	75.0	160

26	26	9.0	11	80	75.0	160
27	27	8.5	15	80	75.0	160
28	28	9.0	15	80	75.0	160
29	29	8.5	11	120	75.0	160
30	30	9.0	11	120	75.0	160
31	31	8.5	15	120	75.0	160
32	32	9.0	15	120	75.0	160

For the smaller diameter roll case, as the mechanical structures of undersize and on-size transfer cannot be modified, the number of rolls was increased to fill the available space of such areas. Table 4.V presents the roller screens configuration used to simulated.

Table 4.V. Roller screens gaps configuration for 63.5 and 75 mm rolls

63.5 mm rolls		75 mm rolls	
Number of gaps	Positions	Number of gaps	Positions
1	1st gap: 2 mm (transport)	1	1st gap: 2 mm (transport)
44	2nd to 45th gaps: 8.5 or 9.0 mm (undersize)	38	2nd to 39th gaps: 8.5 or 9.0 mm (undersize)
3	46th to 48nd gaps: 2 mm (transport)	3	40th to 42nd gaps: 2 mm (transport)
6	49th to 54th gaps: 14 mm (on-size)	5	43rd to 47th gaps: 14 mm (on-size)
12	55th to 66th gaps: 17 mm (on-size)	10	48th to 57th gaps: 17 mm (on-size)
1	67th gap: 2mm (transport)	1	58th gap: 2mm (transport)

4.4 Double deck roller screen (DDRS)

The main purpose of the double deck roller screen is to remove fines generated by degradation of green pellets during conveying and avoid their entrance into induration machine. The first deck works to reduce the high concentration of pellets in lower deck to optimize fines removal.

Vargem Grande actual design consists of a partial upper deck gapped 18 mm without oversize removal conveyor and a lower deck 8.2 mm gapped (Figure 4.14a). Decks are angled 21° and equipped with 94 mm rolls at 108 rpm.

A complete new double deck screen was designed not only to favor fines removal but also to segregate larger pellets at the top and smaller ones at the bottom (Figure 4.14b) since pellets physical quality is strongly influenced by the heat gradient along the bed height. The first and second decks have gaps equal to 12.5 and 8.2 mm gapped respectively. Both are angled 17°. Configurations containing 94 and 89 mm diameter rolls are then evaluated. Roll speeds are remained unaltered in comparison to the original design used in the plant.

As previously mentioned, pellets sintering is determined by a time-thermal dependent reaction (Equation 2.1). Thermal exchanges and the temperature profile along the depth of the bed of pellets has been studied (SPOSARO, 1962; BATTERHAM, 1986; SESHADRI, 1986; PORMELAU, 2005). As the burners are inserted above the bed and the heat transfer is done under forced convection downstream, the thermal input to top layers is much higher than to the ones at the bottom. At the same time, pellets induration kinetics is topochemically driven, i.e., particle size has great relevance in the process. The finer the particle sizes, the highest their reaction rates.

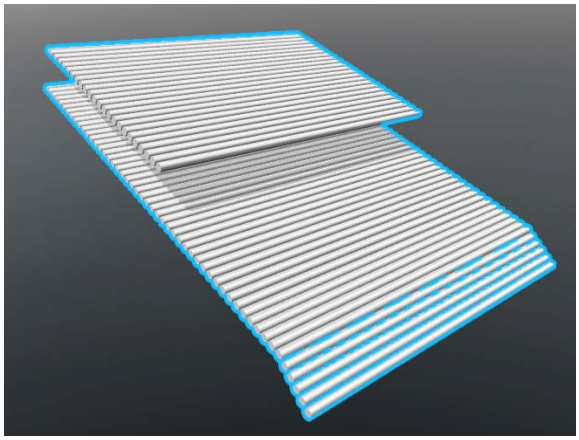

(a)

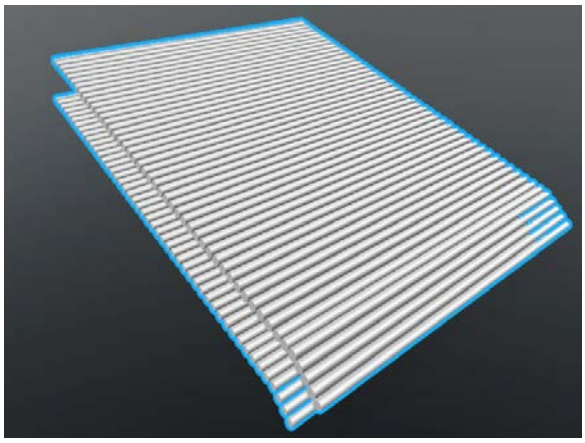

(b)

Figure 4.14. Schematic drawings of (a) actual DRRS; (b) proposed DDRS with complete upper deck.

The size distribution (Figure 4.15) was defined based on samples collected in from the conveyor feed upstream the DDRS. Results for each case will be compared to determine advantages or disadvantages of the proposed design.

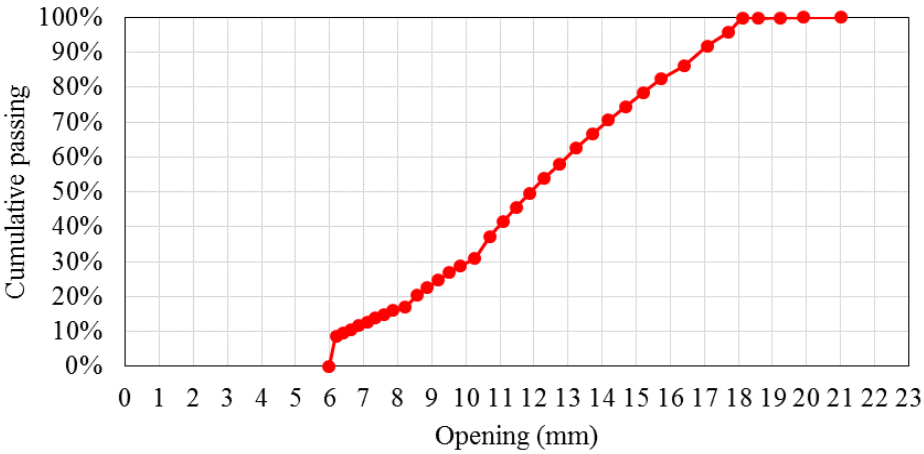

Figure 4.15. Green pellets size distribution fed to DDRS.

5 RESULTS AND DISCUSSION

5.1 Characterization and calibration

5.1.1 Size distribution

A summary of the results obtained are presented in Table 5.I. Usually, the specification pursued in plants is at least 80 to 85 % of green pellets ranging from 8 to 16 mm. As such, results are in good accordance with industrial historic data. The main purpose of green pellets making is to maximize the amount of pellets between 9.5 and 12.5 mm where pellets resistance strength and reducibility are balanced and give the best yield in reduction reactors.

Table 5.I. Green pellets size distribution

Sieve opening (mm)	Retained (%)	Cumulative passing (%)
19.0	0.0	100.0
16.0	1.6	98.4
14.0	5.1	93.3
12.5	18.6	74.7
9.5	59.6	15.1
8.0	11.9	11.9
6.3	2.0	3.2
0.0	1.2	0.0

5.1.2 Hydrostatic bulk density

Green pellets bulk density measured was 3.15 ± 0.48 gcm^{-3}. The variance of such result is fairly wide since the solid is an agglomerate of fines presenting its inherent porosity. In addition, bentonite used as binder, can swell 400 % its own weight by absorbing water.

5.1.3 Moisture content

Pellets moisture content was equal to 9.6 % (weight wet basis). This is the usual range of moisture where agglomerates of hematite iron ores reach their maximum resistance strength.

5.1.4 Drop number test

Table 5.II and Figure 5.1 present the results for the set of pellets tested. The values obtained for the green pellets produced in the laboratory followed the same trend observed by MAYER (1980) and also listed in Table 4.III. It can be verified as well in both aforementioned tables that pellets produced in industrial discs present higher drop number because the magnitude of forces applied are greater than the ones in pilot discs evincing the importance of mechanical forces highlighted by ABOUZEID *et al.* (1979). The compaction is therefore, carried out more effectively in the former.

Table 5.II. Summary of drop number test results

Industrial Disc	Pilot Disc
7.6	5.5

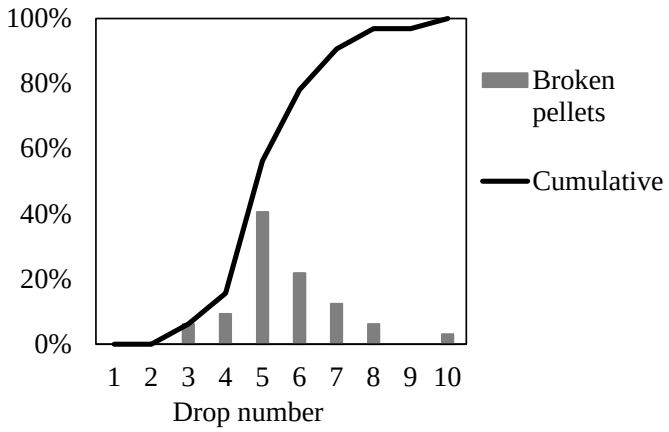

Figure 5.1. Drop number distribution results for green pellets contained in size range 12.5-9.5 mm.

Values close to average obtained are also often found in plants and published in the literature (Table 5.III).

Table 5.III. Typical results for green pellets characteristics (MEYER, 1980).

	Pelletizer		
Parameter	Industrial disc	Pilot disc	Airplane tire
Diameter (m)	6	1	-
Green strength (N/pellet)	7.8	7.6	7.0
Drop number (46 cm)	5.8	4.6	2.6
Moisture (%)	9.3	8.9	7.9

5.1.5 Shape

The pellet surface area and volume of the selected pellet analyzed were 326.7 mm^2 and 555.4 mm^3, respectively (Figure 5.2). A perfect sphere with the same diameter has a surface area equal to 342 mm^2 and a volume of 579.6 mm^3. The ratio between them is 0.96 and suggests that simulating green pellets as perfect spheres is quite reasonable.

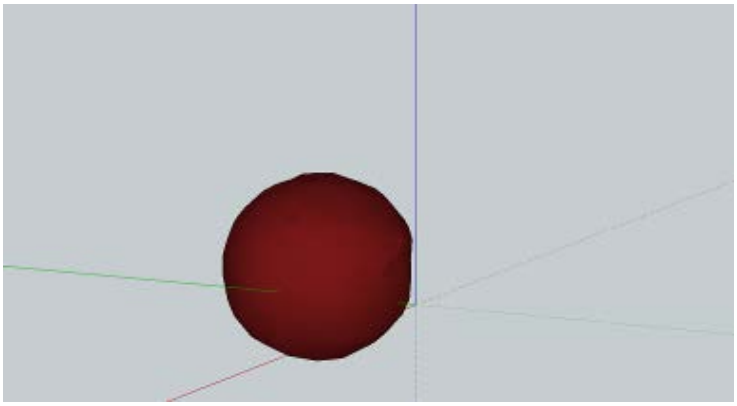

Figure 5.2. Green pellet 3D view on Sketchup®.

5.1.6 Green and dried pellets resistance strength

Green pellets strength values (Table 5.IV) were higher than the plant historic average, which is 14.0 N/pellet. No particular causes were identified for this occurrence. In the case of dried pellet strength, values obtained from the pellets produced in lab were equivalent to those from pellets produced in the industrial scale.

Table 5.IV. Summary of compression test results

	Compression strength (N/pellet)
Green strength	20.8 ± 5.9
Dry strength	32.0 ± 7.5

Equation 5.1 relates Young's, and shear modulus and Poisson rate. Results for the tested set of hematite green pellets is presented in Figure 5.1, which shows single pellet results for each curve represented by a different combination of marker and color. An average response curve was plotted and it is represented by the continuous black line. According to results, pellets mean stiffness is around 4.5 MPa. Shear modulus can then be estimated from Equation 5.1, giving 1.8 MPa. These values are slightly lower than the ones used by WANG *et al* (2015) whose base results were collected from the work by FORSMO *et al* (2006). The Poisson ratio value, equal to 0.25, was assumed, giving

$$G = \frac{E}{2(1+\upsilon)} \tag{5.1}$$

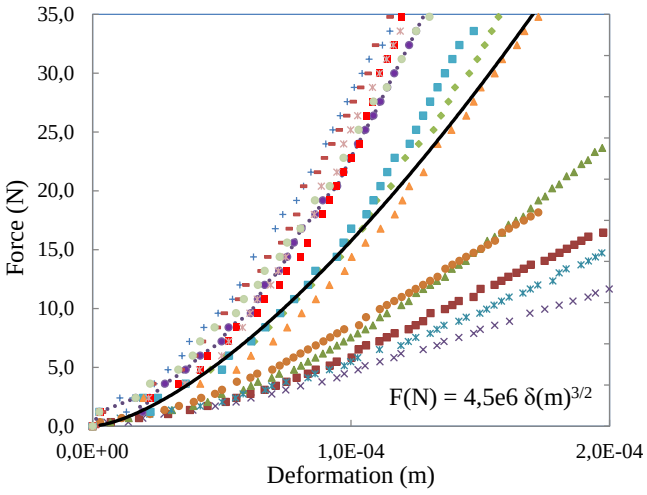

Figure 5.3. Force versus displacement histories for tested green pellets contained in the size range 12.5-9.5 mm.

5.1.7 Angle of repose

The mean repose angle obtained was approximately 27°. The final pellets disposal profile is shown in Figure 5.4 being the cohesive and adhesive forces very relevant on determining the repose angle.

Figure 5.4. Repose angle test: final pile disposal profile.

5.1.8 Restitution

Pellets results have confirmed pellets high amenability to dissipate energy of collisions. Table 5.V summarizes restitution calculated after 1m drop height tests on each different test surface.

Table 5.V Coefficient of restitution test results.

Pellet-Pellet (Mixture layer)	Pellet-Steel	Pellet-Rubber
0.05	0.08	0.05

5.1.9 Handling bench test

Hertz-Mindlin (no-slip) model was discarded due to its inability to reproduce green pellets stick and soft properties. Hysteretic Spring and Hertz-Mindlin with JKR models were then compared since the former simulates plastic deformation when a given overlap is reached between colliding particles and the latter confers to solids some specific surface energy particularly important to describe adhesion of systems such as dry powers or moist particles. It is important to mention that if both models are used

together, EDEM 2.7® does not show any conflict between them, however the forces will be calculated twice i.e., one time by each contact model.

As it can be seen in Figures 5.5 e 5.6, the representation of pellets motion on the handling bench experiment was compared for intermediate and the final moments of the experiment. Details such as the rolling angle made by the pellets at the edge of the angled bulkhead below the feed box (highlighted red circle) and the pile shape at the bottom device at the ending time indicated that the Hertz-Mindlin with JKR contact model (Figures 5.5b and 5.6b) is better suited to reproduce the physical test than the Hysteretic Spring model did (Figures 5.5c and 5.5c).

(a) (b) (c)

Figure 5.5. Handling bench physical experiment and calibration after 4 seconds from beginning (a) Physical experiment (b) Simulation contact model: Hertz-Mindlin with JKR – pellet/pellet: 1.5 J/m^2, pellet/rubber: 0.5 J/m^2, pellet/steel: 0.5 J/m^2 (c) Simulation contact model: Hysteretic Spring – Damping factor: 0.2, Stiffness factor: 0.7.

(a) (b) (c)

Figure 5.6. Handling bench physical experiment and calibration at the end (a) Physical experiment (b) Simulation contact model: Hertz-Mindlin with JKR – pellet/pellet: 1.5J/m^2, pellet/rubber: 0.5 J/m^2, pellet/steel: 0.5 J/m^2 (c) Simulation contact model: Hysteretic Spring – Damping factor: 0.2, Stiffness factor: 0.7.

5.1.10 Tumbling

Observations made when the steel mill rotated at 40 rpm allowed to estimate that green pellets experienced rolling over themselves, being elevated to a shoulder angle up to approximately 330 ° (Figure 5.7). When rotational speed is increased up to 54 rpm, pellets bed rolled the shoulder angle reached 0 ° (Figure 5.8), leading to the occurrence of isolated catarate motion of some individual pellets. The contact parameters used in the simulations were selected by trial-and-error and are presented in Table 5.VI.

Table 5.VI. Summary of material and contact parameters of the no-slip Hertz-Mindlin model

Input parameter	Pellet	Steel	Rubber
Poisson's ratio	0.25	0.25	0.25
Density (kg/m^3)	3150	7800	860

	Interaction		
	Pellet-Pellet	Pellet-Steel	Pellet-Ruber
Coefficient of static friction	0.3	0.35	0.71
Coefficient of rolling friction	0.1	0.25	0.05

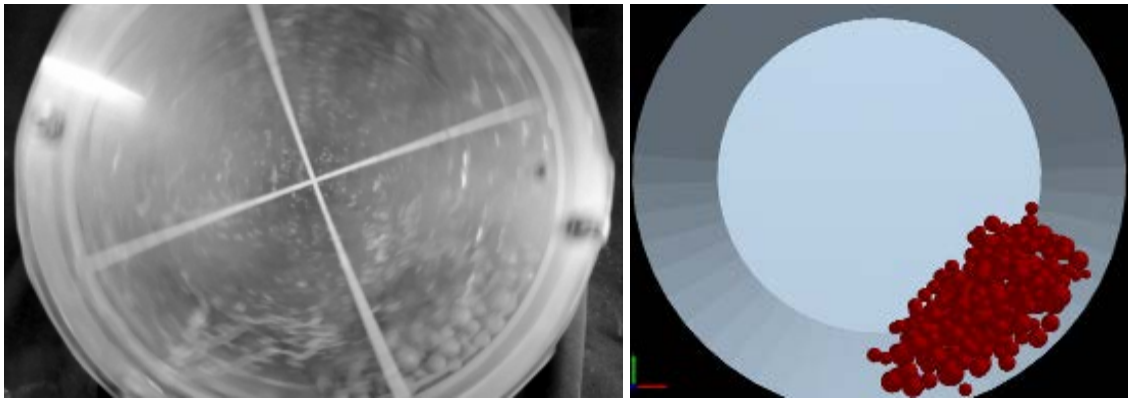

Figure 5.7. Validation of green pellets motion in tumbling mill at 40 rpm rotational speed: experiments (left) and simulation (right).

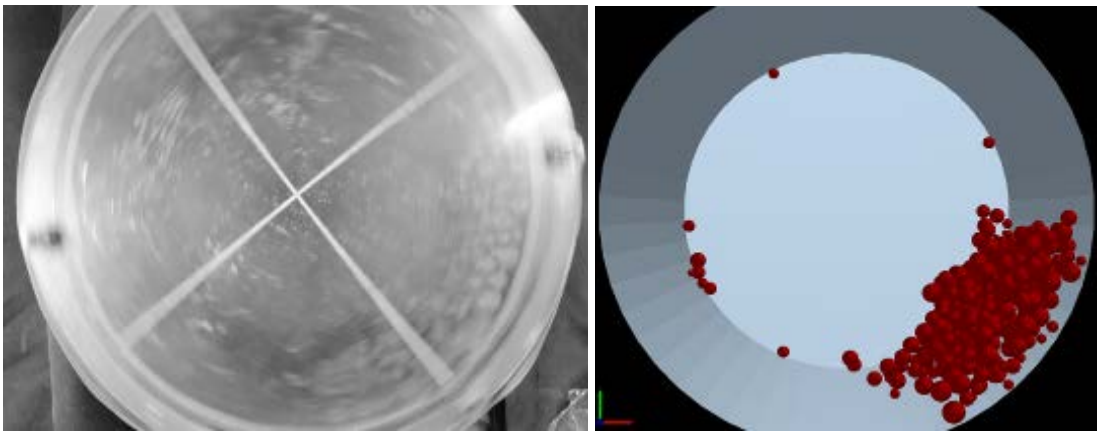

Figure 5.8. Validation of green pellets motion in tumbling mill at 54 rpm rotational speed: experiments (left) and simulation (right).

5.2 Validation and modelling accuracy to exploratory cases

5.2.1 Base case

With the aid of Minitab16® from Minitab Incorporation licensed to VALE SA, the summary of statistical data of daily discs return rate is presented in Figure 5.9. Numbers were collected along 2016 for occasions when the mean discs feed rate was between 125 to 135 t/h; rollers screens equipped with 75 mm rolls at 80 rpm and 8.8 mm gaps for undersize (green in Figure 4.11); and, 14 mm and 18 mm to on-size sieving (yellow and blue in Figure 4.11 respectively).

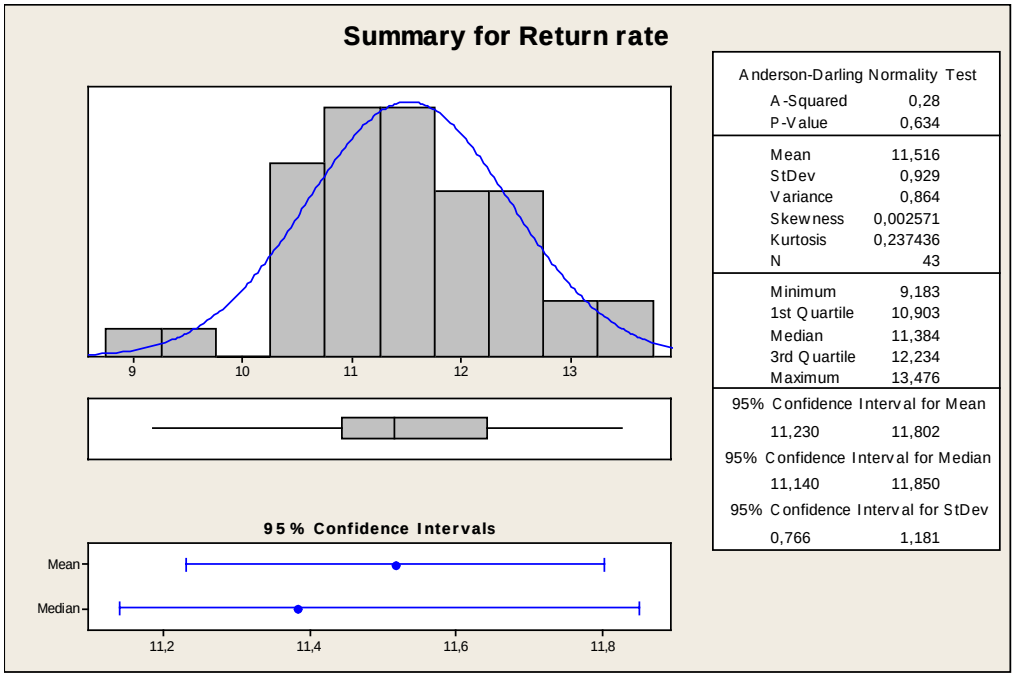

Figure 5.9. Descriptive statistics of the daily discs return rate for Vargem Grande balling circuit in the year of 2016.

The statistical analysis of the operation data, provided the base numbers for the DEM simulation, which required a total number of 213,000 pellet particles. Operation parameters were the following: feed rate was set was to 36 kg/s, i.e., approximately 130 t/h. By the analysis of the flow rates of the three roller screens output, it was observed that the system required a total time of 40 s in order to reach steady-state conditions from the simulation begin when no particles were in simulation. This result can be seen in Figure 5.10: at the beginning only feed is recorded at the conveyor transfer; after 5 s, undersize pellets start to be removed, stabilizing after 20 s at around 10 t/h. From this

moment on, both on size and oversize flows are almost concomitantly registered, reaching relatively constant values after approximately 25 s of simulation. As such, the time interval of time used for estimating the performance indices of the roller screen corresponded to between 40 and 60 s, when all mass flows reached steady-state.

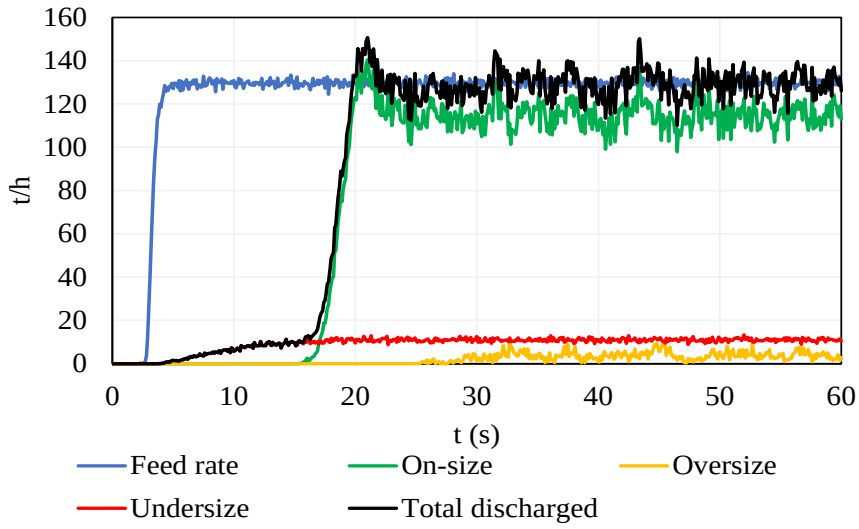

Figure 5.10. Evolution of mass flow registered in simulations for rollers screens screening process for the base case.

A first trial simulation was carried out with pellet particles belonging to only three classes of sizes 6 mm to undersize, 12 mm to on-size and 18 mm to oversize) based on green pellets size distribution historical data from VGR (Table 4.III). Simulations were performed using workstation Dell Precision T7500 equipped with 8 x 3.2 GHz microprocessor, 96 Gb RAM memory and were completed after about 30 h of computation.

Results using three size classes presented a 100 % efficient roller screen, emphasizing the need for a proper representation the size distribution curve of the pellets. As such, the discretization of 36 diameter classes based on the average size distribution of more than 750 samples collected at industrial discs discharge was created as shown in Figure 4.15, being the smallest class 5.9 mm diameter spheres. If smaller particles were allowed, short time steps would be necessary demanding even longer simulations time and generating record files that would be exceedingly large for efficient computation.

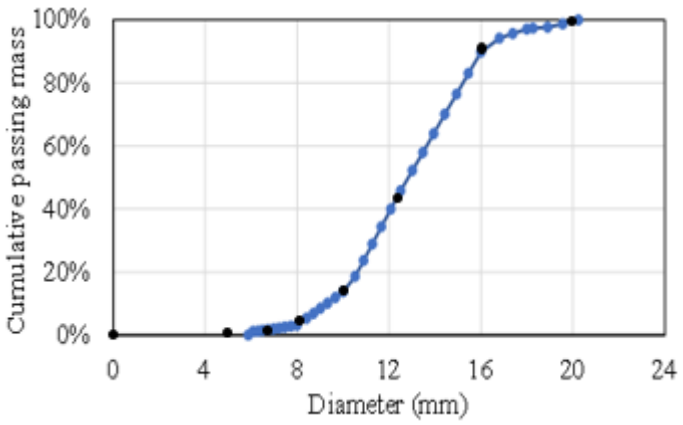

Figure 5.11. Size distribution of green pellets input in EDEM® for 36 particle size classes: black - industrial data, blue – discretization of 36 classes.

Simulation results following a size distribution containing 36 size classes are summarized in Table 5.VII. To make comprehension easier, all numbers presented in all analyzes are given on the basis of Vargem Grande's balling sector, equipped with 11 discs. Simulated discs return rate is in very good agreement with the average value of the industrial data presented in Figure 5.9, being equal to 11.53 % and 11.52 %, respectively. Figure 5.12 illustrates the partition curves for the undersize/on-size and on-size/oversize. The dashed lines represent the undersize and on-size gaps respectively. The percentage of pellets in the left of such lines are the by-pass of each area that corresponds to on-size contamination with fines and the loss of product pellets to oversize respectively.

Table 5.VII. Summarized results of full-scale simulation for the base case in EDEM®.

Responses	
Production loss in undersize	80.2 t/h
Production loss in oversize	2.8 t/h
Total production loss	83.0 t/h
Product share in undersize	66.6 %

Production share in oversize	6.4%
Discs return rate	11.53 %
Discs undersize return rate	8.50 %
Discs oversize return rate	3.03 %
On-size contamination	3.97 t/h
On-size contamination share	0.32 %
Fines screening efficiency	90.7 %
Product screening efficiency	93.7%

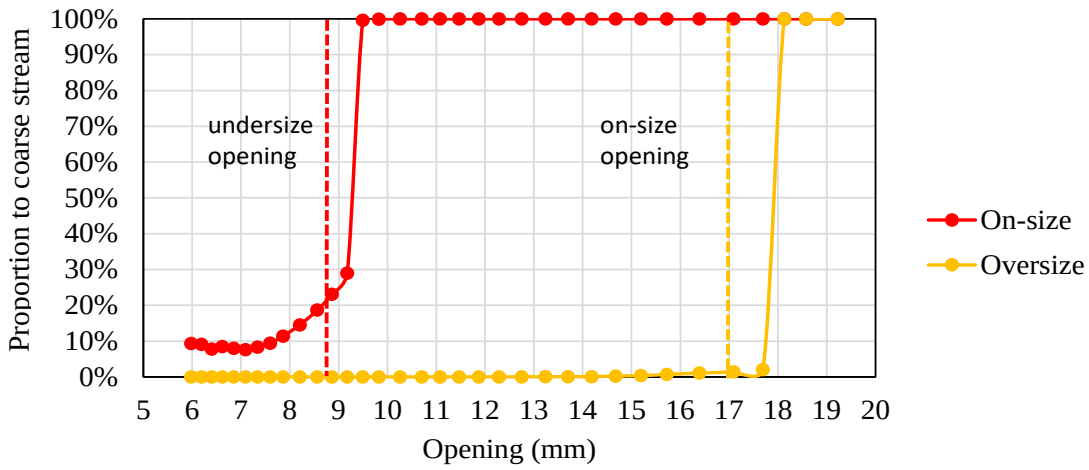

Figure 5.12. Partition curve results.

In order to make a direct assessment of how credible and reliable the modelling is, some exploratory cases were performed by changing some important input parameters. Modelling responses were then verified and compared to real situations.

5.2.1 Moisture content (interaction amongst solids contacts)

One of the most common uncontrolled problems in a pelletizing plant is the raise of feed moisture content in balling. It can happen for many reasons: increase in specific

surface area due to the change in the iron ore mineralogy, change in pH of the slurry that can make filtration very challenging, vacuum inefficiency in filtration or even occurrences of rain when the intermediate pile (reground, filtered and pressed stock) is reclaimed. In those operational situations, the screening process is directly affected. The cohesion among pellets and between them and fines increase substantially and they are carried as a sticked/glued as a compact mass over the rolls. Fines removal efficiency (FRE) considerably drops and on-size contamination is very considerable and harmful to pellets bed permeability in pallets cars.

In order to mimic these cases, the energy of surface of JKR contact model was arbitrarily increased from 1.5 to 2.7 J/m^2 to simulate an increase in moisture content. Results shown in Figure 5.13 and Table 5.VIII are in agreement to observations of real situations afore described. Cohesion among pellets increased to a certain level hauling masses fluxes downstream. Fines by-pass raised approximately 580 % and fines screening efficiency sharply dropped from 92 % to 54 %. Burnt pellets specification consider as product the fraction of pellets ranging from 8 to 18 mm. From such point of view, the loss of production to oversize suffered little impact. Nevertheless, some balling analysts look closely at the range of pellets with sizes from 8 to 16 mm. In this case, the loss of production is more than seven times larger. This is the worst bed condition of operation to green pellets induration sintering process.

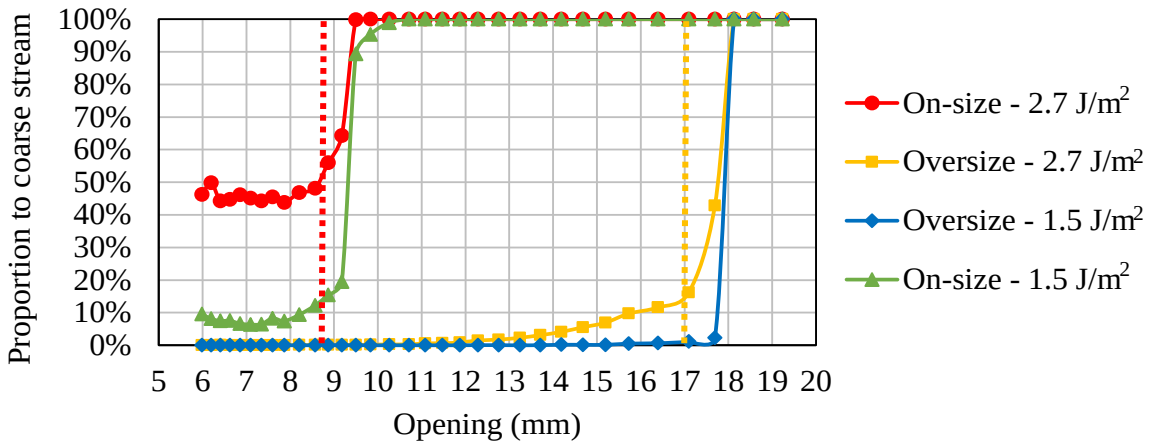

Figure 5.13. Partition curves results with 2.7 and 1.5 J/m^2, representing a high moisture content simulation respectively, of energy of surface in JKR contact model.

Table 5.VIII. Summarized results for simulations involving different moisture contents represented by the choice of different cohesion in the JKR model

Response	JKR Surface Energy Pellet-Pellet	
	1.5 J/m^2	2.7 J/m^2
Production loss in undersize	85.2 t/h	47.1 t/h
Production share in undersize	67.5 %	66.1 %
Production loss in oversize	2.1 t/h	53.4 t/h
Total production loss	87.3 t/h	100.5 t/h
Production share in oversize	7.7 %	57.3 %
Discs return rate	10.95 %	11.61 %
Discs undersize return rate	9.0 %	5.0 %
Discs oversize return rate	1.97 %	6.58 %
On-size contamination	3.48 t/h	20.17 t/h
On-size contamination share	0.28 %	1.61 %
Fines removal efficiency (FRE)	92.4 %	54.4 %
Product screening efficiency (PSE)	92.88 %	91.71 %
Global screening efficiency (GSE)	85.82 %	48.89 %

5.2.2 Gap

The present work deals with a range of solids with sizes that vary in a narrow size range. The differences pursued for discs return rates, although may influence some millions of dollars if analyzed on the basis of annual amounts, are reasonably small (0.5 – 2.5 %). The actual case analysis is carried out for undersize gap lengths of 7.5 mm and 9.0 mm. Both openings have already been used in actual operation at Vargem Grande. All the others input parameter and geometry dimension are maintained constant.

Results are plotted in Figure 5.14. For a narrower gap, it is evident that the loss of production practically vanishes, since the finer product pellets (8-10 mm) are unable to pass through the undersize gaps. However, on-size contamination is 3.4 times greater than when the 9.0 mm gapped screen is used. 20 % of fines by-pass is a substantial amount comparable for example to hydrocyclones separation process. Indeed, this narrower setting is not advisable in practical application due to the high amount of fines contaminating the on-size stream and results are in very good agreement with results

reported by WELLSTEAD *et al.* (1978). At the same time, due the narrower gap, the 7.5 mm gapped screen works with a higher amounts of pellets at the on-size screening area. As consequence, the loss of product to oversize is 4.5 times larger. The global screening efficiency (GSE), i.e, the product of fines removal and product screening efficiencies (FRE and PSE, respectively) is almost 7 % smaller for the narrower gap as detailed in Table 5.IX.

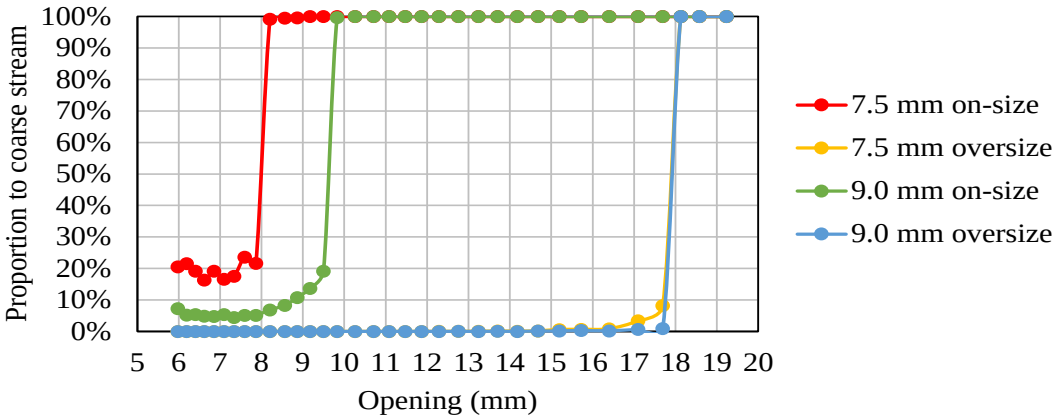

Figure 5.14. Partition curves results for 7.5 and 9.0 mm undersize gaps.

Table 5.IX. Summarized results for 7.5 mm and 9.0 mm undersize gaps length.

Response	Undersize gap length	
	7.5 mm	9.0 mm
Production loss in undersize	0.4 t/h	111.1 t/h
Production share in undersize	1.2 %	72.6 %
Production loss in oversize	4.5 t/h	1.0 t/h
Total production loss	5.0 t/h	112.0 t/h
Production share in oversize	10.1 %	2.3 %
Discs return rate	5.67 %	13.68 %
Discs undersize return rate	2.5 %	10.7 %
Discs oversize return rate	3.14 %	2.96 %
On-size contamination	8.74 t/h	2.60 t/h
On-size contamination share	0.65 %	0.21 %
Fines removal efficiency (FRE)	80.0 %	94.3 %
Product screening efficiency (PSE)	99.46 %	91.61 %

Global screening efficiency (GSE)	79.55 %	86.42 %

5.2.3 Pellets stiffness influence on modelling results

A theoretical comparison of situations was carried out in order to evaluate how modelling responses vary to distinct pellets stiffness. The shear modulus input parameter was set 1 MPa and 2.4 MPa for equal simulations, i.e., all other input parameter remained unaltered. Results are presented in Figure 5.15 and Table 5.X.

One of the important findings from the model calibration was the significant influence of shear modulus on the simulation outcome. As it can be noticed in Figure 5.3, results of compression tests showed the inherent variance among pellets, even though produced under controlled conditions in laboratory and reflected that mean shear modulus can range in some extent (further details are discussed by FORSMO *et al.*, 2006). When the shear modulus is set to a larger value, i.e., pellets are more rigid, the result is an increase of the oversize amount in some extent that did not correspond to real situations. In contrast to that, softer particles exhibited larger elastic deformation, i.e., let higher overlaps take place (Figure 5.16), being pulled through rolls gaps and increase the undersize stream. Fines by-pass is slightly higher for softer particles because production pellets occupy the gap passage hauling fines downstream. For the same reason the smaller production pellets (9 to 10 mm) share in on-size is lower for the low-level case as they were screened in undersize. Global screening efficiency decreased substantially indicating the highly relevant is the role of elastic-plastic deformation for pellets classifying in roller screens.

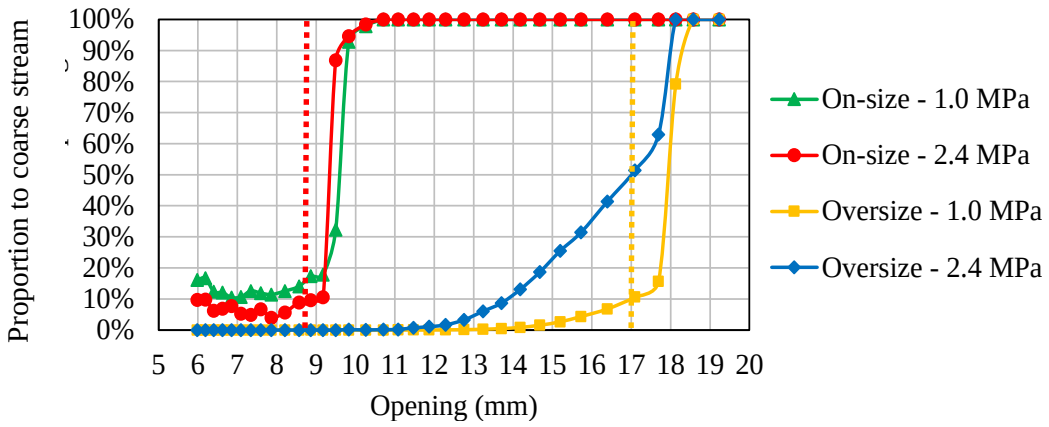

Figure 5.15. Partition curves results for 1.0 MPa and 2.4 MPa shear modulus pellets.

Table 5.X. Summarized results for softer and more rigid solids.

Response	Shear modulus	
	1.0 MPa	2.4 MPa
Production loss in undersize	38.6 t/h	36.3 t/h
Production share in undersize	68.7 %	65.5 %
Production loss in oversize	31.6 t/h	219.7 t/h
Total production loss	70.22 t/h	255.96 t/h
Production share in oversize	23.8 %	68.0%
Discs return rate	13.28 %	26.39 %
Discs undersize return rate	3.9 %	3.9 %
Discs oversize return rate	9.33%	22.52 %
On-size contamination	5.14 t/h	1.65 t/h
On-size contamination share	0.42 %	0.16 %
Fines removal efficiency (FRE)	86.2 %	89.9 %
Product screening efficiency (PSE)	94.53 %	77.74 %
Global screening efficiency (GSE)	81.49 %	69.89 %

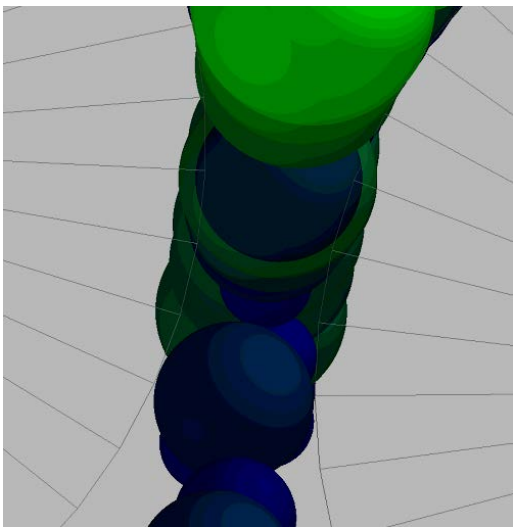

Figure 5.16. Snapshot of roller screen simulation showing pellets passing through rolls gap. Deformation simulated through overlaps for the case with a shear modulus of 1.0 MPa.

5.2.4 Feed size distribution sensibility

Two distinct feed size distributions (fine and coarse) were simulated to evaluate its effect on roller screen performance obtained through simulations. These size distributions are based on the first and third quartiles of pellets mean historical diameter. They are illustrated in Figure 5.17.

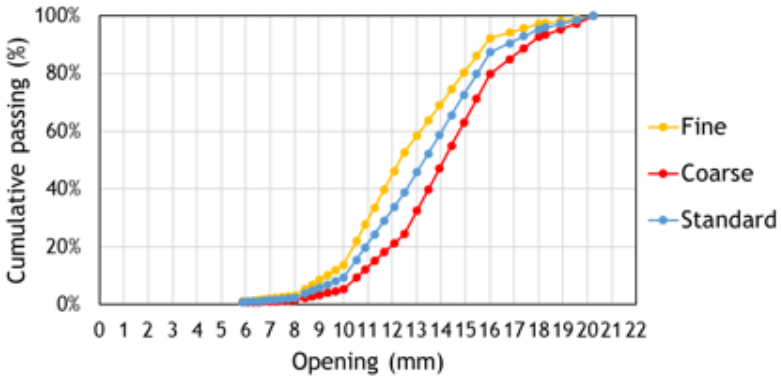

Figure 5.17. Fine and coarse size distributions.

Results shown in Figure 5.18 and Table 5.XI are in accordance to observations of real situations. When discs produce smaller (higher specific surface area, low moisture content, fine feed fineness, higher addition of bentonite etc) or larger pellets for any reason, the response of discs return rate is immediate and balling yield unavoidable decreases. Discs control and maintenance are very relevant to reach success on pellets making and higher rates balling outputs.

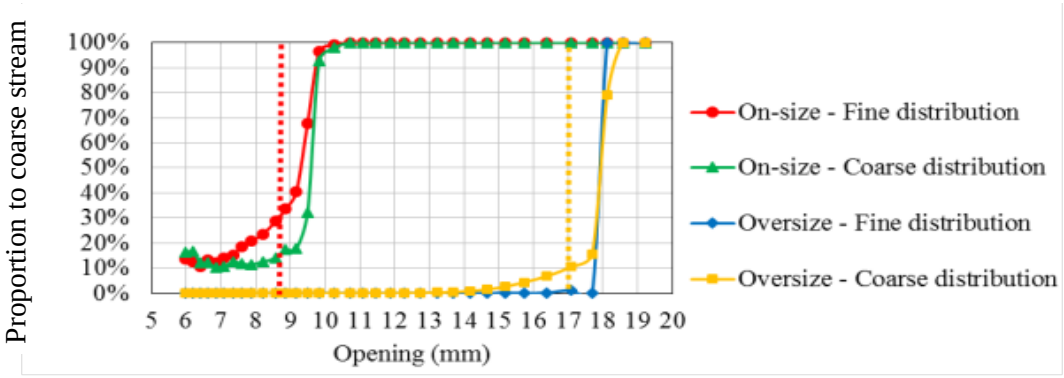

Figure 5.18. Partition curves results for feeds containing fine and coarse pellet size distributions.

Table 5.XI. Summarized results for fine and coarse distribution.

Response	Size distribution	
	Fine	Coarse
Production loss in undersize	78.9 t/h	38.6 t/h
Production share in undersize	67.7 %	68.7 %
Production loss in oversize	0.6 t/h	31.6 t/h
Total production loss	79.46 t/h	70.22 t/h
Production share in oversize	1.3 %	23.8 %
Discs return rate	11.16 %	13.28 %
Discs undersize return rate	8.2 %	3.9 %
Discs oversize return rate	2.95 %	9.33 %
On-size contamination	6.44 t/h	5.14 t/h
On-size contamination share	0.51 %	0.42 %
Fines removal efficiency (FRE)	84.4 %	86.2 %
Product screening efficiency (PSE)	93.64 %	94.53 %
Global screening efficiency (GSE)	79.07 %	81.49 %

5.2.5 Resolution of the geometries

Another noticed difference was detected when simulating solid parts of the geometry of the system such as the steel rollers, with different degrees of details. The circular sides of a cylinder geometry built on EDEM® are described as circumferences with 50 segments/faces. Nevertheless, more or less accurate surfaces can be constructed using other graphics/CAD platforms and then be imported into the simulator. This is particularly critical in the case of the rolls that make up the screen surface (Figure 5.19). It was observed that changes on geometries modified the motion of particles since more/less interactions take place. For higher resolution geometries, for instance, when the cylindrical circular faces were represented by more than 50 segments, interactions between pellets and rolls increased classification performance, i.e., undersize flowrate increased and oversize flowrate reduced (Figure 5.20). Table 5.XII compares results obtained from identical simulations ran with distinct resolution geometries. It shows that simulation results are, indeed, influenced by the level of detail used to describe the

rolls being very relevant to results since differences pursued are little. Such observations are in accordance to conclusions from THORNTON *et al.* (2017) conclusions that contacts models involving adhesive interactions may only be used after careful calibration and validation.

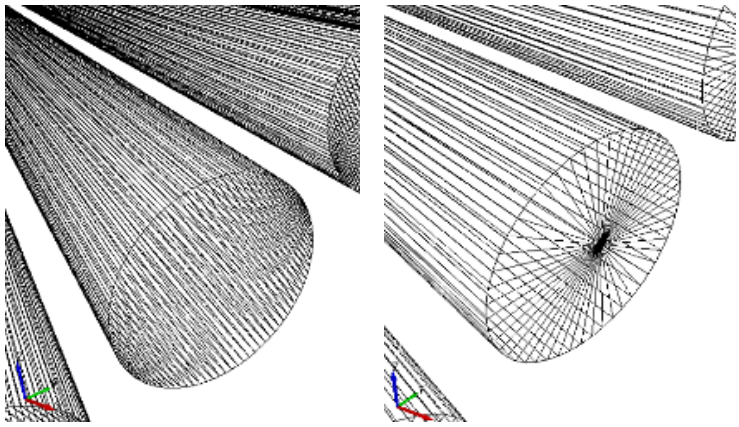

a b

Figure 5.19. (a) High resolution rolls (b) Low resolution rolls

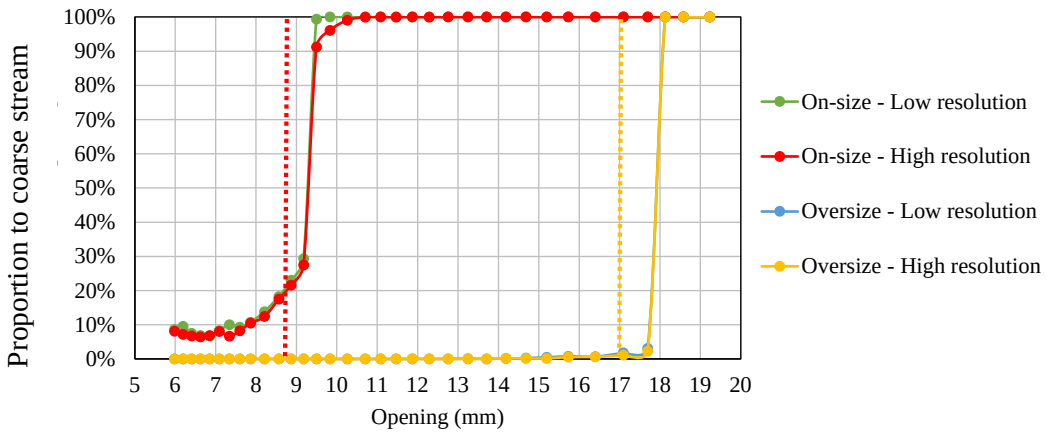

Figure 5.20. Partition curves results for low and high resolution of the rolls.

Table 5.XII. Results for different geometric resolutions of the rolls

Response	Geometry refinement	
	Low resolution	High resolution
Production loss in undersize	80.6 t/h	85.2 t/h

Production share in undersize	66.6 %	67.5 %
Production loss in oversize	3.1 t/h	2.1 t/h
Total production loss	83.7 t/h	87.3 t/h
Production share in oversize	6.9 %	7.7 %
Discs return rate	11.63 %	10.95 %
Discs undersize return rate	8.50 %	8.98 %
Discs oversize return rate	3.13 %	1.97 %
On-size contamination	3.8 t/h	3.5 t/h
On-size contamination share	0.30 %	0.28 %
Fines removal efficiency (FRE)	91.1 %	92.4 %
Product screening efficiency (PSE)	93.5 %	92.9 %
Global screening efficiency (GSE)	85.2 %	85.8 %

5.3 Simulation strategy

Computational resources and research scope (object and time) are key issues that must be always equalized. 30 h simulations, as done for the base case, would force a reduction of scope of work and could limit the number of variables of interest to be evaluated. With the aim of reducing simulation time and still making it possible to get reliable results, the simulation domain was diminished as shown in Figures 5.21 (a) to (d). For the half domain case, Figure 5.21b, a very low friction invisible plane was positioned at the axis of symmetry, along the longitudinal length, of the roller screen. For sliced simulations, 100 and 300 mm in Figures 5.21 (c) and (d), periodic boundary tool on x-axis was enabled, i.e., if any solid reaches the limits of the domain, it comes back in the opposite boundary in an analogous position keeping the same interactions to particles even towards opposite boundaries. Table 5.XIII summarizes the results for each case.

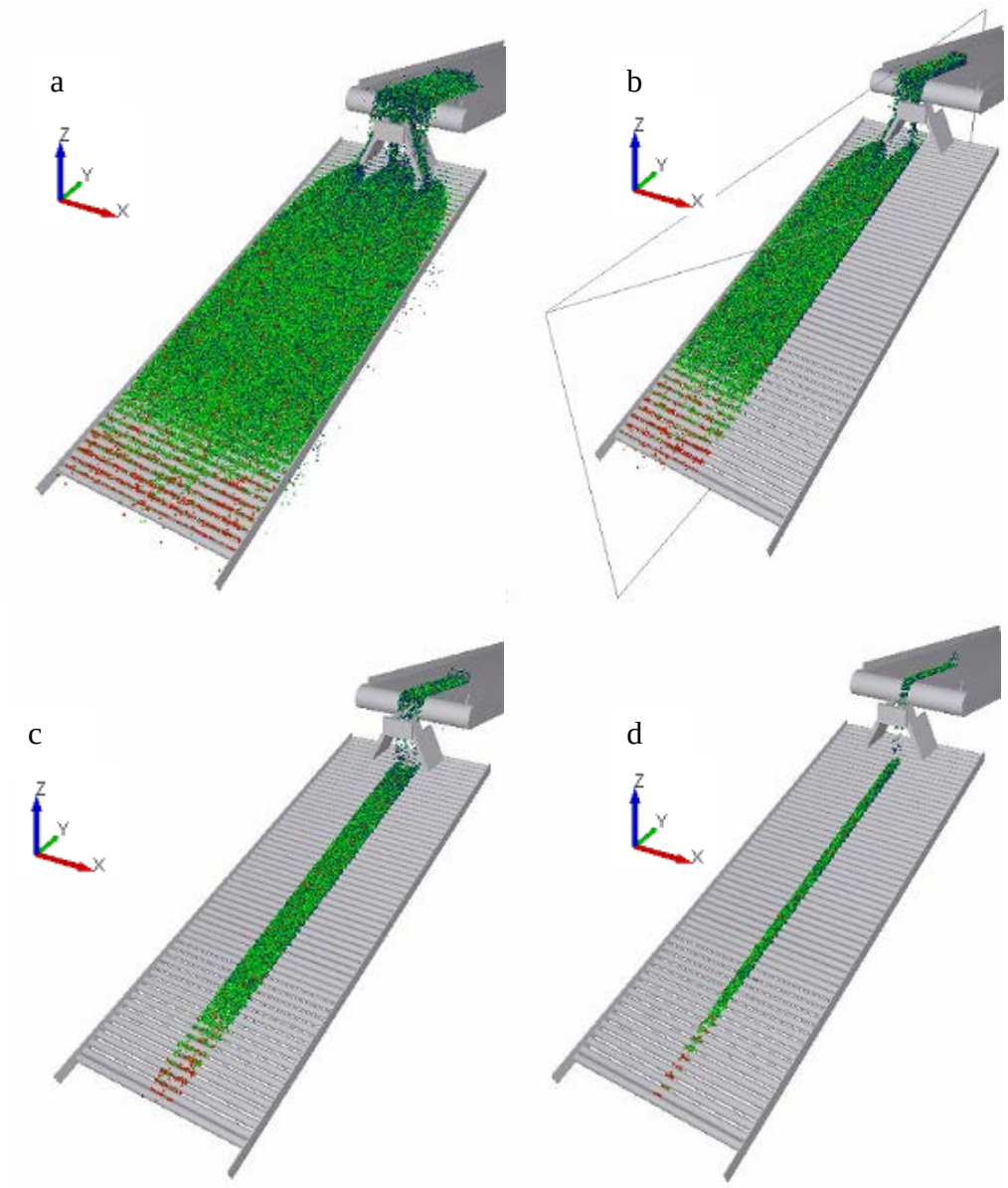

Figure 5.21. Roller screens sieving for different domains (a) full scale (b) half scale – 900 mm – with no friction split wall (c) 300 mm slice with periodic boundary in x-axis (d) 100 mm slice with periodic boundary on x-axis.

Table 5.XIII. Comparison of simulation results for different length domains of analysis.

Response	(a) Full-scale	(b) Half case	(c) 300 mm slice case	(d) 100 mm slice case
Production loss in undersize (t/h)	80.2	80.6	85.4	85.0

Product share in undersize	66.6 %	66.6 %	67.6 %	66.6 %
Production loss in oversize (t/h)	2.8	3.1	2.1	9.6
Total production loss (t/h)	82.9	83.7	87.54	94.60
Production share in oversize	6.4 %	6.9 %	4.9 %	17.1 %
Discs return rate	11.50 %	11.63 %	11.68%	12.27 %
Discs undersize return rate	8.47 %	8.50 %	8.70 %	8.53 %
Discs oversize return rate	3.03 %	3.13 %	2.98 %	3.74 %
On-size contamination (t/h)	3.97	3.82	3.95	4.52
On-size contamination share	0.32 %	0.30 %	0.31 %	0.34 %
Product screening efficiency	93.66 %	93.51 %	94.06 %	92.90 %

It is evident from the simulations that the layer of pellets becomes wider over the rolls as the domain of analysis is gradually reduced and deviates the results from the full case reference and industrial data mean return rate. The screening process efficiency decreased because some particles on the top of the layer did not have the opportunity to reach the gap opening and escape through it. As consequence, larger amounts of fines remain on the pellet bed and contaminate the on-size product. Production loss to oversize is also increased for the same reason. Although the 300 mm slice simulation presents reasonable estimates of discs return rates (total, undersize and oversize), it indicated higher loss of production when compared to full a half scale cases (around 85 t/h versus 80 t/h respectively - Table 5.XIII). In the case of 100 mm slice simulation, results are very different for many responses.

The evaluation of the combined effect of each variable, listed in Chapter 2, is carried out through a Design of Experiments (DOE) methodology (MONTGOMERY, 2013) for half scale simulations drawn at an only geometry resolution level.

Different response variables were considered in the simulations, which are analyzed as follows.

5.3.1 Return rate

The first analysis of the experimental design was carried out in order to identify the relevant factors and interactions which may influence the return rate (Figure 5.22) and described on Table 5.XIV.

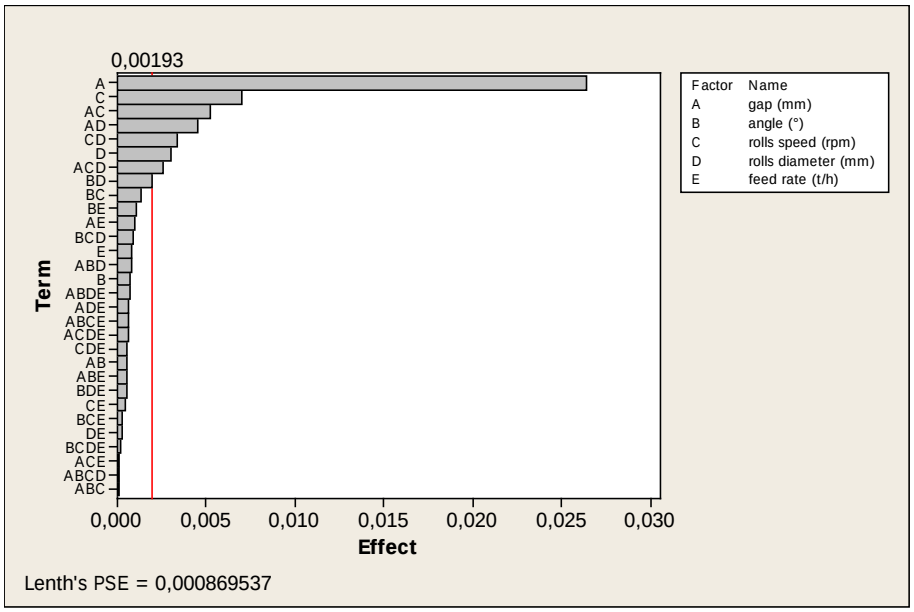

Figure 5.22. Pareto chart of 30 largest effects for return rate (%), significance level: 0.05.

Table 5.XIV. Summary results for significant effects for return rate

Main factors	
A	Undersize gaps length (mm)
C	Rolls rotational speed (rpm)

D	Rolls diameter (mm)
	Second order interactions
AC	Undersize gaps length (mm) * Rolls speed (rpm)
AD	Rolls rotational speed (rpm)* Rolls diameter (mm)
CD	Rolls rotational speed (rpm) * Rolls diameter (mm)
BD	Angle (°) * Rolls diameter (mm)
	Third order interaction
ACD	Undersize gaps length * Rolls rotational speed (rpm) * Rolls diameter (mm)

Non-significant factors and interactions are excluded from the model and the analysis is carried out for the significant ones. Due to the increase of degrees of freedom, the squared mean error statistic is calculated and the variability of the model response and the residual can be estimated as well. It can be inferred that residuals are normally distributed, without any special observation occurrence, with approximately the same variance along the return rates results and the time (Figure 5.23).

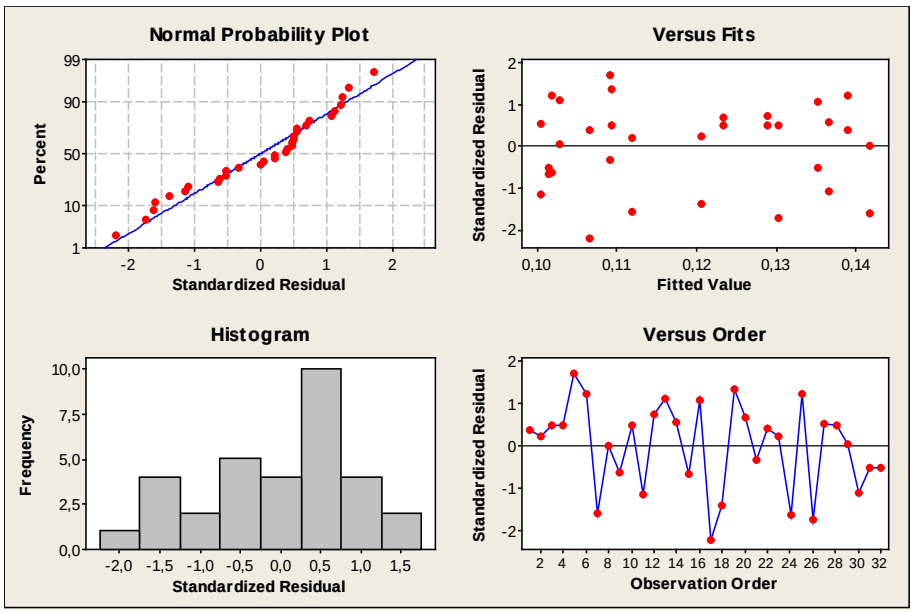

Figure 5.23. Residuals plot for return rate.

Amongst the variables studied, only the gap, the roll speed and the roll diameter were found to influence as individual variables the return rate (Figure 5.24). Angle was only found to have an influence when interacting with other variables. The feed rate, given in percentage of the feed, did not influence the return rate, given in percentage of the feed. Detailed results of the statistical analyzes are presented in Table 5.XV.

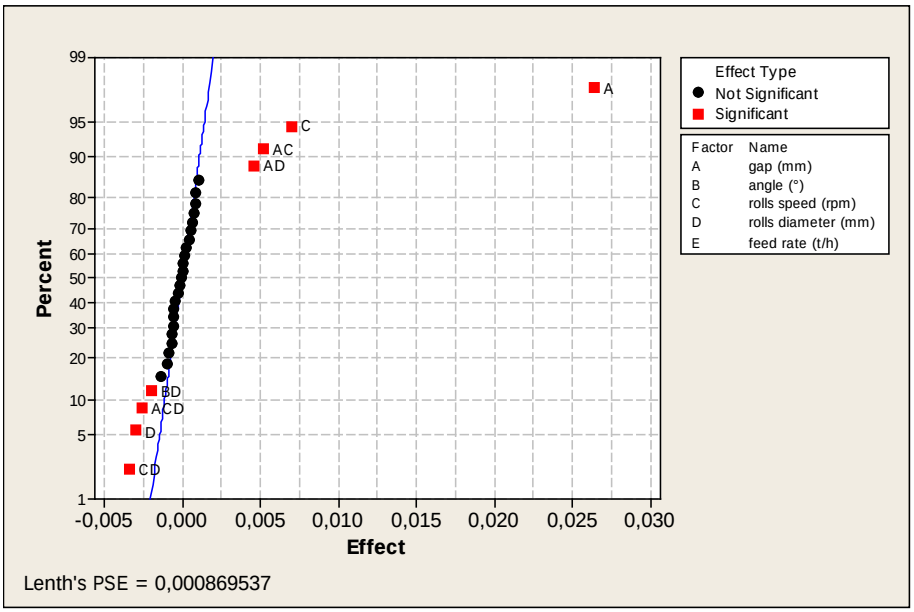

Figure 5.24. Normal plot of the standardized effects for the significant factors and interactions for return rate.

In Figure 5.24, it can be seen in the normal plot of effects the relevant factors and interactions. The model can explain 98.91 % (Table 5.XV) of the variation of the return rate.

Table 5.XV. Summary results for estimated effects and coefficients for return rate (coded units).

Term	Effect	Coef	SE Coef	T	P
Constant		0.118652	0.000321	369.46	0
gap (mm)	0.026419	0.01321	0.000321	41.13	0
angle (°)	0.000734	0.000367	0.000321	1.14	0.266
rolls speed (rpm)	0.00702	0.00351	0.000321	10.93	0

rolls diameter (mm)	-0.003	-0.0015	0.000321	-4.68	0
gap (mm)*rolls speed (rpm)	0.005209	0.002605	0.000321	8.11	0
gap (mm)*rolls diameter (mm)	0.004568	0.002284	0.000321	7.11	0
angle (°)*rolls diameter (mm)	-0.00198	-0.00099	0.000321	-3.09	0.005
rolls speed (rpm)*rolls diameter (mm)	-0.00341	-0.00171	0.000321	-5.31	0
gap (mm)*rolls speed (rpm)*rolls diameter (mm)	-0.00254	-0.00127	0.000321	-3.96	0.001

S = 0.00181670

PRESS = 0.000153619

R-Sq = 98.91 %

R-Sq(pred) = 97.70 %

R-Sq(adj) = 98.47 %

Equation 5.2 is a multiple variable regression expression and cannot be directly used to describe how each factor acts on process. It is only a mathematical representation for the factors levels intervals. Factorial plots illustrate factors (Figure 5.25) and interactions (Figure 5.26 and 5.27) influences for better comprehension.

$$\begin{aligned} &returnrate(\%) = 3.5716 - 0.415438 \cdot gap(mm) - 0.0301437 \cdot rollspeed(rpm) \\ &- 0.0502441 \cdot rolldiameter(mm) + 0.00358239 \cdot gap(mm) \cdot rollspeed(mm) \\ &+ 0.00600987 \cdot gap(mm) \cdot rolldiameter(mm) \\ &- 0.0000862 angle(°) \cdot rolldiameter(mm) \\ &+ 0.000372 rollsspeed(rpm) \cdot rolldiameter(mm) \\ &- 0.00004421 \cdot gap(mm) \cdot rollspeed(rpm) \cdot rollsdiameter(mm) \end{aligned} \tag{5.2}$$

Gap is therefore the factor among all others and their interactions that most influence on return rate within the range of values studied (Figure 5.25). The cube plot means for return rate and the interactions plot are shown in Figures 5.26 and 5.27 respectively.

Still according to the results, the return rate is directly influenced by rolls speed. When rolls rotate faster, the bed of pellets becomes thinner and the distance to reach the

gap openings is reduced. Moreover, the adhesion sticky interaction between pellets roll surfaces (reason why rolls must be often cleaned) promotes the passage of pellets through gaps openings. The relative speed between the precedent and the following roll also promotes more deformation on pellets forcing their passage into the flow of material that passes the screen.

Return rate varies inversely proportional to roll diameters only because there are more gaps available since more rolls are installed in the permanent space of undersize transfer (Table 4.V).

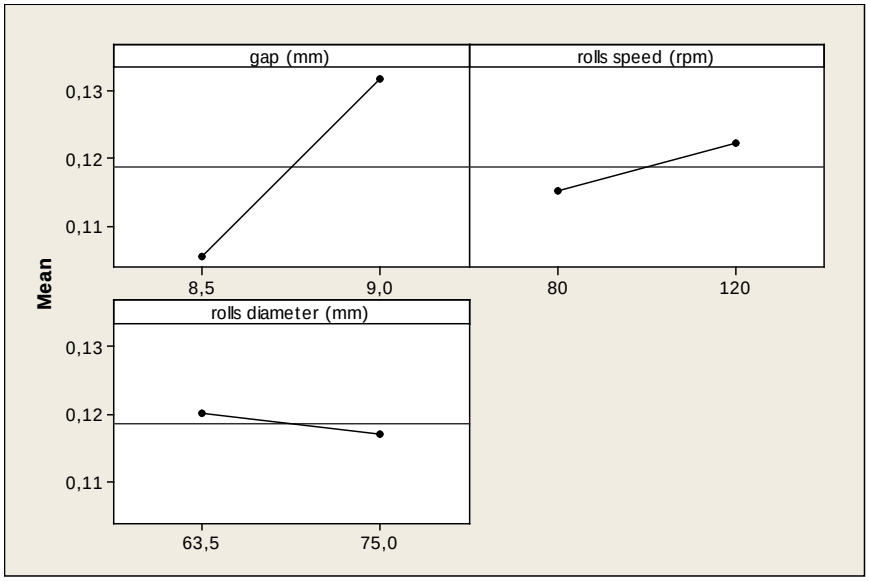

Figure 5.25. Main effects plots for return rate.

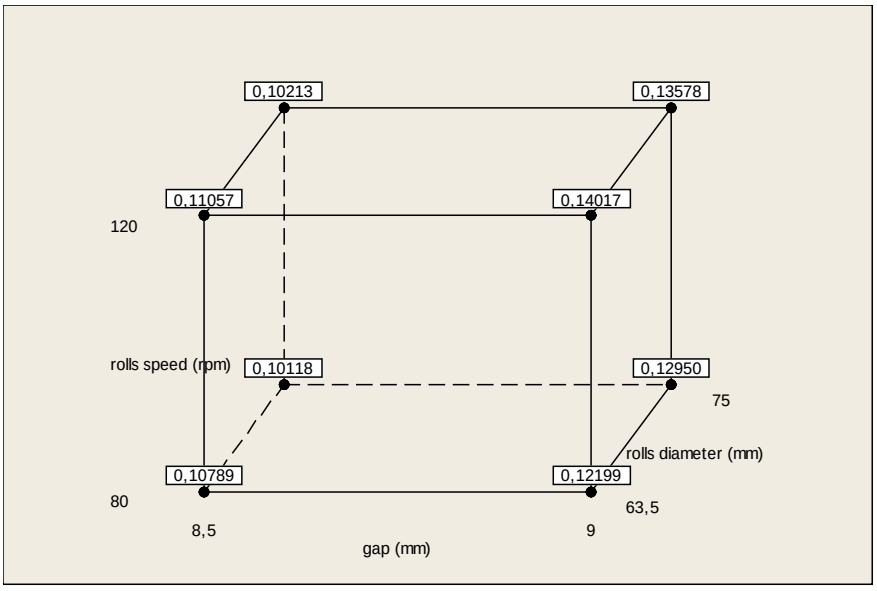

Figure 5.26. Cube plot data means plot for main relevant factors on return rate.

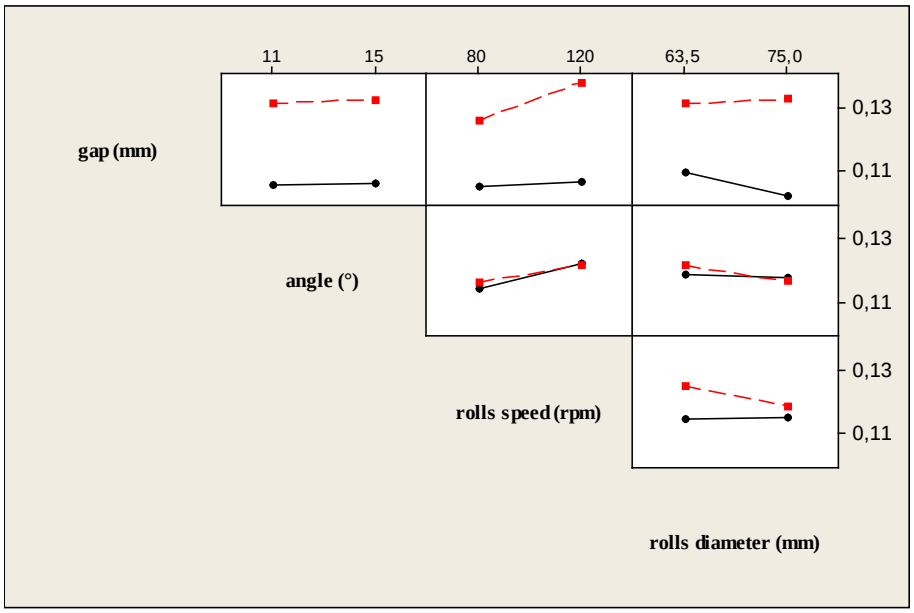

Figure 5.27. Interactions plot for return rate.

Although the analysis of return rate is important, practical recommendations should not be made exclusively based on it. High or low return rates do not mean anything by themselves. Low return rates can be reached by undersize gaps narrowing but on-size contamination with fines can at the same increase and harm bed permeability on travelling grate induration machines. On the other hand, high return rates, although guarantee bed permeability, they can, such as at Vargem Grande, restrict the productivity due the loss of good pellets screened. Other aspects inherent to each plant such as the iron ore nature and its properties (fineness, moisture content, specific surface area), the type of binder, the level of automation, the type and capacity of balling devices (discs or drums), may also influence the results. For such reasons deeper analyzes on the basis of other metrics, such as loss of production, contamination amount in on-size flow, fines removal and product sieving efficiency are conducted.

5.3.2 Fines removal efficiency

As presented before, balling is usually equipped by roller screens downstream balling devices and a double deck roller screen, also called feeder, at induration

machine entrance. One of the main purposes of the former screens is to remove fines to assist operation of the double deck screen since the concentration of pellets at this point is much higher. Fines removal is defined by the ratio of fines screened in undersize stream and fines fed:

$$\text{Fines removal efficiency} = \frac{\text{fines (undersize stream)}}{finesfed} \tag{5.3}$$

A preliminary analysis (Figure 5.28) for fines removal efficiency indicated that all main factors and two-second order interactions, CD and AD, affected it significantly. They are summarized in Table 5.XVI and plotted in Figure 5.29.

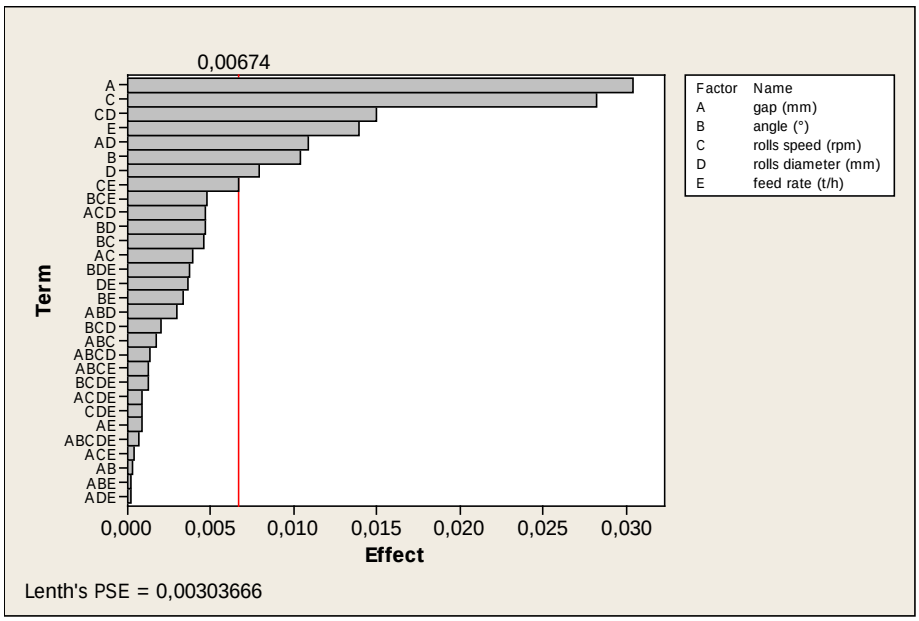

Figure 5.28. Pareto chart of 30 largest effects for return fines removal efficiency, significance level: 0.05.

Table 5.XVI. Summary results for significant effects for fines removal efficiency

	Main factors
A	Undersize gaps length (mm)
B	Angle (°)

C	Rolls rotational speed (rpm)
D	Rolls diameter (mm)
E	Feed rate (t/h)
	Second order interactions
AD	Undersize gaps length (mm) * Rolls diameter (mm)
CD	Rolls rotational speed (rpm) * Rolls diameter (mm)

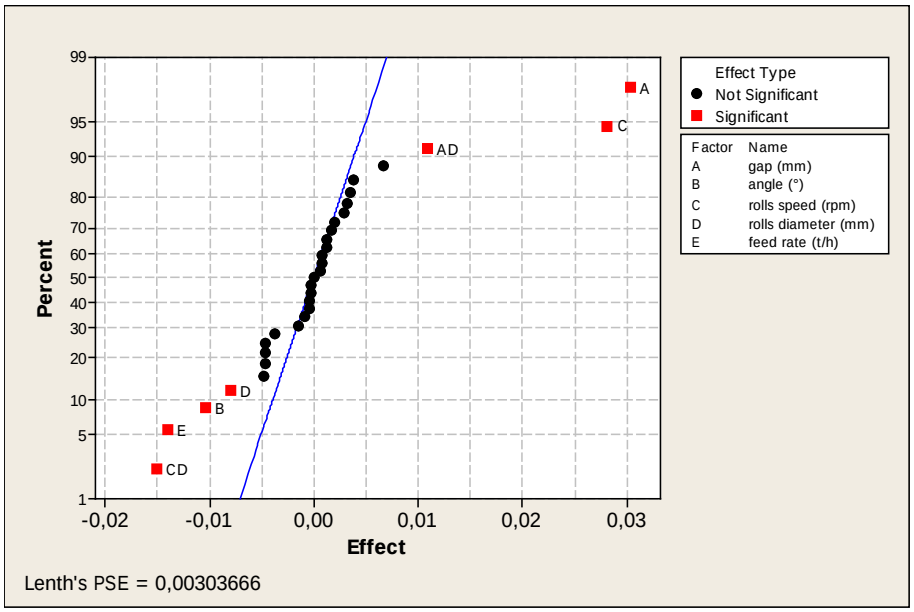

Figure 5.29. Normal plot of the standardized effects for factors and interactions for fines removal efficiency.

No third-order interaction effect influenced fines removal efficiency. The model explains 92.11% of the variability encountered in the data from the simulations (Table 5.XVII).

Table 5.XVII. Summary results for estimated effects and coefficients for fines removal efficiency (coded units).

Term	Effect	Coef	SE Coef	T	P
Constant		0.925058	0.001473	628.1	0
gap (mm)	0.030426	0.015213	0.001473	10.33	0
angle (°)	-0.010396	-0.005198	0.001473	-3.53	0.002
rolls speed (rpm)	0.028225	0.014112	0.001473	9.58	0
rolls diameter (mm)	-0.007905	-0.003952	0.001473	-2.68	0.013
feed rate (t/h)	-0.013912	-0.006956	0.001473	-4.72	0
gap (mm)*rolls diameter (mm)	0.010889	0.005445	0.001473	3.7	0.001
rolls speed (rpm)*rolls diameter (mm)	-0.015003	-0.007502	0.001473	-5.09	0

S = 0.00833139

PRESS = 0

R-Sq = 92.11 %

R-Sq(pred) = 85.97 %

R-Sq(adj) = 89.81 %

$$\begin{aligned} &finesremovalefficiency(\%) = 2.31392 - 0.201431 \cdot gap(mm) - 0.0025991 \cdot angle(°) \\ &+ 0.005222 \cdot rollspeed(rpm) - 0.027305 \cdot rolldiameter(mm) \\ &+ 0.00358239 \cdot gap(mm) \cdot rollspeed(mm) \\ &+ 0.00600987 \cdot gap(mm) \cdot rolldiameter(mm) \\ &- 4.63728 \cdot 10^{-4}\ feedrate(t/h) + 0.003787 \cdot gap(mm) \cdot rolldiameter(mm) \\ &- 6.52309 \cdot 10^{-5} \cdot gap(mm) \cdot rollspeed(rpm) \cdot rolldiameter(mm) \end{aligned} \quad (5.4)$$

Evidently, Equation 5.4 is only valid for the interval modelled. Again, the free term has great influence in the results. Figures 5.30, 5.31 and 5.32 illustrate the effects of the main factors and interactions on fines removal efficiency. It is evident that gap length has the most significant influence on the fines removal efficiency, as expected.

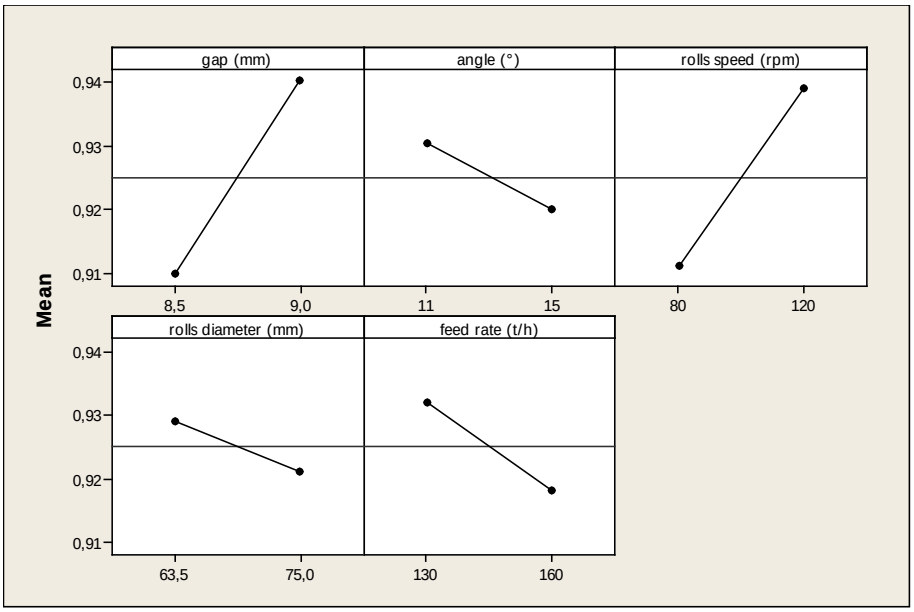

Figure 5.30. Main effects plots for fines removal efficiency.

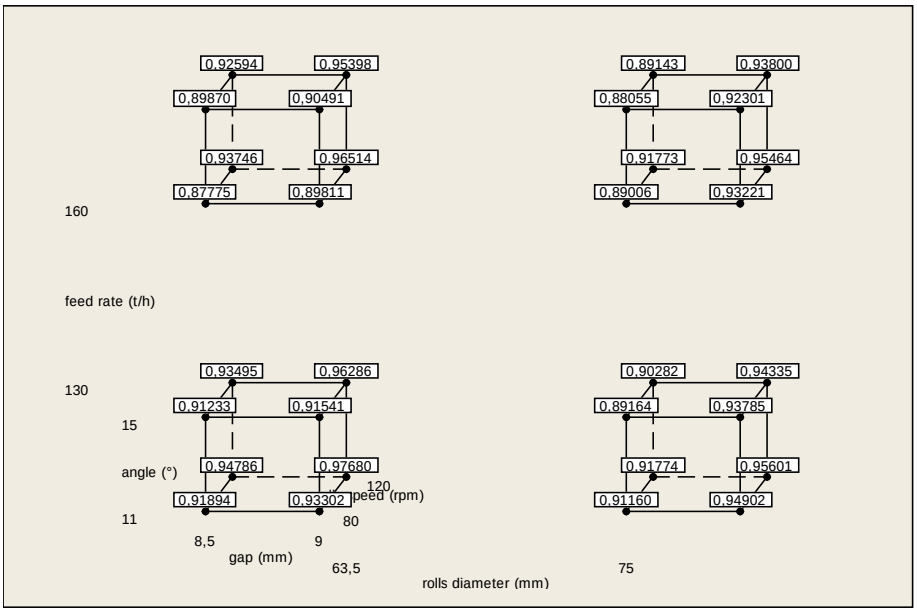

Figure 5.31. Cube plot data means plot for main relevant factors on fines removal efficiency.

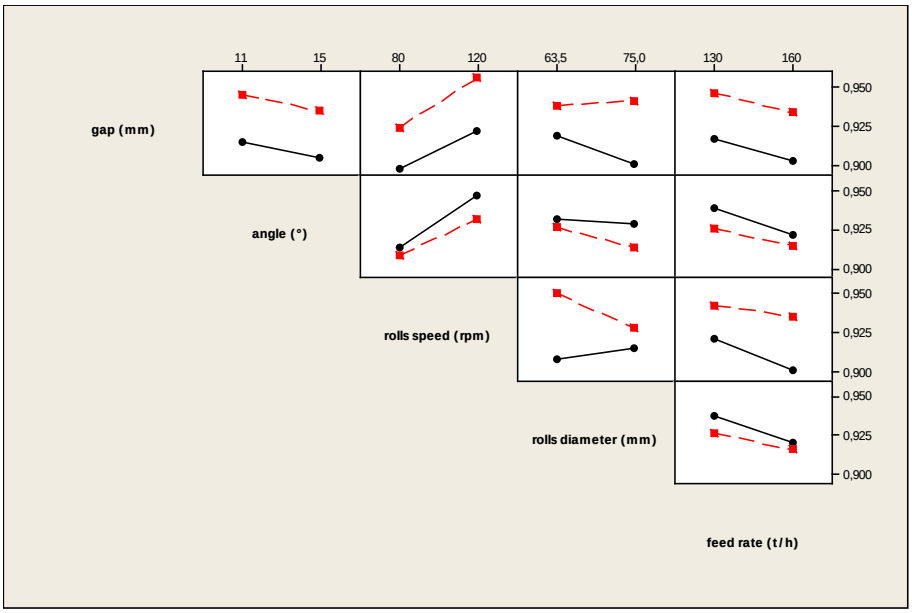

Figure 5.32. Interactions plot for fines removal efficiency.

Figure 5.30 demonstrates that screen angle has a significant role on fines removal efficiency. As the slope of the roller screen increases not only the effective opening (given by the cosine of the angle) becomes narrower but also pellets can more easily escape from rolls gaps and keep moving towards the following rolls.

As rolls rotational speed is raised, the amount of fines removed increases due to the superficial interaction between pellets and rolls surface and the higher torque at gaps throat which increase pellets deformation. Such observations could be demonstrated in industrial scale. The rotation frequency of Vargem Grande screens can be controlled with the aid of a frequency inverter. In Figure 5.33, it can be seen how discs return rate is directly proportional to rolls speed. As fines are screened at discs screens, fewer fines are fed into the double deck screen downstream balling process. The return rate of this screen will then decrease and so will the pressure drop of the pellet bed on the travelling grate.

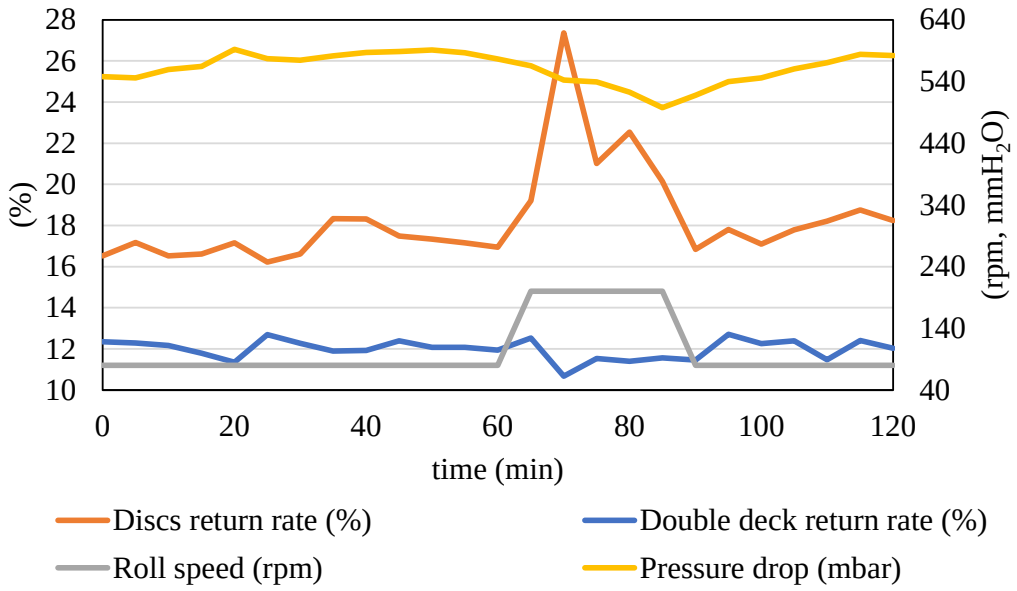

Figure 5.33. Balling immediate response after rolls speed increase at discs discharge.

Figure 5.30 also shows a statistically significant effect of roll diameter. Larger diameter roll screens less fines. As the area of undersize transfer is constant, a smaller number of rolls can be assembled, which results in a smaller number of openings/opportunities to be screened.

Unlike the finding reached for the return rate, Figure 4.30 shows a significant effect of the feed rate. Higher feed rates increase the thickness of the green pellet layer on the rolls, hampering the access of fines to the gaps, thus reducing efficiency of fines removal.

5.3.3 Product screening efficiency

In order to have a holistic understanding about the balling yield, the overall product screening efficiency was also analyzed. The focus of the process is not only to lower return rates and to increase fines removal efficiency but also to guarantee that good pellets properly report to the final product, i.e, sieved as on-size stream at the final quarter rolls of the screen. Product screening efficiency is given by the ratio of product pellets rightly sieved in on-size stream and their amount present at roller screen feed.

$$\text{Product screening efficiency} = \frac{\text{product}(on - \text{size stream})}{\text{product fed}} \tag{5.5}$$

Figure 5.34 shows the magnitude of effects and interactions to determine their importance or not to explain the variability of product screening efficiency response. Table 5.XVIII summarizes the relevant effects on the efficiency.

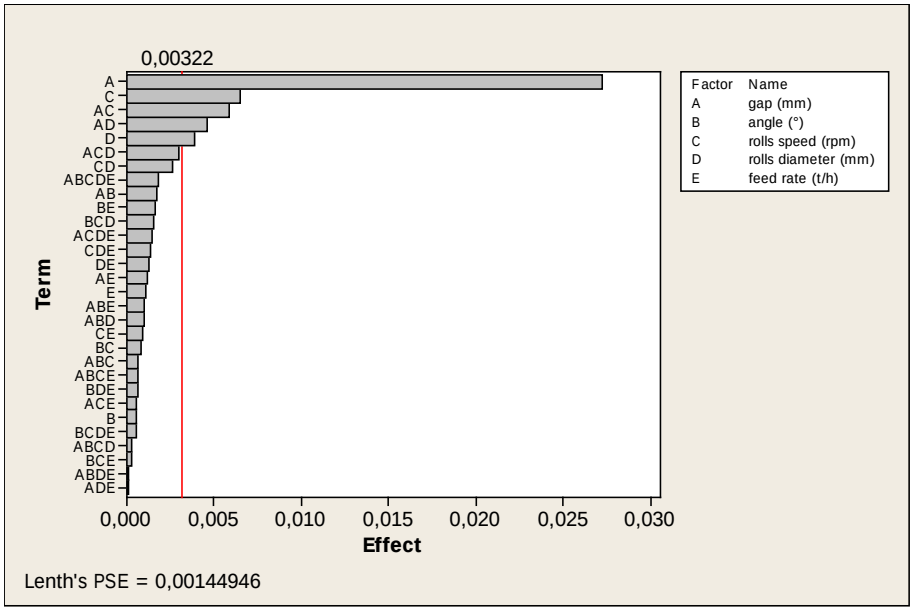

Figure 5.34. Pareto chart of 30 largest effects for product screening efficiency, significance level: 0.05.

Table 5.XVIII. Summary results for significant effects for product screening efficiency

	Main factors
A	Undersize gaps length (mm)
C	Rolls rotational speed (rpm)
D	Rolls diameter (mm)
	Second order interactions
AC	Undersize gaps length (mm) * Rolls rotational speed (rpm)
AD	Undersize gaps length (mm) * Rolls diameter (mm)

Normal plot of standardized effects highlights the relevant factors and interactions in Figure 5.35. Detailed statistical results are summarized in Table 5.XIX.

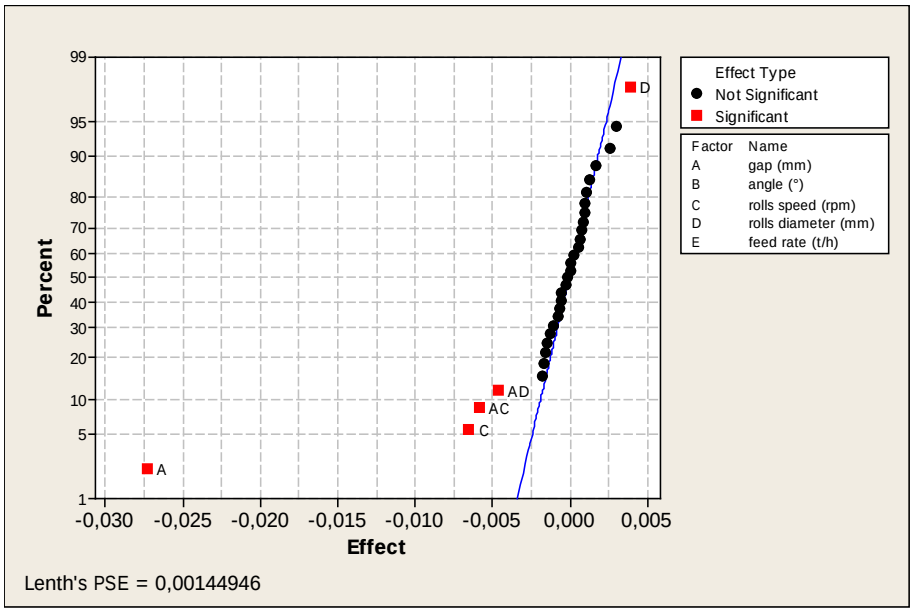

Figure 5.35. Normal plot of the standardized effect of factors and interactions for product screening efficiency.

Table 5.XIX. Summary results for estimated effects and coefficients for product screening efficiency (coded units).

Term	Effect	Coef	SE Coef	T	P
Constant		0.93352	0.000625	1493.55	0
gap (mm)	-0.02732	-0.01366	0.000625	-21.85	0
rolls speed (rpm)	-0.00649	-0.00324	0.000625	-5.19	0
rolls diameter (mm)	0.00392	0.00196	0.000625	3.13	0.004
gap (mm)*rolls speed (rpm)	-0.00584	-0.00292	0.000625	-4.67	0
gap (mm)*rolls diameter (mm)	-0.00464	-0.00232	0.000625	-3.71	0.001

S = 0.00353576

PRESS = 0.000

R-Sq = 95.48 %

R-Sq(pred) = 93.16 %

R-Sq(adj) = 94.62 %

The resulting model can explain 95.48 % of the product screening efficiency for the interval observed:

$$\begin{aligned} &productscreeningefficiency(\%) = -0.083925 + 0.115438 \cdot gap(mm) \\ &+ 0.00494891 \cdot rollspeed(rpm) + 0.0144487 \cdot rolldiameter(mm) \\ &- 5.8412 \cdot 10^{-4} \cdot gap(mm) \cdot rollspeed(rpm) \\ &- 0.00161237 \cdot gap(mm) \cdot rolldiameter(mm) \end{aligned} \tag{5.6}$$

According to results, the response is inversely proportional to undersize gap opening (Figure 5.36, 5.37 and 5.38). As undersize gaps tested are wider than smaller production pellets (8mm) the loss of production increases in the first gaps of the screen.

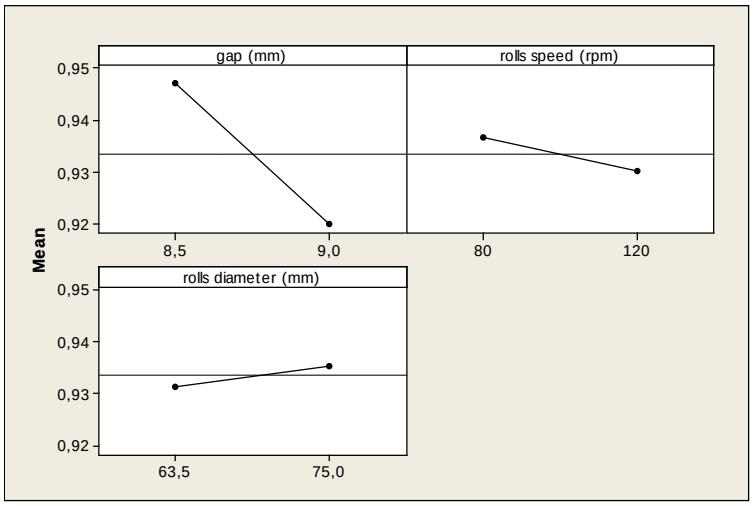

Figure 5.36. Main effects plots for product screening efficiency.

As rolls speed is increased, more fines and production pellets are pulled to the gap due the sticky interaction between these solids surfaces (as earlier verified for fines in Figures 5.30 and 5.33). Due to pellets plasticity (5.16), higher torque of rolls forces pellets deformation and increase the amount sizing near gaps length to undersize flow.

The result observed for rolls diameter is not easily comprehended and it will be analyzed in greater detail in separated streams: loss to undersize and loss to oversize.

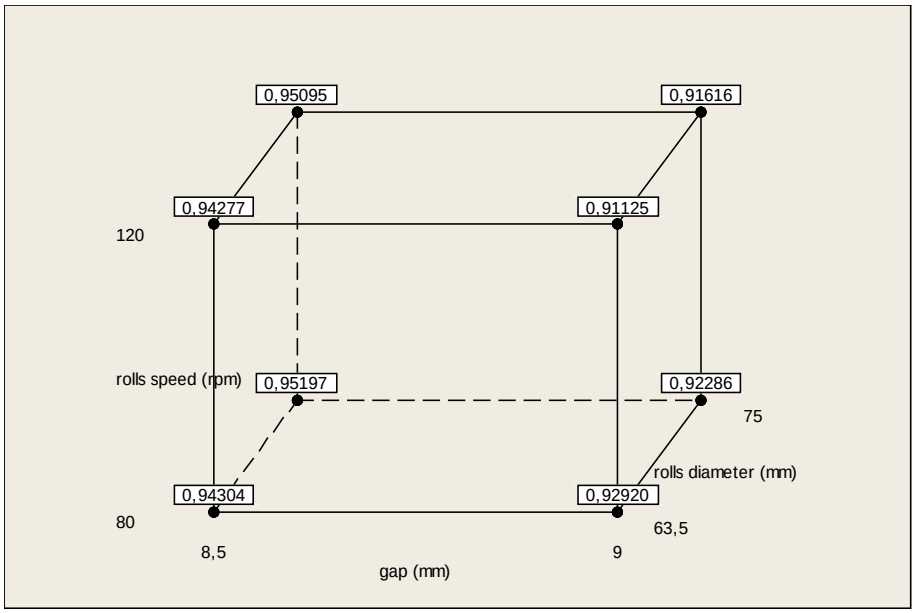

Figure 5.37. Cube plot means plot for main relevant factors on product screening efficiency.

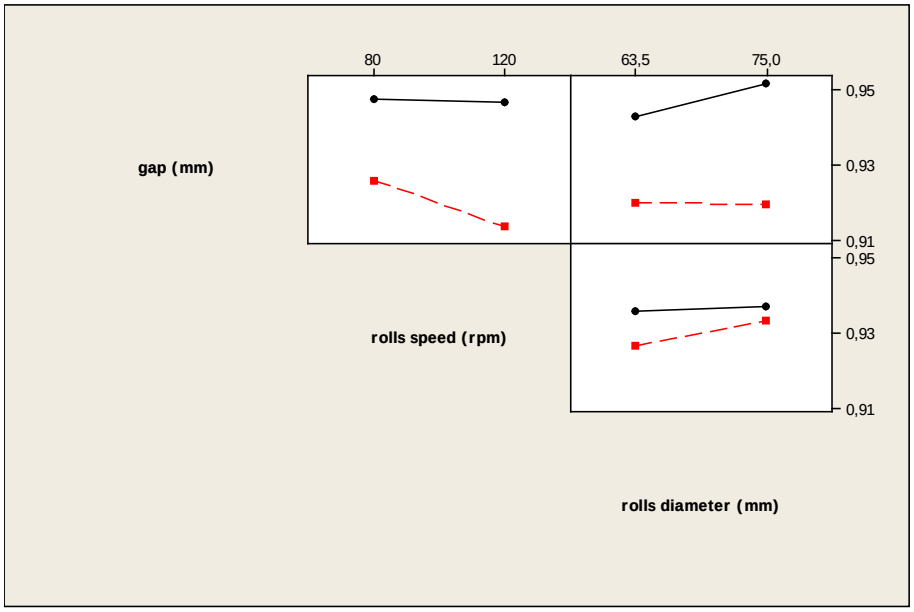

Figure 5.38. Interactions plot for product screening efficiency.

5.3.3.1 Loss of production to undersize

This is the fraction of pellets ranging from 8 to near 9 mm that can be misguided to the underflow stream. Figure 5.39 presents the 30 largest effects and interactions on loss

of production to undersize. Table 5.XX summarizes the relevant factors and interactions for the loss of production to undersize.

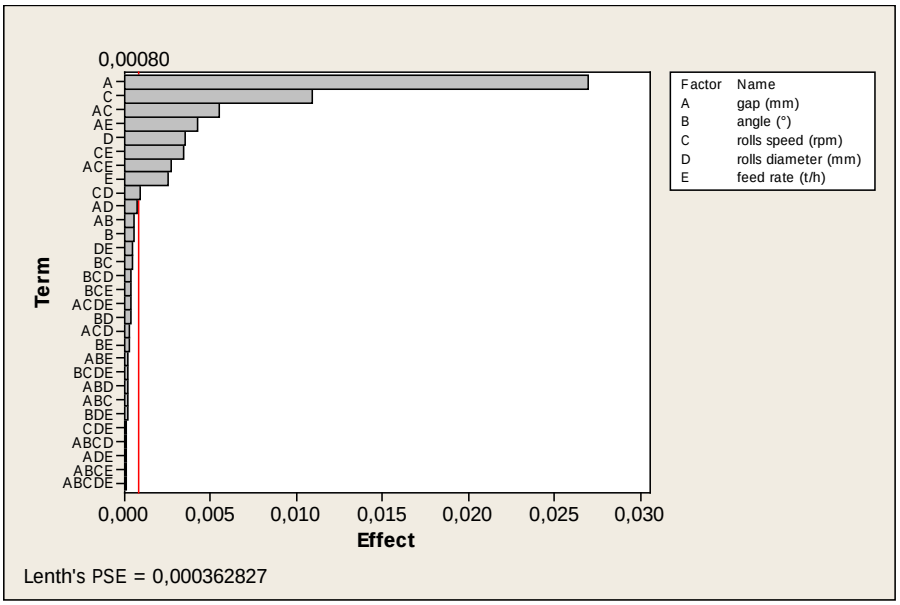

Figure 5.39. Pareto chart of 30 largest effects for loss of production to undersize, significance level: 0.05.

Table 5.XX. Summary results for significant effects for loss of production to undersize

	Main factors
A	Undersize gaps length (mm)
C	Rolls rotational speed (rpm)
D	Rolls diameter (mm)
E	Feed rate (t/h)
	Second order interactions
AC	Undersize gaps length (mm) * Rolls rotational speed (rpm)
AE	Undersize gaps length (mm) * Feed rate (t/h)
CD	Rolls rotational speed (rpm) * Rolls diameter (mm)

CE	Rolls rotational speed (rpm) * Feed rate (t/h)
	Third order interaction
ACE	Undersize gaps length (mm) * Rolls rotational speed (rpm) * Feed rate (t/h)

Relevant effects for factors and interactions which describe the model are highlighted in Figure 5.40.

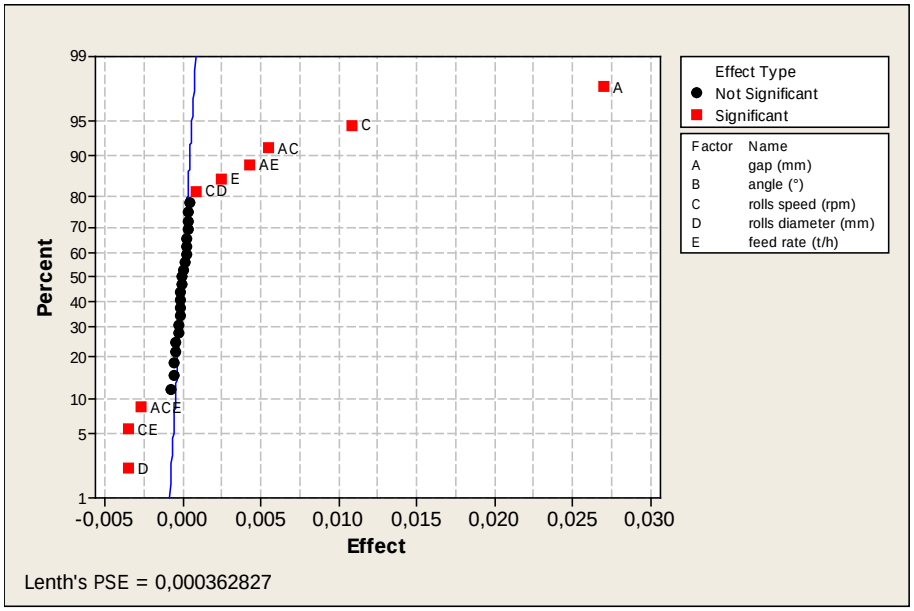

Figure 5.40. Normal plot of the standardized effects for the significant factors and interactions for loss of production to undersize, significance level: 0.05.

According to results in Table 4.XXI, the model obtained can describe 99.83 % of the response. A third order interaction, ACD, was also detected as relevant. Equation 5.7 describes the model for the interval between low and high levels analyzed:

Table 5.XXI. Summary results for estimated effects and coefficients for loss of production to undersize (coded units)

Term	Effect	Coef	SE Coef	T	P
Constant		0.059883	0.000169	353.69	0,000
gap (mm)	0.027036	0.013518	0.000169	79.84	0,000

rolls speed (rpm)	0.01091	0.005455	0.000169	32.22	0,000
rolls diameter (mm)	-0.003513	-0.001756	0.000169	-10.37	0,000
feed rate (t/h)	0.002494	0.001247	0.000169	7.37	0,000
gap (mm)*rolls speed (rpm)	0.005532	0.002766	0.000169	16.34	0,000
gap (mm)*feed rate (t/h)	0.00428	0.00214	0.000169	12.64	0,000
rolls speed (rpm)*rolls diameter (mm)	0.000888	0.000444	0.000169	2.62	0.016
rolls speed (rpm)*feed rate (t/h)	-0.003457	-0.001729	0.000169	-10.21	0,000
gap (mm)*rolls speed (rpm)*feed rate (t/h)	-0.002702	-0.001351	0.000169	-7.98	0,000

S = 0.000957755

PRESS = 0.0000426959

R-Sq = 99.73 %

R-Sq(pred) = 99.43 %

R-Sq(adj) = 99.62 %

$$\begin{aligned} &lossofproductiontoundersize(\%) = 3.00542 - 0.345204 \cdot gap(mm) \\ &- 0.026856 \cdot rollsspeed(rpm) - 6.9142 \cdot 10^{-4} \cdot rollsdiameter(mm) \\ &- 0.026856 \cdot \ feedrate(t/h) + 0.0031654 \cdot gap(mm) \cdot rollsspeed(rpm) \\ &+ 0.002372 \cdot gap(mm) \cdot \ feedrate(t/h) \\ &+ 3.8597 \cdot 10^{-6} \cdot rollsspeed(rpm) \cdot rollsdiameter(mm) \\ &+ 1.5187 \cdot 10^{-4} \cdot rollsspeed(rpm) \cdot \ feedrate(t/h) \\ &- 1.8015 \cdot 10^{-5} \cdot gap(mm) \cdot rollsspeed(rom) \cdot \ feedrate(t/h) \end{aligned} \quad (5.7)$$

Main factors plot (Figure 5.41) show how each variable acts on loss of production to undersize when the level is raised from low to high.

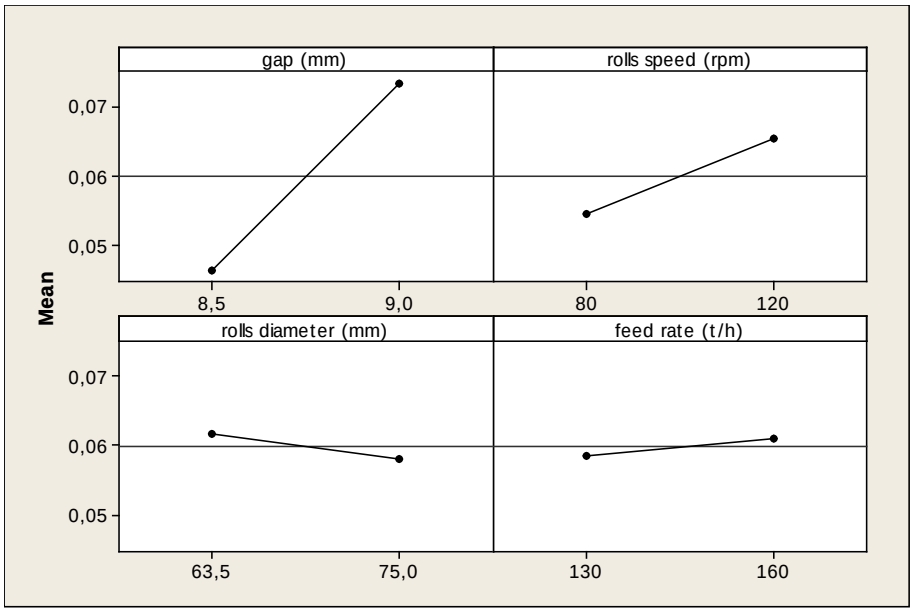

Figure 5.41. Main effects plots for loss of production to undersize.

Figure 5.41 shows a significant effect of gap on the loss of production to undersize. As discussed previously, if the gap length is wider more fines and also finer product pellets are easier sieved as undersize. In Figure 5.40 it may be also verified that a significant effect of rolls speed on the loss of production to undersize, which follows the same trend observed for product screening efficiency. Roll diameter also influences directly the loss of production to undersize. Fewer gaps are available when larger diameter rolls are used in the roller screens. Production pellets then follow to on-size screening area and losses to undersize are reduced.

Cube plots of main and interaction effects are shown in Figures 5.42 and 5.43, respectively.

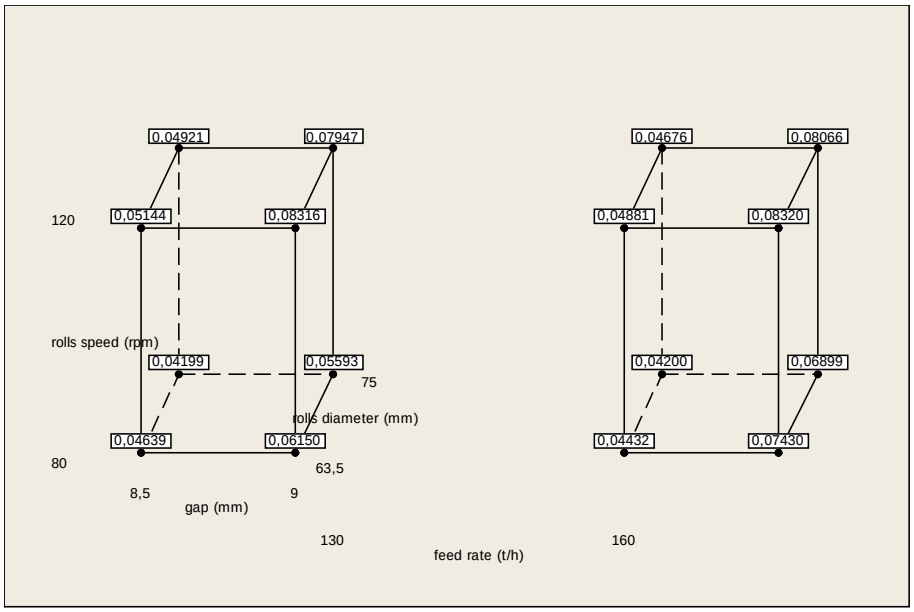

Figure 5.42. Cube plot data means plot for main relevant factors on loss of production to undersize.

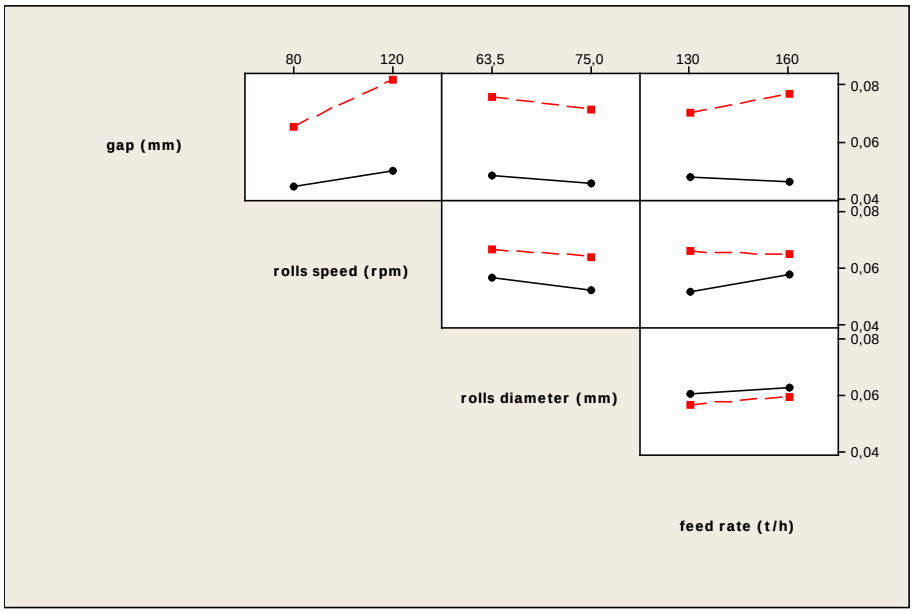

Figure 5.43. Interactions plot for loss of production to undersize.

5.3.3.2 Loss of production to oversize

This is the fraction of on-size pellets which are miscarried to oversize as coarse. Figure 5.44 presents the 30 largest for the mentioned response, showing that effects are

significant. A preliminary summary of results for relevant factors are resumed in Table 5. XXII.

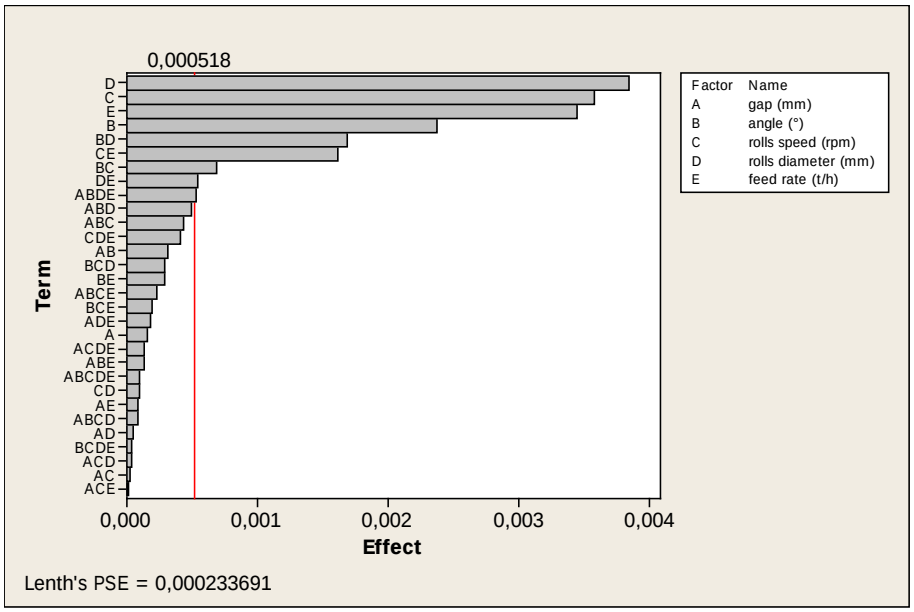

Figure 5.44. Interactions plot for loss of production to oversize.

Table 5.XXII. Summary results for significant effects for loss of production to oversize.

	Main factors
B	Angle (°)
C	Rolls rotational speed (rpm)
D	Rolls diameter (mm)
E	Feed rate (t/h)
	Second order interactions
BC	Angle (°) * Rolls rotational speed (rpm)
BD	Angle (°) * Rolls diameter (mm)
CE	Rolls rotational speed (rpm) * Feed rate (t/h)
DE	Rolls diameter (mm) * Feed rate (t/h)

	Third order interaction
ABDE	Undersize gaps length (mm) * Angle (°) * Rolls diameter (mm) * Feed rate (t/h)

A fourth order interaction, ABDE, was detected as relevant to describe the model variability (Figure 5.45).

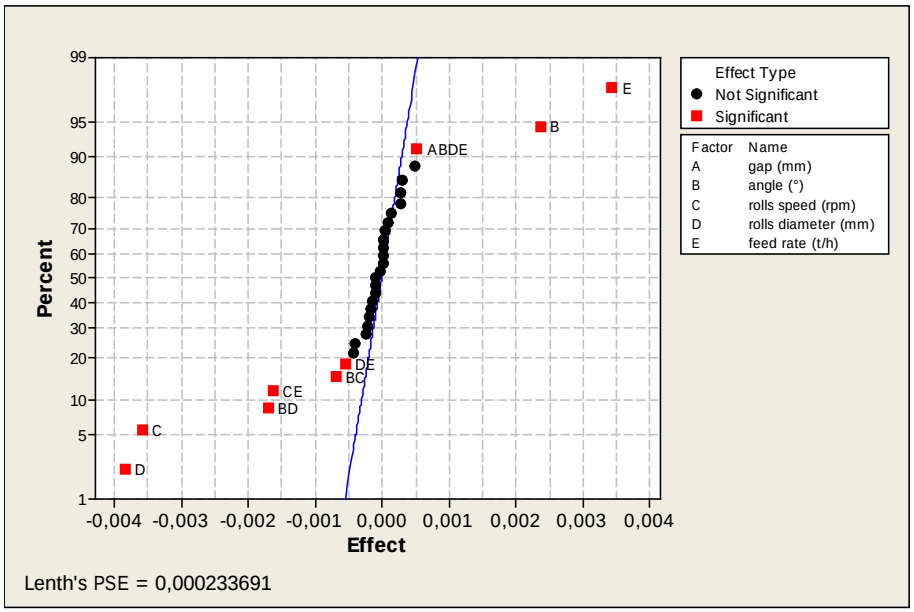

Figure 5.45. Normal plot of the standardized effects for the significant factors and interactions for loss of production to oversize, significance level: 0.05.

The model obtained for the loss of production to oversize explains 97.98 % of the variability in the data (Table 5.XXIII).

Table 5.XXIII. Summary results for estimated effects and coefficients for loss of production to oversize (coded units).

Term	Effect	Coef	SE Coef	T	P
Constant		0.00456	0.00011	40.59	0
gap (mm)	-0.0002	-8E-05	0.00011	-0.69	0.496
angle (°)	0.00237	0.00119	0.00011	10.55	0
rolls speed (rpm)	-0.0036	-0.0018	0.00011	-15.92	0

rolls diameter (mm)	-0.0038	-0.0019	0.00011	-17.09	0
feed rate (t/h)	0.00345	0.00172	0.00011	15.33	0
angle (°)*rolls speed (rpm)	-0.0007	-0.0003	0.00011	-3.04	0.006
angle (°)*rolls diameter (mm)	-0.0017	-0.0008	0.00011	-7.5	0
rolls speed (rpm)*feed rate (t/h)	-0.0016	-0.0008	0.00011	-7.19	0
rolls diameter (mm)*feed rate (t/h)	-0.0005	-0.0003	0.00011	-2.39	0.026
gap (mm)*angle (°)*rolls diameter (mm)*feed rate (t/h)	0.00053	0.00027	0.00011	2.36	0.028

S = 0.000635941

PRESS = 0.0000197204

R-Sq = 97.98 %

R-Sq(pred) = 95.32 %

R-Sq(adj) = 97.02 %

The model is non-hierarchical since a fourth order interaction was verified as relevant and any third order was.

Main effects plots are presented in Figure 5.46.

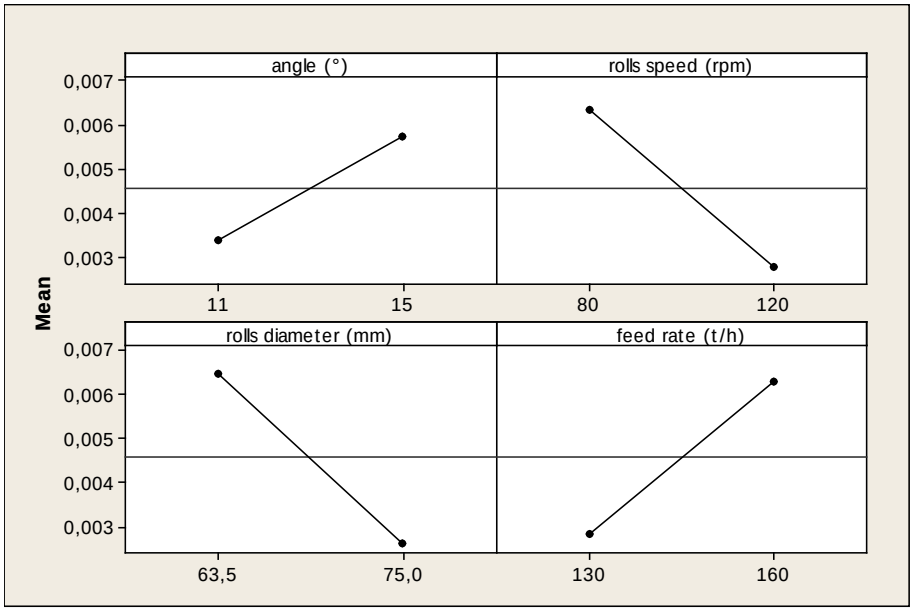

Figure 5.46. Main effects plots for loss of product to oversize.

Roller screen angle is directly proportional to loss of production to oversize, as it is to undersize. As device inclination is raised, the transport on horizontal component of pellets movement on the rolls is faster, reducing the effective gap.

Rolls speed also follows the same trend observed for loss to undersize and were found to affect loss of product to oversize. By increasing rotation frequency, pellets and fines pulled to gap openings being submitted to higher torque and have less chance to escape from the neck between rolls.

Although changing rolls diameters caused the same variation, i.e. directly proportional, on loss of production for undersize and oversize, the reasons for such responses are completely different. As discussed, the area for undersize and on-size screening are kept fixed which means that if the smaller rolls are installed, more gaps are available (Table 4.V) and increase the probability of pellets to be classified through them. The same behavior was also expected for on-size area, nevertheless, the response is in the opposite direction, i.e., pellets rather stayed over the smaller rolls than be sieved through the gaps openings. Even with more gaps openings, the amount of pellets carried as oversize to roller screen discharge raised. This phenomenon is explained by the important relationship between pellets and rolls diameters that change significantly the probability of a determined particle escaping or remaining “imprisoned” between rolls throat. All other factors tested influence such motion but roll diameter is the most important of them for the intervals tested. In Figures 5.47(a) to 5.47(d) a 12 mm diameter pellet is represented into a 10 mm length gap. The difference between drawings is rolls diameter that defines the depth pellets reach into the throat between two rolls. Rolls diameter in Figure 5.47(a) and (b) are 63.5 and 75 mm, respectively, i.e., the low and high levels of this factor respectively. In order to evaluate how imprisoned pellets are into rolls neck, it assumed as 100 % of depth when the point of contact of the pellet and the rolls is horizontally aligned to pellet and rolls centers of mass. It can be also described when the pellet is stuck between the rolls by only two points being its halves equally over and under gap opening. The pellet reached 77.1 % of depth between the 63.5 mm rolls while and 78.7 % for 75 mm rolls case. It can be inferred that it is harder for pellets to escape from larger diameter rolls than when they are into smaller ones. Figures 5.47(c) and 5.47(d) illustrate theoretical rolls of 10 mm and 203.2 mm (8 inches) diameter rolls to demonstrate such difference. For such reason,

even presenting more gaps, the loss of carried pellets to oversize is larger for smaller diameter rolls.

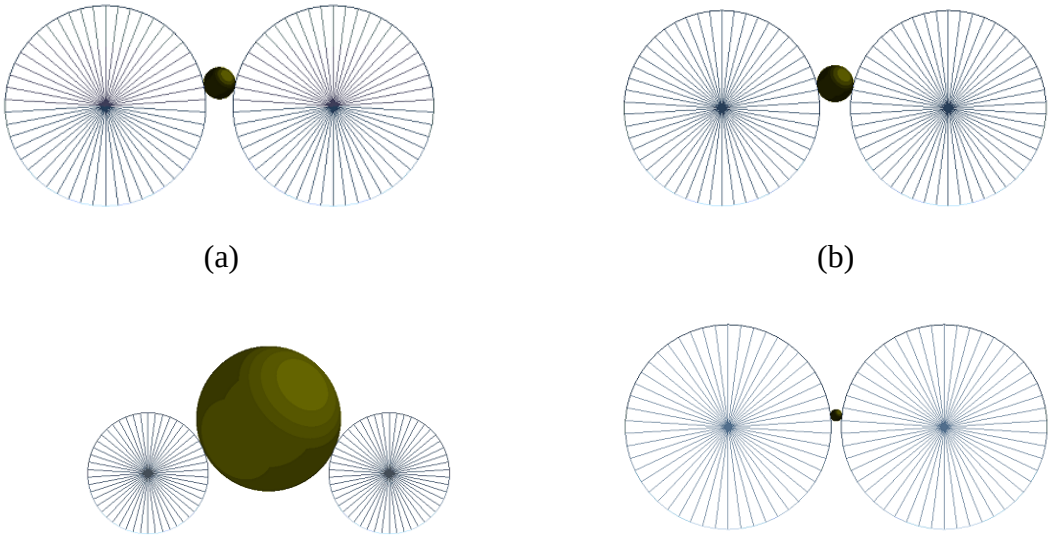

(a) (b)

(c) (d)

Figure 5.47. Illustration of imprisonment of 12 mm pellet into 10 mm gapped horizontal rolls. Rolls diameter – (a) 63.5 mm; (b) 75 mm; (c) 10 mm and (d) 203.2 mm

The cube plot of main effects and interactions for the loss of production to oversize are shown in Figures 5.48 and 5.49, respectively.

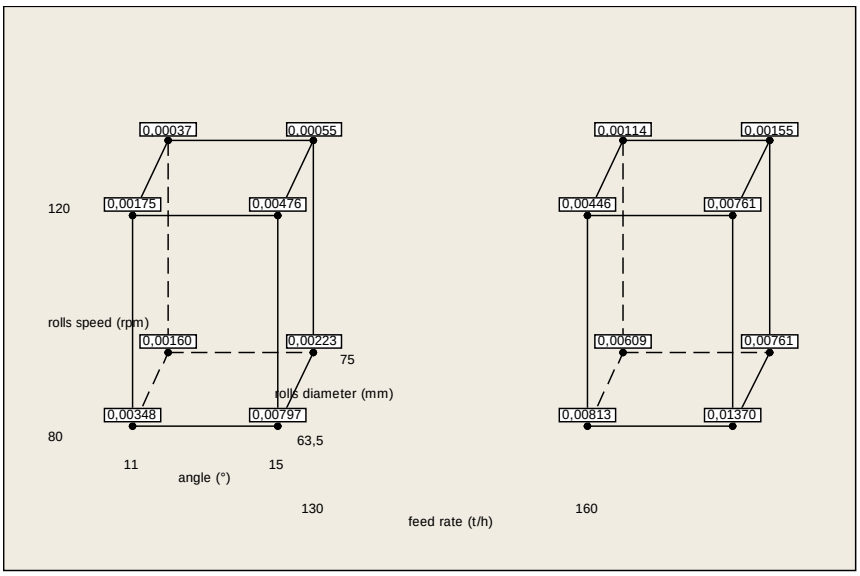

Figure 5.48. Cube plot for main relevant factors on loss of production to oversize.

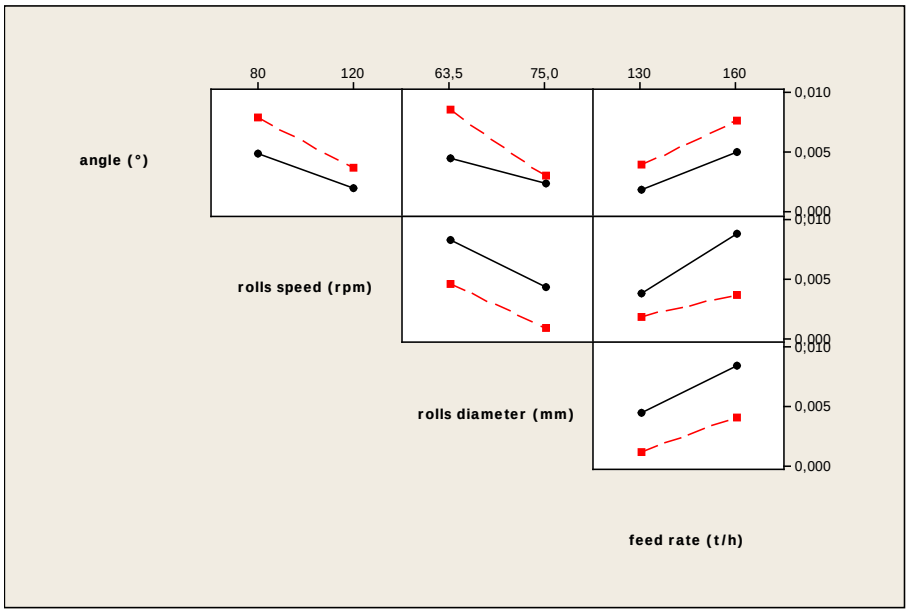

Figure 5.49. Interactions plot for loss of production to oversize.

5.3.4 On-size contamination

On-size contamination is the total amount of fines not screened through undersize gaps that remained on pellet bed and were guided later screened as production pellets. Although they will have a second chance to be removed on double deck roller screens (DDRS), it is opportune their removal at this stage since DDRS is less efficient due to higher mass concentration on it. Such single deck roller screens usually operate at unit flow rates from 15 to 18.5 t/m^2 while a DDRS works with 70 to 75 t/m^2. In Figure 5.50, the results for the 30 largest effects and interactions that may influence on-size contamination are presented.

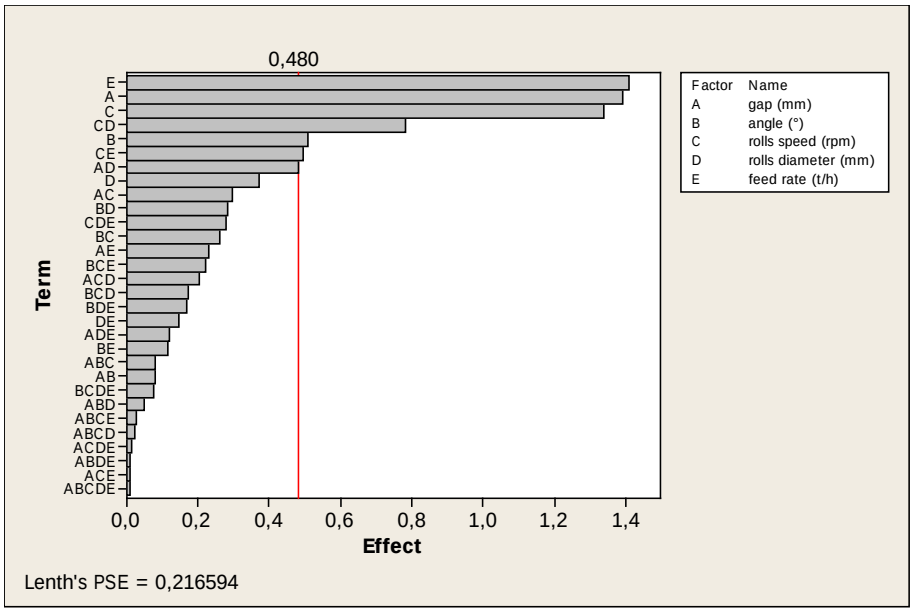

Figure 5.50. Pareto chart of 30 largest effects for on-size contamination (%), significance level: 0.05.

The relevant factors and interactions for on-size contamination are summarized on Table 5.XXIV.

Table 5.XXIV. Summary results for significant effects for on-size contamination

Main factors	
A	Undersize gaps length (m)
B	Angle (°)
C	Rolls rotational speed (rpm)
E	Feed rate (t/h)
Second order interactions	
AD	Undersize gaps length (mm) * Rolls diameter (mm)
CD	Rolls rotational speed (rpm) * Rolls diameter (mm)
CE	Rolls rotational speed (rpm) * Feed rate (t/h)

The resulting model explains 89.15 % of the variability in the data (Table 5.XXV). The factor rolls diameter is non-relevant, with a P-value greater than significance level. Nevertheless, it is inserted in the equation and the results because it appears as part of some statistically significant interactions.

Table 5.XXV. Summary results for estimated effects and coefficients for on-size contamination (t/h) (coded units)

Term	Effect	Coef	SE Coef	T	P
Constant		3.793	0.07996	47.44	0
gap (mm)	-13.923	-0.6962	0.07996	-8.71	0
angle (°)	0.5074	0.2537	0.07996	3.17	0.004
rolls speed (rpm)	-1.34	-0.67	0.07996	-8.38	0
rolls diameter (mm)	0.3717	0.1858	0.07996	2.32	0.029
feed rate (t/h)	14.108	0.7054	0.07996	8.82	0
gap (mm)*rolls diameter (mm)	-0.4838	-0.2419	0.07996	-3.02	0.006
rolls speed (rpm)*rolls diameter (mm)	0.7812	0.3906	0.07996	4.88	0
rolls speed (rpm)*feed rate (t/h)	-0.494	-0.247	0.07996	-3.09	0.005
S = 0.452321					
PRESS = 9.10889					
R-Sq = 92.46 %					
R-Sq(pred) = 85.40 %					
R-Sq(adj) = 89.83 %					

Mathematically, for the interval analyzed, the on-site contamination amount is given by equation below:

$$\begin{aligned} on-sizecontamination(t/h) &= -69.5723 + 8.86759 \cdot gap(mm) \\ &+ 0.126855 \cdot angle(°) - 0.149319 \cdot rollspeed(rpm) \\ &+ 1.16487 \cdot rolldiameter(mm) + 0.129365 \cdot feedrate(t/h) \\ &- 0.168263 \cdot gap(mm) \cdot rolldiameter(mm) \\ &+ 0.0033965 \cdot rollspeed(rpm) \cdot rolldiameter(mm) \\ &- 8.234 \cdot 10^{-4} \cdot rollspeed(rpm) \cdot feedrate(t/h) \end{aligned} \quad (5.8)$$

In Figure 5.51, it can be seen in the normal plot of effects the relevant factors and interactions.

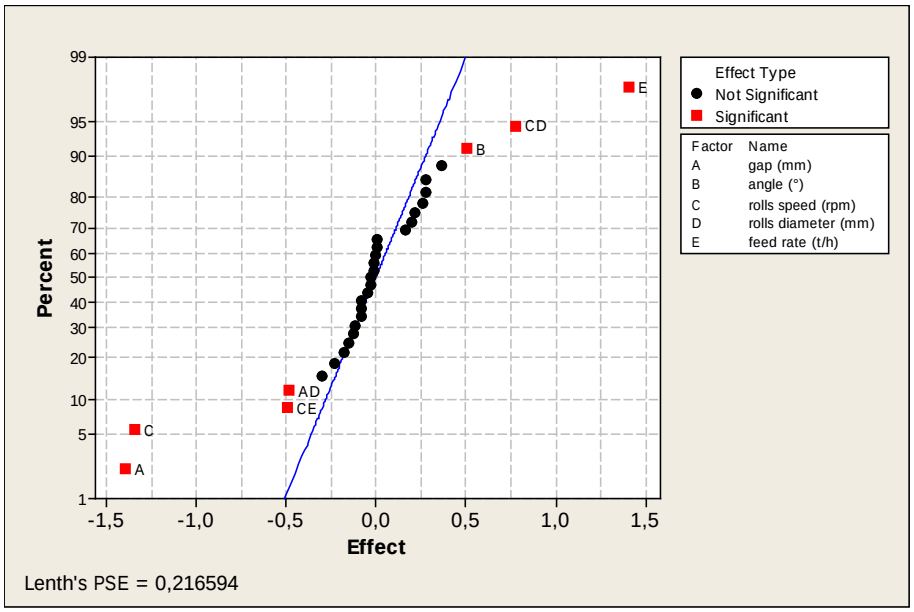

Figure 5.51. Normal plot of the standardized effects for the significant factors and interactions for on-size contamination (t/h), significance level: 0.05.

Main factors plots are presented in Figure 5.52. According to these results, wider gaps increase sieving capability and for such reason avoid the transport of fines not classified to on-size.

Angle also follows the inverse trend. If roller screens are less inclined, the effective gaps opening, given by the product of gaps length and the cosine of screen inclination, is wider. In addition, the movement towards the rolls becomes harder since pellets reach deeper positions into the rolls gaps neck.

By increasing rolls speed, fines and pellets are submitted to higher torque and deformations towards gaps opening. As consequence, less fines are let go to on-size downstream.

If feed rate increases, greater is the height of the pellets bed and fines over the rolls making their passage through undersize gaps harder.

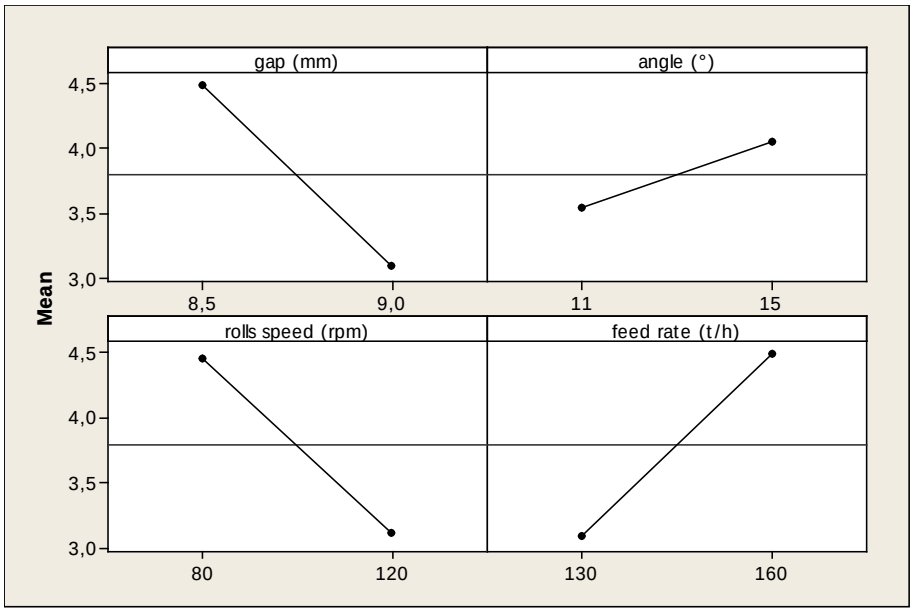

Figure 5.52. Main effects plots for on-size contamination (t/h).

Cube plot for relevant factors illustrates the scenario for on-size contamination (Figure 5.53).

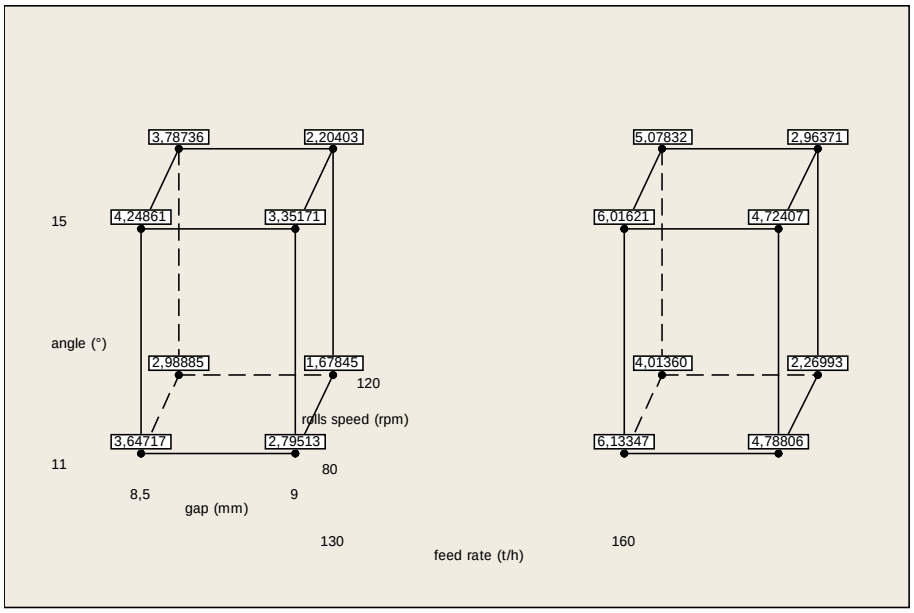

Figure 5.53. Cube plot for main significant factors for on-size contamination (t/h).

Relevant interaction plots are shown in Figure 5.54. It can be verified how the interaction of rolls speed and diameter.

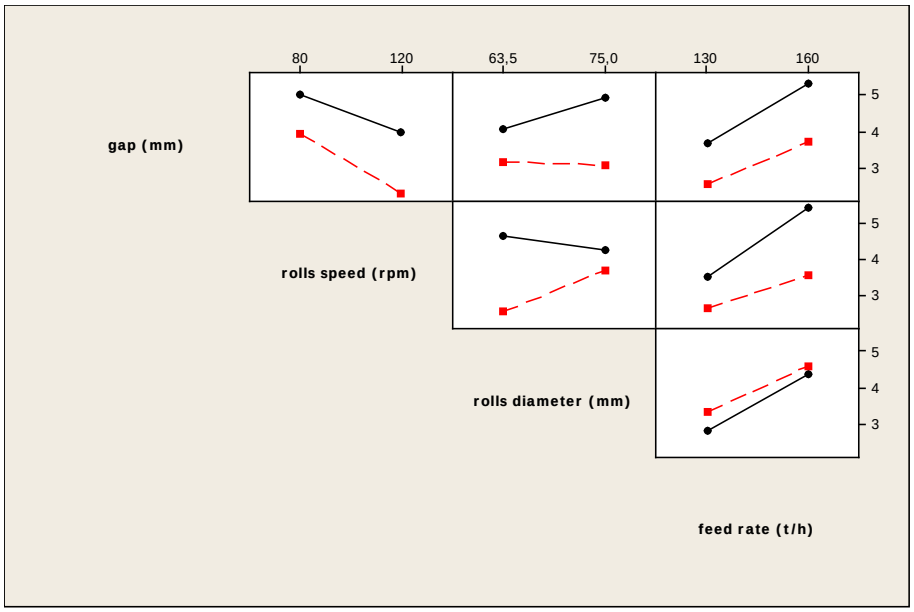

Figure 5.54. Interaction plots for on-size contamination.

5.4 Optimization of single deck screens

Based on results gotten from the DOE analysis and observation of pellets motion in simulations, some changes on roller screens are proposed as follows in order to optimize product screening and fines removal efficiency, i.e., the main objective is to reduce loss of production, return rate and on-size contamination concomitantly.

Proposed modifications:

- Wider gaps length at undersize sieving were benefic to reduce on-size contamination but at same time, they increased the return rate due the loss of production. The first ¾ of the screen are designed to remove fines and this is the main aim at this stage. The concentration of particles in this part of the undersize gaps is high making tougher the screening of fines. Nevertheless, as fines are sieved, the pellets bed height over the rolls diminishes facilitating fines screening but inherently increasing loss of production. For such reason, the undersize gaps were split in two halves: the first one 8.8 mm gapped to intensify fines removal and the second part 8.5 mm gapped to reduce loss of production since concentration of pellets is lower.

- The relation between particles and rolls diameters played a very important influence on determining pellets scape or imprison into gaps throat. The average size of screened particles must be observed to determine the most indicated rolls for each area. Results verified that smaller rolls worked better if installed in undersize area, i.e., when fines are removed. However, their results were worse than thicker rolls in on-size sieving area where coarse and coarser pellets are predominant. Lower product screening efficiency and larger losses of production to oversize were accounted for thinner rolls case. For such reasons, rolls of distinct diameters are suggested: 63.5 mm for undersize and 75 mm for on-size. The bearings of the thinner rolls must be adjusted in order to align the top part of the rolls, avoiding obstacles that can damage pellets during motion.

- The analyses of loss of production to undersize and oversize were the key indicators to propose a change in roll speeds. Rotational speed was set to 80 rpm and l20 rpm for undersize and on-size rolls respectively. This would require a second moto-reduction drive assembly and chains in the opposite side of roller screens to control rolls speed of each area independently.

The other factors, angle and feed rate, would be kept unaltered for comparisons to the base case, which corresponds to current in operation at VGR. Results are present in Table 5.XXVI and plotted in Figure 5.55.

Table 5.XXVI. Results of optimization simulations of single deck tests

Inputs	Base Case	Test A1	Test A2	Test A3
Rolls diameter (mm)	75	75	63.5/75	63.5/75
Rolls speed (rpm)	80	80	80	80/120
Undersize gap (mm)	8.8	8.8-8.5	8.8-8.5	8.8-8.5
Outputs				
Loss to undersize (t/h)	80.6	71.0	74.2	74.2
Loss to oversize (t/h)	3.0	2.7	4.1	0.6
Total loss of production (t/h)	83.7	73.7	78.3	74.8
Return rate	11.6 %	10.7 %	11.2 %	10.8 %
Undersize Return rate	8.5 %	7.8%	8.1%	8.1 %

Oversize return rate	3.1 %	2.9 %	3.1 %	2.7 %
On-size contamination (t/h)	3.82	4.00	3.11	3.28
Fines removal efficiency - FRE	91.1 %	90.1 %	92.4 %	92.9%
Product screening efficiency - PSE	93.5 %	95.0 %	94.1 %	94.4 %
Global efficiency - FRE x PSE	85.2 %	86.6 %	87.0 %	87.7 %

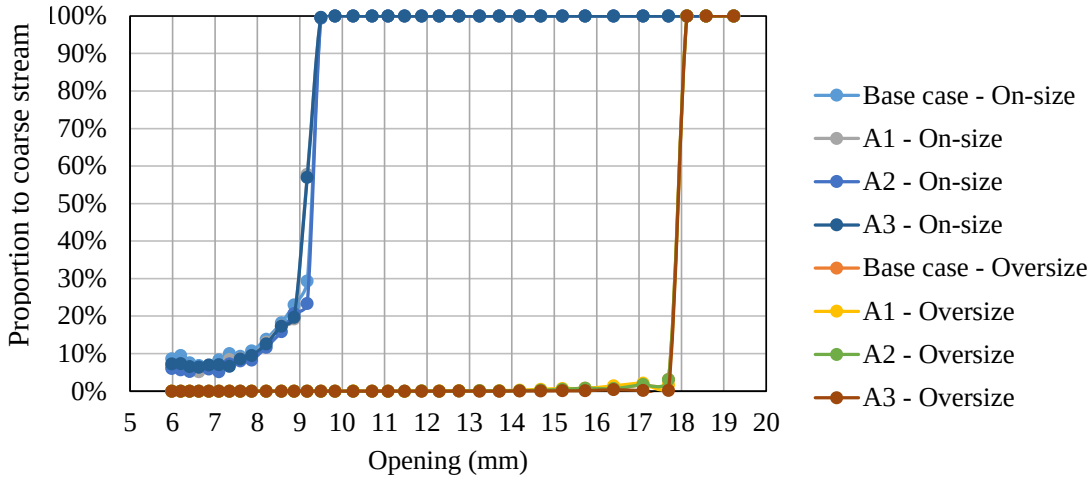

Figure 5.55. Partition curve for tests of optimized screens.

All comparisons are relative to base case. In test A1, all the undersize gaps were split in two halves: the first was gapped at 8.8 mm to remove fines and the second at 8.5 mm to avoid losses. All other factors remained as the actual case. Results obtained were in accordance to perspectives. Losses to undersize and return rate dropped 12 % - from 80.6 to 71.0 t/h – and 7.7% - from 11.6 % to 10.7 % - respectively; nevertheless, on-size contamination raised 4.7 %, from 3.82 t/h to 4.00 t/h. Fines removal efficiency reduced 1 % while product screening efficiency increased in 1.5 %. The global efficiency increased 1.4 %.

For test A2, modifications used in test A1 were maintained and rolls of different diameters were simulated. Loss of undersize decreased 8 % - from 80.6 to 74.2 t/h – while return rate receded 3.4 % - from 11.6 to 11.2 %. On-size contamination dropped 18.5 % - from 3.82 t/h to 3.11 t/h. Fines removal and product screening efficiencies progressed respectively. Global efficiency reached 87.0 %.

A3 test conserved A2 configurations but rolls speed was set to 80 rpm for 63.5 mm rolls in undersize and 120 rpm for 75 mm. Loss of production to undersize was the same obtained in A2 test. Loss to oversize reduced 13 % - from 3.1 % to 2.7 %. Return rate followed the same tendency and fell 7,8 % - from 11.6 % to 10.8 %. On-size contamination decreased approximately 14 % - from 3.82 to 3.28 t/h. Both fines removal and product screening efficiencies advanced 1.9 % and 0.9 % respectively. As consequence, the global efficiency increased almost 3 %.

The changes of such modifications can increase Vargem Grande balling productivity and consequently raise grate index in at least 0.7 t/m^2·dia (2.5 %) which corresponds to approximately 46 kt/y. There are also others gains not measured in this study: as the screening efficiency raised, feed rate can be reduced thus improving discs performance, which would discharge less fines.

5.5 Double deck roller screen feeder (feeder)

The assessment of DDRS cases (Figure 5.56) was carried out for the product contamination, i.e., the amount of fines not screened that follows the induration machine, the loss of production to undersize, return rate and the screen efficiencies as summarized in Table 5.XXVII. Partition curves are illustrated in Figure 5.57. It can be verified that the new DDRS angled at lower angle equipped with the complete upper deck worked better and reduced the amount of fines by-pass into production stream. The global screening efficiency also demonstrated evolution increasing 6.5 % for smaller diameter rolls due the availability of more gaps to screen.

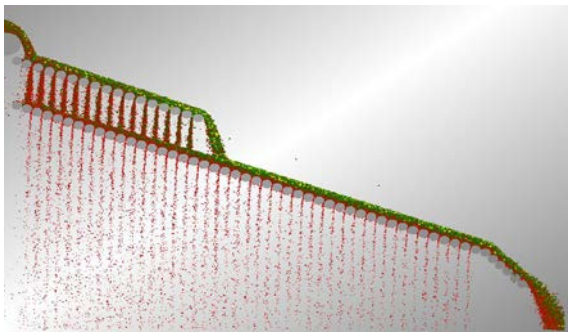

(a)

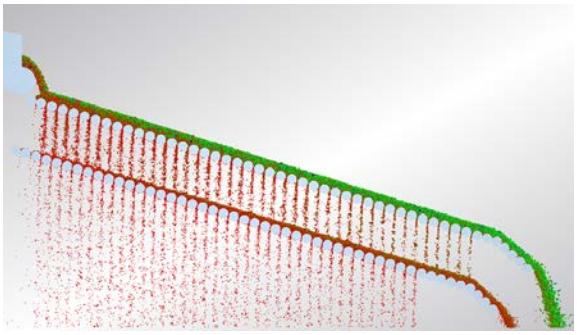

(b)

Figure 5.56. Simulation of the (a) current and (b) proposed DDRS simulations

Table 5.XXVII. Summary of results of DDRS cases.

Response	Actual DDRS	Proposed DDRS (94 mm)	Proposed DDRS (89 mm)
Product contamination (t/h)	55.4	48.1	41.4
Loss of production (t/h)	20.8	23.4	24.6
Return rate	14.18 %	15.07 %	15.36 %
FRE	72.7 %	76.3 %	79.6 %
PSE	97.9 %	97.6 %	97.5 %
GSE	71.1 %	74.5 %	77.6 %

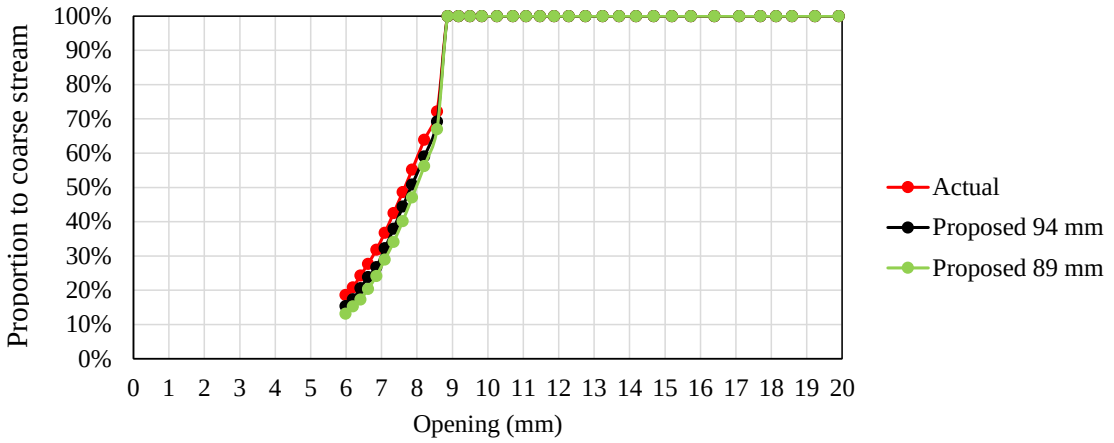

Figure 5.57. Partition curves for DDRS under different conditions.

Pellets segregation layers on pallet cars were also analyzed. Bed voidage fraction information was extracted under steady state conditions (Figure 5.58 and 5.59). Results have shown as evolution of 3 to 5 % (Figure 5.60) when comparing the proposed design to the actual DDRS in operation. Although bed permeability, K_{bed}, cannot be directly measured from EDEM, excellent inferences can be made since its relation to bed porosity is direct as demonstrated in Kozeny-Carman model (CORROCHANO *et al.*, 2015).

$$K_{bed} = \frac{\varepsilon^3 \cdot \left(\phi \cdot d_p\right)^2}{72 \cdot \left(\tau_{bed}{}^{\xi}\right)^2 \cdot \left(1-\varepsilon\right)^2} \tag{5.9}$$

Where

τ_{bed} is semi-empirical bed tortuosity (DIAS *et al.*, 2006) given by:

$$\tau_{bed} = \left(\frac{1}{\varepsilon}\right)^{\zeta} \tag{5.10}$$

Where

ζ is an adjustable parameter for packing method.

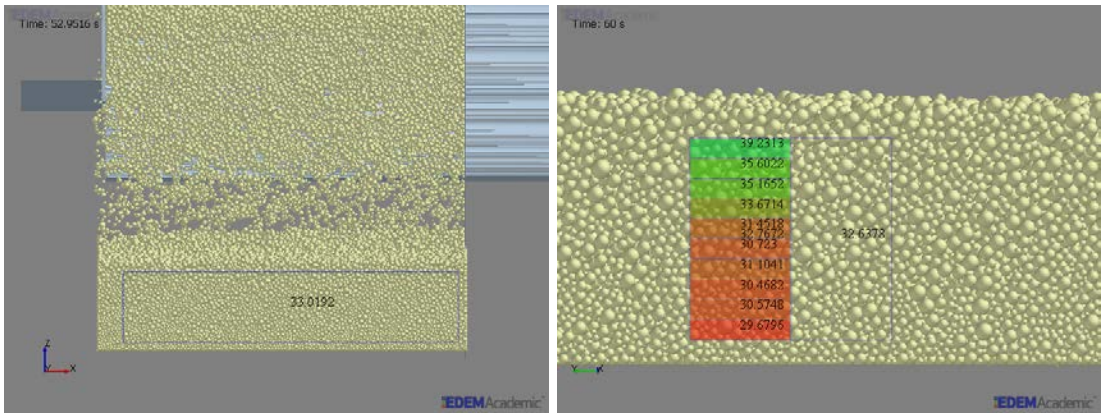

Figure 5.58. Measurements of voidage fraction of pellets bed – actual DDRS case simulation.

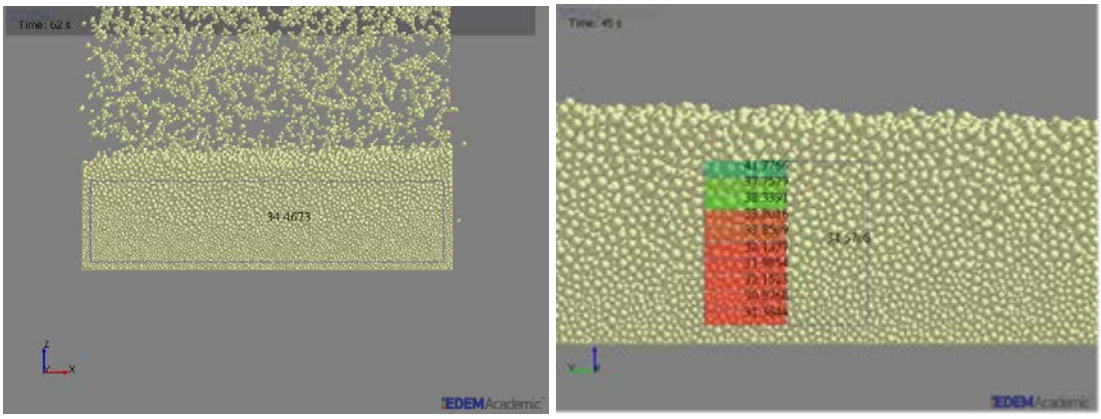

Figure 5.59. Measurements of voidage fraction of pellets bed – proposed DDRS case simulation.

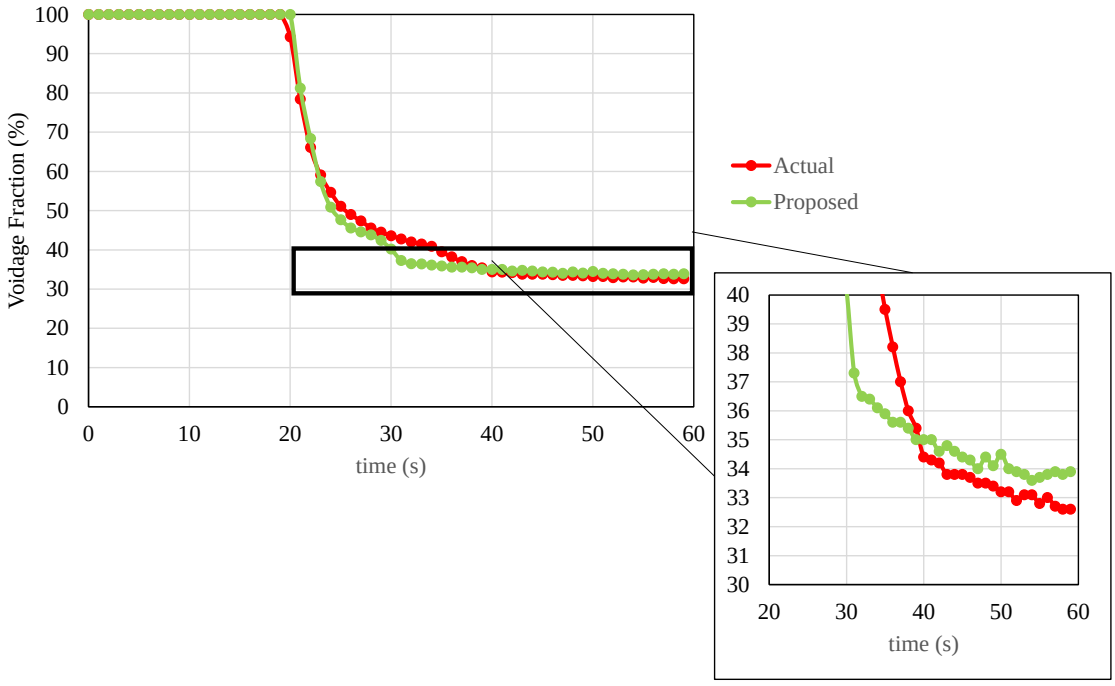

Figure 5.60. Partition curves for DDRS.

6 CONCLUSIONS

DEM application demonstrated to be a useful tool to reproduce green pellets motion and can preview results of green pellets classification on balling area. Even small differences could be verified when any parameter of control is altered. Green pellets individual and bulk properties were characterized and JKR contact model demonstrated to be the most appropriate to simulate their complex moist/sticky and soft behavior. However its use must be carefully carried out. Even geometry resolution cause changes on results that can be relevant depending on the difference/information investigated. The application of such numerical model must not be generalized and has to be individually analyzed since small singularities of each case can misguide conclusions.

DEM simulations of the roller screens using calibrated contact parameter for both pellets and system boundaries showed good agreement to the industrial data. Exploratory simulations have reproduce, at least qualitatively, the effect of important process variables such as moisture content, size distribution, pellets resistance that are verified in reality. Post-processing information also provided information about production losses and screening efficiency never measured and estimated in industrial units.

Controlled variables influence on single deck screening process responses were studied by extending the simulations investigations. Quantitative analysis of their effect conducted and the phenomena understanding were achieved by analyzing the outputs variations. Based on simulations results, new designs were thus proposed. Simulations results indicated that changes suggested increased screening efficiency and balling yield were approximately 2.5 % and representing good perspectives to roller screens equipment improvement.

Double deck roller screen (DDRS) configurations were simulated and results have demonstrated good perspectives for the complete upper deck that segregates production pellets in pallet cars. Its GSE is 6.5 % higher than the actual DDRS in operation. Voidage fraction of pellet beds in pallet cars would increase approximately 3 to 5 % if the proposed DDRS design is installed. Such information can led to following applications of fluid dynamics methods that can evaluate how screening efficiency can impact/improve air percolation and heat exchanges of pellets bed.

7 SUGGESTED FUTURE WORKS

- Evaluate impacts of pellets bed void fraction on process gases fluxes: assembly DEM output to CFD input modelling software in order to preview the impact on process fans energy consumption and heat exchanges that were considered uncountable benefits of better bed permeability in this study.

- Incorporate pellets mechanical degradation in the model

- Study the difference between drums and discs balling on green pellets making

8 REFERENCES

ABOUZEID, A.-Z.M; SEDDIK, A.A; EL-SINBAWY, H.A. Pelletizing Kinetics of an Earthy Iron Ore and the Physical Properties of the Pellets Produced. Powder Technology, 26, pp. 229-236, 1979.

ADETAYO, A.A; ENNIS, B.J. A New Approach to Modeling Granulation Processes for Simulation and Control Purposes. Powder Technology, 108, pp. 202-209, 2000.

ADETAYO, A.A; LITSTER, J.D; PRATSINIS, S.E; ENNIS, B.J. Population Balance Modelling of Drum Granulation of Materials with Wide Size Distribution. Powder Technology, 82, pp. 37-49, 1995.

ALVES, V.K. Metodologia para Simulação e Escalonamento de Prensa de Rolos. D.Sc, Universidade Federal de Minas Gerais, 2012.

BAKER, L.A; THOMAS, C.G; CORNELIUS, R.J; LYNCH, K.S; ARMSTRONG G.J. Effect of Goethite on Production Rate in a Travelling Grate Pellet Plant. Transactions of AIME, 254, pp. 270-278, 1973.

BALL, D.F; DARTNELL, J; GRIEVE, A; WILD, R. Agglomeration of Iron Ores. Heinemann, London, 1973.

BARRIOS, G.K.P; CARVALHO, R.M; KWADE, A; TAVARES, L.M. Contact Parameter Estimation for DEM Simulation of Iron Ore Pellet Handling. Powder Technology, 248, pp. 84-93, 2013.

BATTERHAM, R.J. Modeling the Development of Strenght in Pellets. Metallurgical Transctions B, 17B, pp. 479-285, 1986.

BOECHAT, F.O. Simulation of Mechanical Degradation of Iron Ore Pellets in direct Reduction Furnace Using The Discrete Element Method. M.Sc, Universidade Federal do Rio de Janeiro, 2013.

BORIM, J.C; FREITAS, R.O. Controle Automático da Distribuição Granulométrica de Pelotas de Minério de Ferro em uma Planta de Pelotização. Controle & Automação, 148, 2009.

CASTRO, A.A. Avaliação de Propriedades em Altas Temperaturas de Pelotas para Alto-Forno, M.Sc., Universidade Federal de Ouro Preto, 2006.

CAVALCANTE, M.V.S; FIGUEIRA, R.M; NUNES, S.F. Relationship between the Voids Found in Pellets Bed in a Furnace Type Traveling Grate with Energy Costs and Productivity. 45th Ironmaking and Raw Materials Seminar, 16th Brazilian Symposium on Iron Ore, 3rd Brazilian Symposium on Agglomeration of Iron Ore, Rio de Janeiro, Brazil, 2015.

CAVALCANTE, M.V.S; FIGUEIRA, R.M; NUNES, S.F; FONSECA, M.C; BERNARDO, B.S. Evaluation of Void in Bed Raw Pellets and its Relationship with the Parameters of Operational Control Measured in Pot Grate. 45th Ironmaking and Raw Materials Seminar, 16th Brazilian Symposium on Iron Ore, 3rd Brazilian Symposium on Agglomeration of Iron Ore, Rio de Janeiro, Brazil, 2015.

CLEARY, P.W. DEM Simulation of Industrial Particle Flows: Case Studies of Dragline Excavators, Mixing in Tumblers and Centrifugal Mills. Powder Technology, 109, pp. 83-104, 2000.

CLEARY, P.W. Recent Advances in DEM Modelling of Tumbling Mills. Minerals Engineering, 14, pp. 1295-1319, 2001.

CLEARY, P.W; METCALFE, G; LIFFMAN, K. How Well Do Discrete Element Granular Flow Models Capture the Essentials of Mixing Process? Applied Mathematical Modelling, 22, pp. 995-1008, 1998.

CLEARY, P.W; SINNOTT, M.D; MORRISON, R.D. Separation Performance of Double Deck Banana Screens – Part I: Flow and Separation for Different Accelerations. Minerals Engineering, 22, pp. 1218-1229, 2009.

CLEARY, P.W; SINNOTT, M.D; MORRISON, R.D. Separation Performance of Double Deck Banana Screens – Part II: Quantitative Predictions. Minerals Engineering, 22, pp. 1218-1229, 2009.

CORROCHANO, B.R; MELROSE, J.R; BENTLEY, A.C; FRYER, P.J; BAKALIS, S. A New Methodology to Estimate the Steady-state Permeability od Roast and Ground Coffee in Packed Beds. Journal of Food Engineering, 150, pp. 106-116, 2015.

COSTA, R.V.P. Otimização da Resistência à Compressão de Pelotas de Minério de Ferro para Redução Direta pela Aplicação de Projeto Robusto. M. Sc., Universidade Federal de Ouro Preto, 2008.

CUNDALL, P.A; STRACK, O.D.L. A Discreet Numerical Model for Granular Assemblies. Géotechnique, 29, no.1, pp. 47-65, 1979.

EDEM 2.6 User Guide, DEM Solutions, 2014.

EISELE, T.C; KAWATRA, S.K. A Review of Binders in Iron Ore Pelletization. Mineral Processing & Extractive Metallurgy Review, 24, pp. 1-90, 2003.

ENNIS, B.J. A Microlevel-based Characterization of Granulation Phenomena. Powder Technology, 65, pp. 257-272, 1991.

ENNIS, B.J; LI, J; TARDOS, G.I; PFEFFER, R. The Influence of Viscosity on the Strength of an Axially Strained Pendular Liquid Bridge. Chemical Engineering Science, 45, pp. 3071-3088, 1990.

ERGUN, S. Flow Through Packed Columns. Chemical Engineering Progress, 48, n.02, pp.89-94, 1952.

FONSECA, M.C; FERREIRA, H.O; OTAVIANO, M.M; PERIN, V. Coal Dosage Influence on Fired Pellets Quality. 39th Ironmaking and Raw Material Seminar, 10th Brazilian Symposium on Iron Ore, Ouro Preto, Brazil, 2009.

FORSMO, S.P.E; APELQVIST, A.J; BJÖRKMAN, B.M.T; SAMSKOG, P.-O. Binding Mechanisms in Wet Iron Ore Green Pellets with Bentonite Binder. Powder Technology, 169, pp. 147-158, 2006.

GILROY, A. How Low Can Iron Ore Prices Go from Here? Market Realist, New York, October 9th, 2015. Available on: < http://marketrealist.com/2015/10/impacts-iron-ore-miners-break-even-costs/>. Accessed on June 18th, 2016.

GODIN, E; WILHELMY, J.F. Development of a New Layered Pellet. 2nd COREM Symposium on Iron Ore Pelletizing, Quebec City, Canada, 2008.

HALEY, K.M; APULI, W.E. Pelletising on a horizontal grate machine. Interscience, New York, pp. 958-963, 1962.

HELE, P.D. Advanced Granulation Theory at Particle Level. Copenhagen, Denmark, 2006.

HOTTA, K; TAKEDA, K; IINOYA, K. The Capillary Bonding Force of a Liquid Bridge. Powder Technology, 10, pp. 231-242, 1974.

IVESON, S.M; LITSTER, J.D; HAPGOOD, K; ENNIS, B.J. Nucleation, Growth and Breakage Phenomena in Agitated Wet Granulation Processes: a Review. Powder Technology, 117, pp. 3-39, 2001.

JOHNSON, K.L; KENDALL, K; ROBERTS, A.D. Surface Energy and the Contact of Elastic Solids. Proceedings of Royal Society of London, Mathematical and Physical Sciences, 324, pp. 301-313, 1971.

KAMINSKA, J; DANKO, J. Analysis of the Granulation Process Mechanism – Stand and Scope of Experimental Investigations. Metallurgy and Foundry Engineering, 37, pp. 81-87, 2011.

KAPUR, P.C; ARORA, S.C.D; SUBBARAO, S.V.B. Water-bentonite Interaction in Balling of Iron Ores. Chemical Engineering Science, 28, pp. 1535-1540, 1973.

KAPUR, P.C; FUERSTENAU, D.W. Kinetics of Green Pelettization. Transactions of AIME, 229, pp. 348-466, 1964.

KAPUR, P.C; KAPUR, P; FUERSTENAU, D.W. An Auto-layering Model for the Granulation of Iron Ore Fines. International Journal of Mineral Processing, 39, pp. 239-250, 1993.

KAPUR, P.C; RUNKANA, V. Balling and Granulation Kinetics revisited. International Journal of Mineral Processing, 72, pp. 417-427, 2003.

KAWATRA, S.K; RIPKE, S.J. Developing and Understanding The Bentonite Fiber Bonding Mechanism. Minerals Engineering, 14, pp. 645-659, 2001.

KAWATRA, S.K. Binders in Iron Ore Pelletization. Michigan Tech University. Course on 3rd International Meeting On Ironmaking, 38th Edition of the Ironmaking Seminar, São Luís, Brazil, 2008.

LEONEL, C.M.L. Estudo do Processo de Calcinação como Operação Unitária Adicional na Pelotização de Minérios de Ferro com Altos Valores de PPC. D.Sc, Universidade Federal de Minas Gerais, 2011.

LIAN, G; THORNTON, C; ADAMS, M.J. A Theoretical Study of the Liquid Bridge Forces between Two Rigid Spherical Bodies. Journal of Colloid and Interface Science, 161, pp. 138-147, 1993.

LIAN, G; THORNTON, C; ADAMS, M.J. Discrete Particle Simulation of Agglomerate Impact Coalescence. Chemical Engineering Science, 53, pp. 3381-3391, 1998.

LITSTER, J.D; WATERS, A.G; NICOL, S.K. A Model for Predicting the Size Distribution of Product from a Granulating Drum. Transactions ISIJ, 26, pp. 1036-1044, 1986.

LIU, L. X; IVESON, S.M; LITSTER, J.D; ENNIS, B.J. Coalescence of Deformable Granules in Wet Granulation Processes. AIChE, 46, pp. 529-539, 2000.

LYNCH, A.J. Mineral Crushing and Grinding Circuits: Their Simulation, Optimization, Design and Control. Elsevier, Amsterdan, 1979.

MAYERHOFER, F.C. Study of Grinding Circuit of Pellet Feed in Vargem Grande Pelletizing Plant. Pós-graduação em Gestão de Negócios no Setor Mínero-metalúrgico. Ouro Preto, 2012.

MEYER, K. Springer-Verlag Berlin, Heidelberg, e Verlag Stahleisen mbH, Dusseldorf, 1980.

MISHRA, B.K; THORNTON, C; BHIMJI, D. A Preliminary Numerical Investigation of Agglomeration in a Rotary Drum. Minerals Engineering, 15, pp. 27-33, 2002.

MONTGOMERY, D.C. Design and Analysis of Experiments. 8th edition, Wiley, 2013.

NAGESWARARAO, K. Further Developments in the Modelling an Scale up of Industrial Hydrocycones. PhD Thesis, University of Queensland (JKMRC), 1978.

NAGESWARARAO, K. A Generalized Model for Hydrocyclone Classifiers. AusIMM Proceedings, vol. 2, 300, pp. 21, Parkville, 1995.

OptProcess Manual, 2009.

O'SULLIVAN, C. Particulate Discrete Element Modeling. A Geomechanics Perspective. Applied Geotechnics, volume 4. London, 2011.

PORMELAU, D; HODOUIN, D; POULIN, E. A First Principle Simulator of an Iron Oxide Pellet Induration Furnace – An Application to Optimal Tuning. Canadian Metallurgical Quarterly, 44, pp. 571 – 582, 2005.

QUIST, J.C.E. DEM Modelling and Simulation of Cone Crushers and High Pressure Grinding Rolls, Tese de doutorado, Chalmers Institute of Technology, Gothenburg, 2017.

RABINOVICH, Y.I; ESAYANUR, M.S; MOUDGIL, B.M. Capillary Forces between Two Spheres with a Fixed Volume of Liquid Bridge: Theory and Experiment. Lagmuir, 21, pp. 10992-10997, 2005.

RHODES, M. Introduction of Particle Technology. John Wiley & Sons Ltd., Chichester, 1998.

RUMPF, H. The Strength of Granules and Agglomerates in W.A. Knepper: Agglomeration, American Institute of Mining. Metallurgical, and Petroleum Engineers, INC., Interscience Publishers, New York, pp. 379-418, 1962.

SASTRY, K.V.S. Similarity Size Distribution of Agglomerates During Their Growth by Coalescence in Granulation or Green Pelletization. International Journal of Mineral Processing, 2, pp. 187-203, 1975.

SASTRY, K.V.S. How to Produce Designer Pellets of Our Choice Through a Process Engineering Approach. 2nd COREM Symposium on Iron Ore Pelletizing, Quebec City, Canada, 2008.

SASTRY, K.V.S; FUERSTENAU, D.W. Mechanisms of Agglomerate Growth in Green Pelletization. Powder Technology, 7, pp. 97-105, 1973.

SASTRY, K. V. S; DONTULA, P; HOSTEN, C. Investigation of the Layering Mechanism of Agglomerate Growth during Pelletiztion. Powder Technology, 130, pp. 231-237, 2003.

SCHRADER, M. E. Young-Dupre Revisited. Langmunir, 11, pp. 3585-3589, 1995.

SESHADRI, V; PEREIRA, R.O.S. Comparison of Formulae for Determining Heat Transfer Coefficient of Packed Bed. Transactions ISIJ, 26, pp. 604-610, 1986.

SILVA, B.B; CORDEIRO, F.S.O; OSORIO, L.G; PAIVA, J.A. Balling Control and Benefits of Narrower Granulometry Dispersion of Green Pellets on Indurated Pellets Metallurgical Properties. 3rd COREM Symposium on Iron Ore Pelletizing, Quebec City, Canada, 2013.

SOUZA, R.M.P; DANTAS, L.H.T; BARROS, M.V; DUARTE, C.L.L; COSTA, A.L.B; BONZI, J.S.A; SILVA, T.G; JUNIOR, F.L.C.C; SILVA, B.B; MAYERHOFER, F.C. Efeito da Variação do PPC do Minério no Processo de Pelotização da Vale. 44th Ironmaking and Raw Materials Seminar, 15th Brazilian Symposium on Iron Ore, 2nd Brazilian Symposium on Agglomeration of Iron Ore, Belo Horizonte, 2014.

SPOSARO, A.W. Packed Bed Heat Transfer. M.Sc. Newark College of Engineering, 1962.

TAVARES, L.M, CARVALHO, R.M; SILVEIRA, M.W; PEREIRA, H.C; BIANCHI, M.R; OTAVIANO, M.M; PEREIRA, B.C.E. Mechanical Degradation of Iron Ore Pellets During Handling. Part 1: Mathematical Model and Simulator. 45th Ironmaking and Raw Materials Seminar, 16th Brazilian Symposium on Iron Ore, 3rd Brazilian Symposium on Agglomeration of Iron Ore, Rio de Janeiro, 2015.

TAVARES, L.M, CARVALHO, R.M; SILVEIRA, M.W; PEREIRA, H.C; BIANCHI, M.R; OTAVIANO, M.M; PEREIRA, B.C.E. Mechanical Degradation of Iron Ore Pellets During Handling. Part 2: Simulation Case Studies. 45th Ironmaking and Raw Materials Seminar, 16th Brazilian Symposium on Iron Ore, 3rd Brazilian Symposium on Agglomeration of Iron Ore, Rio de Janeiro, 2015.

TAVARES, L.M; KING, R.P. Single-Particle Fracture under Impact Load. International Journal of Mineral Processing, 54, pp. 1-28, 1998.

THOMPSEN, L; PATZELT, N; KNECHT, J. High-pressure Grinding for Copper at Cyprus Sierrita. Mining Engineering, pp. 23-26, 1996.

THORNTON, C; CUMMINS, S. J; CLEARY, P.W. On elastic-plastic normal contact force models, with and without adhesion. Powder Technology, 315, pp. 339-346, 2017.

Vargem Grande Final Technical Report.

VELLOSO, C.M. Otimização da Operação do Alto-forno 1 da V&M do Brasil com “Stave Cooler” através da Distribuição de Carga no Topo do Forno, M.Sc, Universidade Federal de Minas Gerais, 2006.

WALTON, O.R., BRAUN. R.L. Stress calculations for Assemblies of Inelastic Spheres in Uniform Shear. Acta Mechanica, 63, PP. 73-86, 1986.

WANG, D; SERVIN, M; BERGLUND, T; MICKELSSON, K.-O; RÖNNBÄCK, S. Parametrization and Validation of a Nonsmooth Discrete Element Method for Simulating Flows of Iron Ore Green Pellets. Powder Technology, 283, pp. 475-487, 2015.

WEERASEKARA, N.S; POWELL, M.S; CLEARY, P.W; TAVARES, L.M; EVERTSSON,M; MORRISON, R.D; QUIST, J. CARVALHO, R.M. The contribution of DEM to the science of comminution. Powder Technology, 248, pp. 3-24, 2013.

WELLSTEAD, P.E; CROSS, M; MUNRO, N; IBRAHIM, D. On the Design and Assessment of Control Schemes for Balling-Drum Circuits Used in Pelletising. International Journal of Mineral Processing, 5, pp. 45-67, 1978.

WILLET, C.D; ADAMS, M.J; JOHNSON, S.A; SEVILLE, J.P.K. Capillary Bridges between Two Spherical Bodies. Langmuir, 16, pp. 9396-9405, 2000.

YU, A.B; STANDISH, N. An Analytical-Parametric Theory of the Random Packing of Particles. Powder Technology, 55, pp. 171-186, 1988.

ZHU, H; ZHOU, Z; YANG, R; YU, A. Discrete Particle Simulation of Particulate Systems: a Review of Major Applications and Findings. Chemical Engineering Science, 63, pp. 5728–5770, 2008.

APENDIX 1 DOE COMPLETE RESULTS

StdOrder	RunOrder	CenterPt	Blocks	gap (mm)	angle (°)	rolls speed (rpm)	rolls diameter (mm)	feed rate (t/h)	Production loss to undersize (t/h)	Product share in undersize	Production loss in oversize (t/h)	Total production loss (t/h)
1	1	1	1	8.5	11	80	63.5	130	61.65	60.21 %	5.77	67.42
2	2	1	1	9.0	11	80	63.5	130	82.77	66.62 %	4.18	86.95
3	3	1	1	8.5	15	80	63.5	130	62.07	60.54 %	11.20	73.27
4	4	1	1	9.0	15	80	63.5	130	81.53	66.75 %	11.60	93.14
5	5	1	1	8.5	11	120	63.5	130	69.13	62.19 %	2.82	71.95
6	6	1	1	9.0	11	120	63.5	130	111.68	72.05 %	2.19	113.88
7	7	1	1	8.5	15	120	63.5	130	68.66	62.33 %	6.75	75.41
8	8	1	1	9.0	15	120	63.5	130	110.57	72.12 %	6.87	117.45
9	9	1	1	8.5	11	80	75	130	60.01	59.71 %	2.53	62.54
10	10	1	1	9.0	11	80	75	130	100.58	70.48 %	2.05	102.63
11	11	1	1	8.5	15	80	75	130	59.11	59.93 %	2.58	61.69
12	12	1	1	9.0	15	80	75	130	98.63	70.34 %	3.81	102.43
13	13	1	1	8.5	11	120	75	130	66.10	61.88 %	0.63	66.74
14	14	1	1	9.0	11	120	75	130	112.05	72.54 %	0.42	112.47
15	15	1	1	8.5	15	120	75	130	64.74	61.76 %	0.58	65.32
16	16	1	1	9.0	15	120	75	130	111.06	72.61 %	0.98	112.04
17	17	1	1	8.5	11	80	63.5	160	66.24	58.21 %	13.99	80.23
18	18	1	1	9.0	11	80	63.5	160	90.98	65.16 %	14.65	105.62
19	19	1	1	8.5	15	80	63.5	160	70.99	59.33 %	24.45	95.44
20	20	1	1	9.0	15	80	63.5	160	91.99	65.25 %	23.79	115.78
21	21	1	1	8.5	11	120	63.5	160	80.88	61.43 %	6.90	87.79

22	22	1	1	9.0	11	120	63.5	160	131.40	71.55 %	8.79	140.19
23	23	1	1	8.5	15	120	63.5	160	80.09	61.49 %	14.78	94.86
24	24	1	1	9.0	15	120	63.5	160	128.67	71.34 %	12.02	140.69
25	25	1	1	8.5	11	80	75	160	68.74	58.80 %	13.04	81.77
26	26	1	1	9.0	11	80	75	160	113.25	69.18 %	8.40	121.65
27	27	1	1	8.5	15	80	75	160	68.69	59.03 %	12.10	80.79
28	28	1	1	9.0	15	80	75	160	112.73	69.27 %	14.68	127.41
29	29	1	1	8.5	11	120	75	160	77.05	60.78 %	2.45	79.50
30	30	1	1	9.0	11	120	75	160	133.43	72.08 %	1.56	134.99
31	31	1	1	8.5	15	120	75	160	76.31	61.24 %	2.55	78.85
32	32	1	1	9.0	15	120	75	160	130.60	72.00 %	2.90	133.50

StdOrder	RunOrder	CenterPt	Blocks	gap (mm)	angle (°)	rolls speed (rpm)	rolls diameter (mm)	feed rate (t/h)	Production share in oversize	Discs return rate	Discs undersize return rate	Discs oversize return rate
1	1	1	1	8.5	11	80	63.5	130	11.57 %	10.71 %	7.2 %	3.51 %
2	2	1	1	9	11	80	63.5	130	8.85 %	12.10 %	8.8 %	3.33 %
3	3	1	1	8.5	15	80	63.5	130	20.86 %	11.00 %	7.2 %	3.78 %
4	4	1	1	9	15	80	63.5	130	21.00 %	12.41 %	8.5 %	3.87 %
5	5	1	1	8.5	11	120	63.5	130	5.87 %	11.18 %	7.8 %	3.37 %
6	6	1	1	9	11	120	63.5	130	4.91 %	14.06 %	10.9 %	3.15 %
7	7	1	1	8.5	15	120	63.5	130	14.56 %	10.95 %	7.7 %	3.24 %
8	8	1	1	9	15	120	63.5	130	14.18 %	14.15 %	10.8 %	3.40 %
9	9	1	1	8.5	11	80	75	130	5.79 %	10.09 %	7.0 %	3.05 %
10	10	1	1	9	11	80	75	130	4.64 %	13.09 %	10.0 %	3.09 %

11	11	1	1	8.5	15	80	75	130	6.07 %	9.88 %	6.9 %	2.98 %
12	12	1	1	9	15	80	75	130	8.41 %	13.00 %	9.8 %	3.17 %
13	13	1	1	8.5	11	120	75	130	1.51 %	10.44 %	7.5 %	2.95 %
14	14	1	1	9	11	120	75	130	1.02 %	13.72 %	10.8 %	2.89 %
15	15	1	1	8.5	15	120	75	130	1.52 %	10.05 %	7.4 %	2.68 %
16	16	1	1	9	15	120	75	130	2.33 %	13.68 %	10.7 %	2.96 %
17	17	1	1	8.5	11	80	63.5	160	21.33 %	10.32 %	6.5 %	3.77 %
18	18	1	1	9	11	80	63.5	160	22.00 %	11.85 %	8.0 %	3.83 %
19	19	1	1	8.5	15	80	63.5	160	33.10 %	11.13 %	6.9 %	4.25 %
20	20	1	1	9	15	80	63.5	160	31.29 %	12.44 %	8.1 %	4.36 %
21	21	1	1	8.5	11	120	63.5	160	11.99 %	10.87 %	7.6 %	3.31 %
22	22	1	1	9	11	120	63.5	160	15.05 %	13.94 %	10.6 %	3.36 %
23	23	1	1	8.5	15	120	63.5	160	22.73 %	11.22 %	7.5 %	3.74 %
24	24	1	1	9	15	120	63.5	160	19.29 %	13.91 %	10.3 %	3.57 %
25	25	1	1	8.5	11	80	75	160	20.41 %	10.37 %	6.7 %	3.66 %
26	26	1	1	9	11	80	75	160	14.58 %	12.75 %	9.4 %	3.32 %
27	27	1	1	8.5	15	80	75	160	20.36 %	10.14 %	6.7 %	3.43 %
28	28	1	1	9	15	80	75	160	23.07 %	12.96 %	9.3 %	3.65 %
29	29	1	1	8.5	11	120	75	160	4.63 %	10.28 %	7.3 %	3.03 %
30	30	1	1	9	11	120	75	160	3.15 %	13.48 %	10.6 %	2.85 %
31	31	1	1	8.5	15	120	75	160	5.04 %	10.07 %	7.2 %	2.91 %
32	32	1	1	9	15	120	75	160	5.58 %	13.44 %	10.4 %	2.99 %

StdOrder	RunOrder	CenterPt	Blocks	gap (mm)	angle (°)	rolls speed (rpm)	rolls diameter (mm)	feed rate (t/h)	On-size contamination (t/h)	On-size contamination share	Fines screening efficiency	Product screening efficiency
1	1	1	1	8.5	11	80	63.5	130	3.47	0.27 %	91.9 %	94.45 %
2	2	1	1	9	11	80	63.5	130	3.17	0.25 %	93.3 %	92.55 %
3	3	1	1	8.5	15	80	63.5	130	3.86	0.31 %	91.2 %	93.91 %
4	4	1	1	9	15	80	63.5	130	3.52	0.28 %	91.5 %	93.01 %
5	5	1	1	8.5	11	120	63.5	130	2.44	0.19 %	94.8 %	93.99 %
6	6	1	1	9	11	120	63.5	130	1.23	0.10 %	97.7 %	90.84 %
7	7	1	1	8.5	15	120	63.5	130	3.15	0.25 %	93.5 %	94.56 %
8	8	1	1	9	15	120	63.5	130	1.81	0.15 %	96.3 %	91.03 %
9	9	1	1	8.5	11	80	75	130	3.82	0.30 %	91.2 %	95.41 %
10	10	1	1	9	11	80	75	130	2.42	0.20 %	94.9 %	92.27 %
11	11	1	1	8.5	15	80	75	130	4.64	0.36 %	89.2 %	95.55 %
12	12	1	1	9	15	80	75	130	3.18	0.26 %	93.8 %	92.23 %
13	13	1	1	8.5	11	120	75	130	3.54	0.28 %	91.8 %	94.95 %
14	14	1	1	9	11	120	75	130	2.13	0.17 %	95.6 %	91.49 %
15	15	1	1	8.5	15	120	75	130	4.43	0.35 %	90.3 %	94.96 %
16	16	1	1	9	15	120	75	130	2.60	0.21 %	94.3 %	91.61 %
17	17	1	1	8.5	11	80	63.5	160	6.51	0.42 %	87.8 %	94.82 %
18	18	1	1	9	11	80	63.5	160	5.94	0.39 %	89.8 %	93.22 %
19	19	1	1	8.5	15	80	63.5	160	5.65	0.37 %	89.9 %	94.03 %
20	20	1	1	9	15	80	63.5	160	5.22	0.34 %	90.5 %	92.91 %
21	21	1	1	8.5	11	120	63.5	160	3.31	0.21 %	93.7 %	94.56 %
22	22	1	1	9	11	120	63.5	160	1.89	0.13 %	96.5 %	91.07 %
23	23	1	1	8.5	15	120	63.5	160	4.10	0.27 %	92.6 %	93.99 %

24	24	1	1	9	15	120	63.5	160	2.45	0.16 %	95.4 %	91.56 %
25	25	1	1	8.5	11	80	75	160	5.75	0.37 %	89.0 %	95.07 %
26	26	1	1	9	11	80	75	160	3.63	0.24 %	93.2 %	92.17 %
27	27	1	1	8.5	15	80	75	160	6.38	0.41 %	88.1 %	94.75 %
28	28	1	1	9	15	80	75	160	4.23	0.28 %	92.3 %	92.48 %
29	29	1	1	8.5	11	120	75	160	4.71	0.30 %	91.8 %	95.39 %
30	30	1	1	9	11	120	75	160	2.65	0.18 %	95.5 %	91.82 %
31	31	1	1	8.5	15	120	75	160	6.06	0.39 %	89.1 %	95.09 %
32	32	1	1	9	15	120	75	160	3.48	0.23 %	93.8 %	91.55 %

APENDIX 2 RESIDUALS ANALYSIS FOR FINES REMOVAL EFFICIENCY

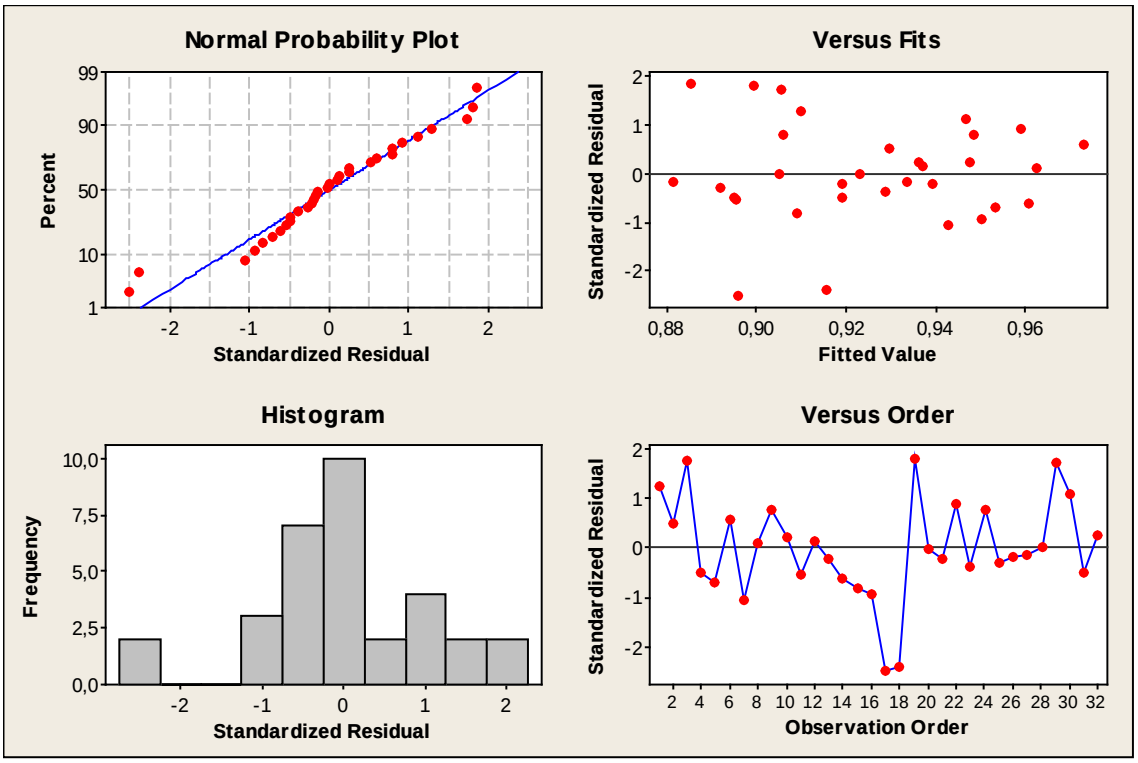

Residuals plot for fines removal efficiency.

None unusual observation was detected on residuals plot analysis for fines removal efficiency

APENDIX 3 RESIDUALS ANALYSIS FOR PRODUCT SCREENING EFFICIENCY

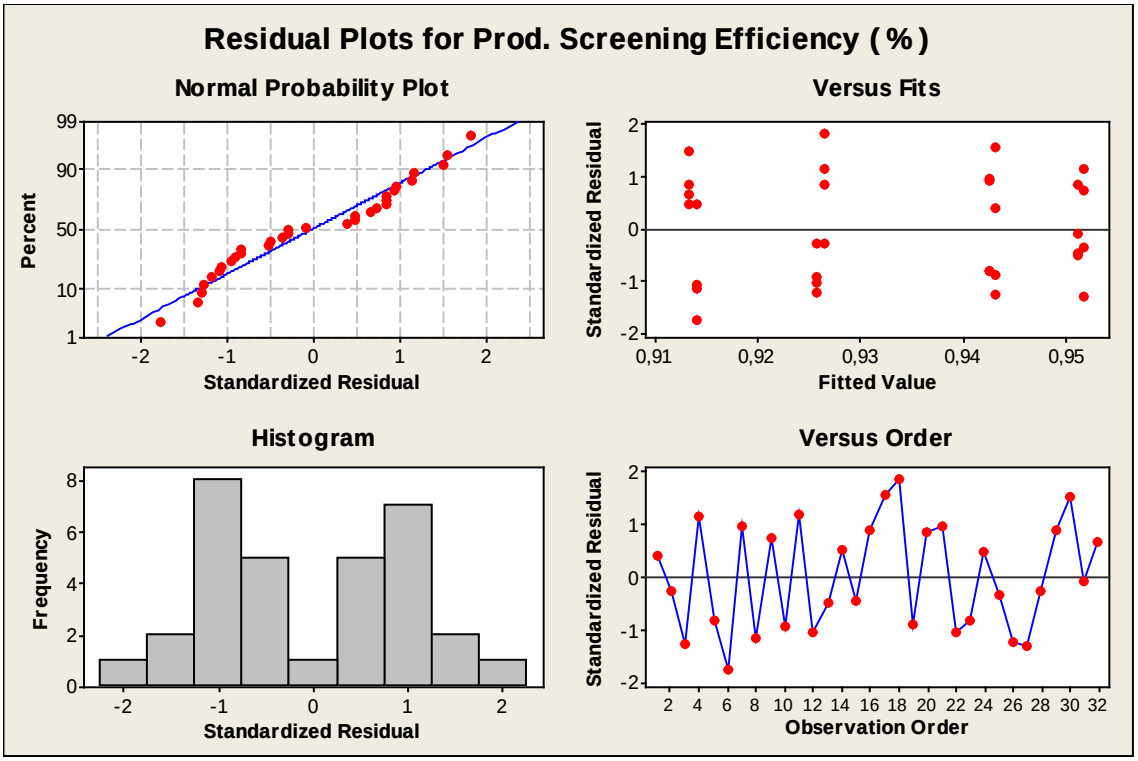

Normal plot of the standardized effects for the significant factors and interactions for product screening efficiency.

Residuals are normally distributed along the simulations execution order and variability is kept approximately constant for all the values of product screening efficiency.

APENDIX 4 RESIDUALS ANALYSIS FOR PRODUCT SCREENING EFFICIENCY

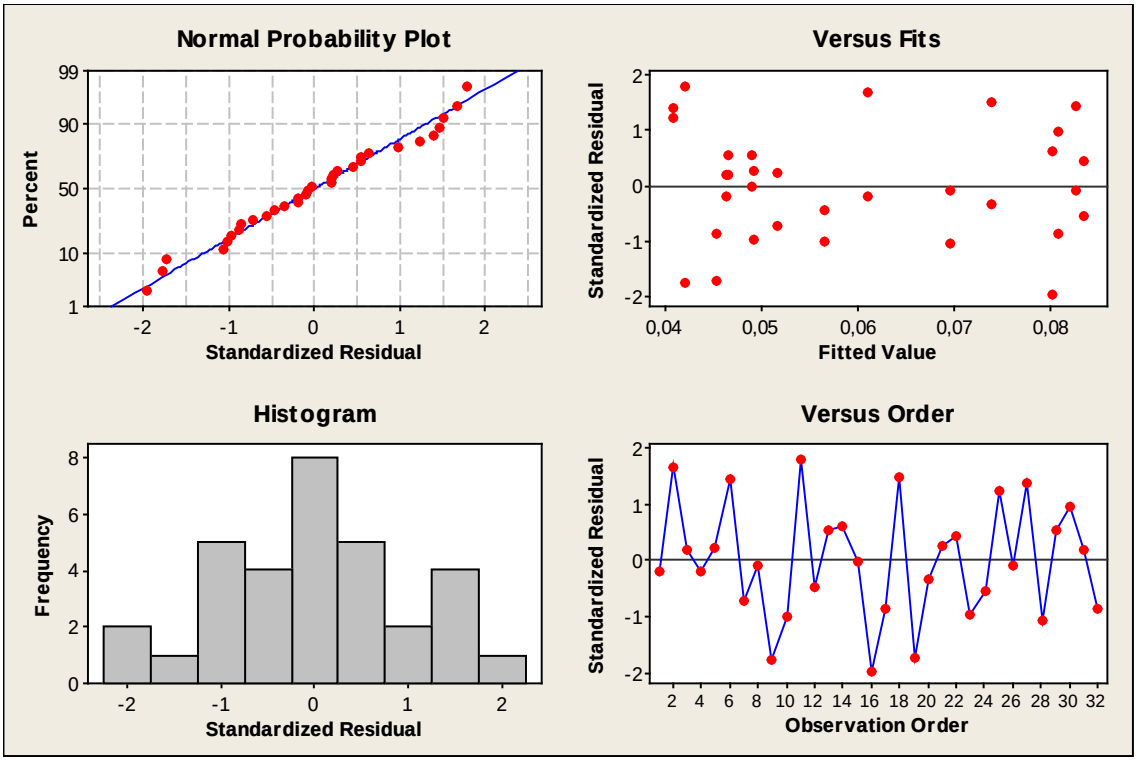

Normal plot of the standardized effects for the significant factors and interactions for loss of production to undersize.

There is not any special observation verified in residuals analysis. They are normally distributed along their mean, variance and occurrence.

APENDIX 5 RESIDUALS ANALYSIS FOR LOSS OF PRODUCTION TO OVERSIZE

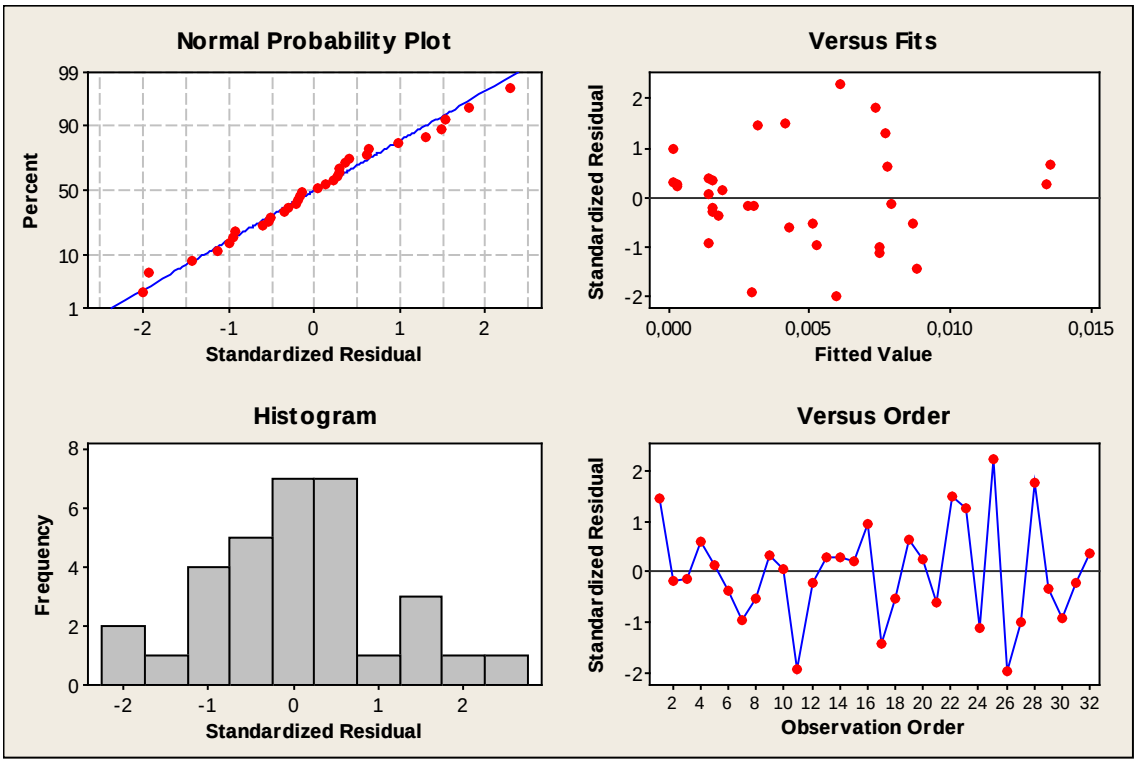

Normal plot of the standardized effects for the significant factors and interactions for loss of production to oversize.

There is not any special observation of residuals for the loss of production to oversize results.

APENDIX 6 RESIDUALS ANALYSIS FOR ON-SIZE CONTAMINATION (t/h)

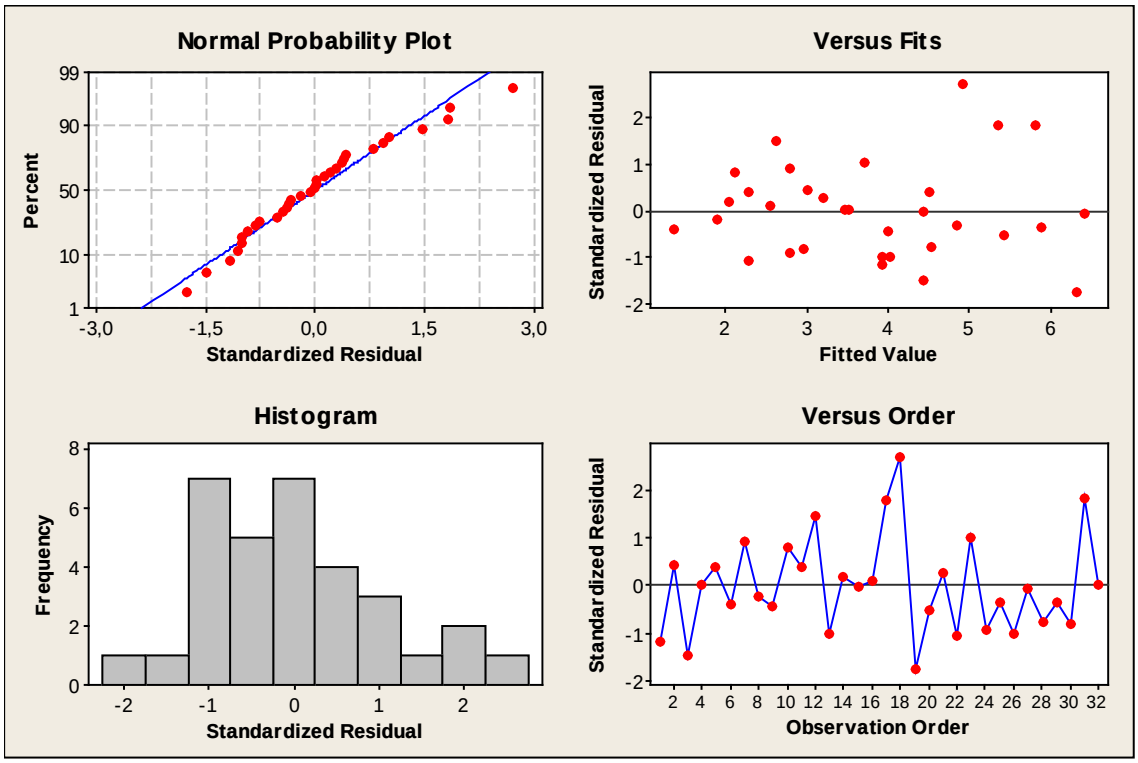

Normal plot of the standardized effects for the significant factors and interactions for on-size contamination (t/h).

Residuals are normally distributed along their mean, variance and occurrence.